

國立清華大學

National Tsing Hua University

碩士論文

Master Thesis

親輕子徐(Zee)模型的現象學限制研究

Phenomenological Constraints on the Leptophilic Zee Model

系別：物理系 Department of Physics

學號：110022421

研究生：黎德傳 Duc Truyen LE

指導教授：張維甫 We-Fu CHANG

中華民國一一三年〇九月

R.O.C. 113-09

摘要

在本研究中，我們探討了親輕子的徐(Zee)模型，其中額外的二重態純量場在樹級僅與希格斯基底中的輕子耦合。我們特別研究了由帶電輕子衰變和中微子振盪所給出來的現象學限制。我們也研究了由極化 μ 子衰變導出的Michel參數[1, 2] 及其對Zee模型參數空間的影響。

本論文的架構如下：第一章介紹了中微子振盪，並簡要回顧了中微子質量生成機制。第二章詳細討論了輕子親和Zee模型的理論架構及混合質量矩陣所帶來的限制。第四章和第五章討論了來自輕子味變（LFV）衰變的限制，如 $l_i \rightarrow l_i \bar{l}_m l_n$ 和 $L \rightarrow l \gamma$ 等衰變。第三章研究了透過 π 介子衰變進行的輕子普適性測試，然而此限制較弱。第六章詳細研究了Zee模型中的 μ 子衰變，結合了LFV衰變的全面研究及中微子振盪資料。最後，第七章給出了結論、粗略的數值結果以及未來研究的展望。



致謝

能夠有機會完成這篇論文，並在此寫下這些話，我真心想對所有在我身邊支持、幫助、相信我的人說一聲感謝。

首先，我要向我的導師張維甫教授表達我最真誠的感謝。在我的整個求學生涯和研究道路上，他給了我巨大的支持。沒有他的指導，是不可能有今天的。從他那裡獲得的專業知識和建議是無價的，特別是在我從以前的學習中所欠缺的物理見解和視角的培養上。他的指導幫助我在科學研究道路上變得更加成熟。我衷心想對我的親愛的老師說一聲“謝謝”，感謝他在我的旅程中扮演如此重要的角色。

我還要感謝清華大學給了我這樣一個優良環境中學習的機會，這對我完成論文起到了至關重要的作用。此外，我要感謝物理系的全體工作人員，他們的細心幫助讓我受益匪淺。特別感謝我的研究小組成員，震宇和士賢，感謝你們的支持、學習討論，以及一起度過的難忘時光。我的美好時光不僅體現在專業上的成長，也包括文化交流和豐富的學生生活，這一切都將成為我永遠珍藏的回憶。

我藉此機會向理論物理系的所有老師表達感激之情：張維甫教授、黃一平教授、張敬民教授、史馬丁教授和徐百嫻教授。沒有他們啟發性的講座，或許就沒有今天的我對物理史的熱情。徐百嫻

最後，我要感謝我的父母和家人，他們一直在我身邊，關心、相信並支持我追逐成為物理學家的夢想。所有的感激之情都不足以形容他們對我的無價之愛，而正是這種愛讓我每天都變得更堅強，勇敢面對一切困難。

Abstract

In this study, we investigated the leptophilic Zee model, where the extra doublet scalar only couples to leptons in Higgs basis at tree level. We specially study the phenomenological constraints arising from Charged Lepton decays and Neutrino Oscillation. We also study the Michel parameters [1, 2] derived from polarized muon decay, and its impact on the parameter space of the Zee model.

The structure of this thesis is as follows: Chapter 1 provides an introduction to the neutrino oscillation and briefly review the neutrino mass generation mechanisms. The theoretical framework of the leptophilic Zee model and the constraint from the mixing mass matrix are detailed in Chapter 2. Chapters 4 and 5 discuss the strong constraints from Lepton Flavor Violation (LFV) decays, such as $l_i \rightarrow l_i \bar{l}_m l_n$, $L \rightarrow l \gamma$. The Universality test in Pion decay is also studied in Chapter 3, however, the constraint obtained is rather weak. Chapter 6 presents a detailed study on the muon decay in the Zee model, leveraging comprehensive studies of LFV decays along with neutrino oscillation data. Finally, Chapter 7 gives the conclusions, a rough numerical result and perspectives for future research.

Acknowledgements

To have the opportunity to complete this thesis and write such words here, I really want to say thank you all, who side by side have been supporting, helping, believing in me.

First of all, I would like to express my sincere gratitude to my supervisor, Prof. Chang We-Fu, who has supported me tremendously throughout both my student life and study path. Without his guidance, my achievements today would not have been possible. The professional knowledge and advice I have gained from him are invaluable, particularly in developing the physics insights and perspectives I lacked from my previous studies. His mentorship has been instrumental in helping me become more mature and sustainable in my research path. I genuinely want to say "thank you" to my dear teacher for being such an important part of my journey.

I am also grateful to Tsing Hua University for giving me the opportunity to work in such a renowned scientific environment, which was instrumental in accomplishing my thesis. Additionally, I would like to thank all the staff members of the Department of Physics for their thoughtful assistance. Special thanks go to my group members, Zhen-Yu and Shi-Xian, for their support, study discussions, and for sharing indelible moments together. My great time here has been enriched not only by professional growth but also by cultural exchanges and the vibrant student life, all of which I will cherish as lasting memories.

I take this opportunity to express gratitude to all of my teachers at the Department of Theoretical Physics: Prof. We-Fu, Yi-Ping, Kingman, Martin, Jennifer. Without their inspiring lectures, there might be not my passion today.

The last, to my parents, my family, who are always by my side, concern, believe, and favor me in the way of my dream of becoming a physicist. All my gratitude is not enough to describe their invaluable love for me, which makes me stronger every single day, dare to cope with all difficulties.



Tsingda, September 2024

Hsinchu city, Taiwan

LE Duc Truyen

Contents

Abstract (Chinese)	I
Acknowledgements (Chinese)	II
Abstract	III
Acknowledgements	IV
Contents	VI
List of Figures	IX
List of Tables	X
1 Neutrino Oscillation	1
1.1 Neutrino Oscillation	1
1.2 Neutrino mass generation	4
2 Zee's model	9
3 Universality test in Pion decay	14
4 Trilepton decay $l_i \rightarrow l_j \bar{l}_m l_n$ constraint	20
5 Lep-to-lep-gamma $L \rightarrow l\gamma$	23



6	Muon decay	27
6.1	Michel paramters	27
6.2	Fermi constant	29
6.3	Zee model constraints in Muon decay	30
7	Conclusion and outlook	35
	Bibliography	39
	Appendices	42
A	Fierz transformation	43
B	Full massive Lorenz index two-body phase pace	45
C	Effective Field Theory model	47
C.1	Charged vector boson	47
C.2	Charged scalar boson	51
C.3	Feynman rule	52
D	Michel parameters	56
E	$L \rightarrow l\gamma$ decay process	61
E.1	Gauge invariant and Anapole vanishing	61
E.2	Charged vector form factors	63
E.3	Charged scalar form factors	65
E.4	$L \rightarrow l\gamma$ and $(g - 2)_l$	67
E.4.1	$L \rightarrow l\gamma$ LFV decay	67
E.4.2	$(g - 2)_l$ anomalous magnetics dipole moment	68
F	EFT Coupling Constraints in muon decay experiments	72
F.1	Case of universal coupling	72

F.2	a_l contributions from new charged bosons	74
F.3	Case of non-universal coupling	77
F.4	Coupling pattern from UV models	80
G	$L \rightarrow l\gamma$ form factor full expression	82
G.1	Charged vector form factors of diagrams Fig. E.1	82
G.2	Charged scalar form factor of diagrams Fig. E.2	87



List of Figures

1.1	Feynman diagram for generating Majorana neutrino mass	8
7.1	Parameter space constraint of Zee model from experiments	37
E.1	$l_j \rightarrow l_i \gamma$ with new charged vector contribution	63
E.2	$l_j \rightarrow l_i \gamma$ with new charged scalar contribution	65
F.1	Yukawa couplings in muon parameters experiment values	73
F.2	Vector couplings in muon experiment values	74
F.3	MDM values from new scalar's contribution in muon decay experiment's constrained region.	75
F.4	MDM values from new vector's contribution in muon decay experiment's constrained region.	76
F.5	Electron MDM anomaly in the scalar's non-universality coupling . .	77
F.6	Muon MDM anomaly in the vector non-universality coupling	78
F.7	The new vector non-universality coupling's constraint	79
F.8	2HDM constraint	80

List of Tables

4.1	Trilepton $l_i \rightarrow l_j \bar{l}_m l_n$ decay constraints table	21
4.2	Simple expression of Trilepton $l_i \rightarrow l_j \bar{l}_m l_n$ decay constraints	22
5.1	$L \rightarrow l \gamma$ constraints table	26
7.1	Order of magnitude of roughly constraints	35
F.1	2HDM type of couplings	81



Chapter 1

Neutrino Oscillation

Neutrino oscillation, a dynamic phenomenon discovered in 1998 by the Super-Kamiokande group through their analysis of atmospheric neutrinos, stands as a pivotal exploration in elementary particle physics. Over the years, the neutrino oscillation has been established across various sources, including atmospheric, solar, accelerator, and reactor neutrinos. This groundbreaking revelation challenges the traditional understanding embedded within the SM framework, proposing a new approach that necessitates the incorporation of neutrino mass and mixing into the theoretical models. As a result, the mechanism which generates neutrino masses and the observed oscillation pattern are crucial for theories to go beyond the Standard Model.

1.1 Neutrino Oscillation

From the quantum mechanics point of view, the origin of oscillation is understood to stem from the studied states and the Hamiltonian eigenstates are not the same. That is, the studied states here, called flavor states ν_α^L , produced and detected through the physical processes are actually a mixture of different mass states deemed as Hamiltonian eigenstates ν_i . As the neutrino travels, the different

mass states evolve differently due to their distinct masses. This difference causes the probability of detecting a particular flavor to change over time and distance. In vacuum, assumed that $E \sim p \gg m$, then $E = \sqrt{m^2 + p^2} \simeq p + \frac{m^2}{2p}$, the probability when a flavor state ν_α^L evolves to ν_β^L after traveling a distance of L

$$\begin{aligned} \mathbf{Pr}(\nu_\alpha \rightarrow \nu_\beta) &\cong \left| \sum_i U_{\beta i}^\nu U_{\alpha i}^{\nu*} e^{-i \frac{m_i^2}{2E} L} \right|^2 = \sum_{i,j} U_{ij}^{\alpha\beta} e^{i 2X_{ij}} \\ &= \delta_{\alpha\beta} - 4 \sum_{i>j} \sin^2(X_{ij}) \operatorname{Re} [U_{ij}^{\alpha\beta}] - 2 \sum_{i>j} \sin(2X_{ij}) \operatorname{Im} [U_{ij}^{\alpha\beta}], \end{aligned} \quad (1.1)$$

where $U_{ij}^{\alpha\beta} \equiv U_{\alpha i}^\nu U_{\beta i}^{\nu*} U_{\beta j}^\nu U_{\alpha j}^{\nu*}$ and $X_{ij} \equiv \frac{m_i^2 - m_j^2}{4E} L$. The last term in Eq. 1.1 is sensitive to the CP violation in the lepton sector, which apparently does not show up in the survival probability¹

$$\mathbf{Pr}(\nu_\alpha \rightarrow \nu_\alpha) = 1 - 4 \sum_{i>j} |U_{\alpha i}^\nu|^2 |U_{\alpha j}^\nu|^2 \sin^2(X_{ij}). \quad (1.2)$$

The weak eigenstates ν_α^L are presented in terms of mass eigenstates $\nu_\alpha^L = \sum_{i=1}^3 U_{\alpha i}^\nu \nu_i$ by an 3×3 unitary mixing matrix U^ν , the so-called Pontecorvo-Maki-Nakagawa-Sakata (PMNS) matrix which is characterized by the following standard parametrization

$$\begin{aligned} U^\nu &= \begin{pmatrix} 1 & 0 & 0 \\ 0 & c_{23} & s_{23} \\ 0 & -s_{23} & c_{23} \end{pmatrix} \times \begin{pmatrix} c_{13} & 0 & s_{13} e^{-i\delta_{CP}^D} \\ 0 & 1 & 0 \\ -s_{13} e^{i\delta_{CP}^D} & 0 & c_{13} \end{pmatrix} \times \begin{pmatrix} c_{12} & s_{12} & 0 \\ -s_{12} & c_{12} & 0 \\ 0 & 0 & 1 \end{pmatrix} \times \operatorname{Diag} \left(1, e^{i\frac{\mu_1}{2}}, e^{i\frac{\mu_2}{2}} \right) \\ &= \begin{pmatrix} c_{12}c_{13} & s_{12}c_{13} & s_{13}e^{-i\delta_{CP}^D} \\ -s_{12}c_{23} - c_{12}s_{23}s_{13}e^{i\delta_{CP}^D} & c_{12}c_{23} - s_{12}s_{23}s_{13}e^{i\delta_{CP}^D} & s_{23}c_{13} \\ s_{12}s_{23} - c_{12}c_{23}s_{13}e^{i\delta_{CP}^D} & -c_{12}s_{23} - s_{12}c_{23}s_{13}e^{i\delta_{CP}^D} & c_{23}c_{13} \end{pmatrix} \times \operatorname{Diag} \left(1, e^{i\frac{\mu_1}{2}}, e^{i\frac{\mu_2}{2}} \right) \end{aligned} \quad (1.3)$$

¹Survial probability means the probability a type of flavor neutrino is still in the same flavor as the source when it reaches the detector, e.g. $\operatorname{Pr}(\nu_e \rightarrow \nu_e)$.

in terms of mixing angles $c_{ij}(s_{ij}) \in [0, 1]$ and CP phases $\{\mu_i, \delta_{CP}^D\} \in [0, 2\pi]$. Therein we assumed the 3-flavor neutrino mixing ν_l^L for $l = \{e, \mu, \tau\}$, which was compatible with data from invisible Z boson decay width, and three of massive neutrinos $\{\nu_1, \nu_2, \nu_3\}$. Nevertheless, the number of massive neutrinos, in general, is larger than 3, that is recently hinted at by experiments implying the possibility of the presence of light sterile neutrinos mixing with the flavor neutrinos [3, 4].

The complex phase's d.o.f of the PMNS matrix counted as

$$\# \text{Phase d.o.f} = \begin{cases} \frac{n(n+1)}{2} - (2n - 1) = \frac{(n-1)(n-2)}{2} & \text{Dirac neutrinos} \\ \frac{n(n+1)}{2} - n = \frac{n(n-1)}{2} & \text{Majorana neutrinos} \end{cases}, \quad (1.4)$$

is similar to the CKM matrix of the quark sector in the case of Dirac neutrinos. Given n flavor, Eq. 1.4 says, in the Dirac case there are $(2n - 1)$ redundant phase d.o.f by the unphysical field rephasing ($2n$ chiral fields), and factor (-1) is the overall phase which does not change anything. However, for the Majorana phases only the LH neutrinos are involved. Therefore, only n d.o.f are deducted. As a corollary, at least 3-flavor Dirac neutrinos are required to yield 1 CP phase, in contrary, only 2-flavor Majorana neutrinos are needed for the Majorana CP phase to exist.

In SM, the neutrino is massless, and the PMNS matrix is the identity matrix. The observed neutrino oscillation detected in 1998, was the smoking gun evidence of NP beyond the SM. And the weak eigenstate, the interaction basis with the W boson, and the mass eigenstate of neutrino are different. The mass eigenstate is usually regarded as the “physical” state due to the invariance under Lorentz transformation, with a definite mass generated in the Yukawa sector.

The flavor index l of LH neutrinos ν_l^L stands for the charged lepton accompanying in the SM charged current (CC) interaction, described by the Lagrangian

$$\mathcal{L}_{\text{CC}} = -\frac{g}{\sqrt{2}}W_{\mu}^{+} \sum_{l=\{e,\mu,\tau\}} \bar{\nu}_l^L \gamma^{\mu} l^L + \text{h.c.} \quad (1.5)$$

The neutrino flavor is determined by the flavor of the associated charged lepton in CC interaction in oscillation experiment. Depending on the sources, the oscillation experiments are categorized into atmospheric and accelerator (probing ν_{μ} and $\bar{\nu}_{\mu}$), solar (ν_e) and reactor ($\bar{\nu}_e$). The mixing angle and mass squared difference are thus coined accordingly. For instance, the neutrino solar mixing angle and mass squared differences are labeled as $c_{12} \equiv c_{\odot}$ and $\Delta m_{21}^2 \equiv \Delta m_{\odot}^2$, while $c_{23} \equiv c_A$ and $\Delta m_{31}^2 \equiv \Delta m_A^2$ for the atmospheric neutrino. Due to the smallness of (1,3) mixing, both solar and atmospheric neutrino oscillations can be approximated by the 2-flavor oscillation.

Note that, most neutrino oscillation experiments are of the disappearance type measuring “ ν survival probability” as they travel from the experiment source till passing the neutrino detector, they apparently cannot be used to search for CP violation. Moreover, these conventional lepton-number-conserving neutrino oscillations depend only on the Dirac phase, which is characterized by the rephasing invariant J_{CP}

$$J_{CP} = \frac{\text{Im} (U_{in}^{\nu} U_{jm}^{\nu} U_{im}^{\nu*} U_{jn}^{\nu*})}{\sum_k \epsilon_{ijk} \sum_l \epsilon_{nml}} = c_{12} c_{13}^2 c_{23} s_{12} s_{13} s_{23} \sin (\delta_{CP}^D), \quad (1.6)$$

which is known as the Jarlskog invariant [5]. Hence, neutrino oscillation experiments cannot tell us whether neutrinos are Dirac or Majorana particles.

1.2 Neutrino mass generation

In the Standard Model, the masses of the charged fermions are generated via a Yukawa coupling of the scalar Higgs doublet H , with a fermion right-handed

and left-handed component, particularly, the lepton mass is conventionally built up by $SU(2)_L$ invariant combination of left-handed lepton doublet L with the right-handed charged lepton field l^R

$$\mathcal{L}_{Yuk} \supset -Y_{ij}^l \bar{L}_i H l_j^R + h.c. \quad (1.7)$$

After spontaneous symmetry breaking, Higgs gets VEV $\langle H \rangle = \frac{v}{\sqrt{2}} \begin{pmatrix} 0 \\ 1 \end{pmatrix}$, these terms lead to charged lepton masses

$$m_{ij}^l = Y_{ij}^l \frac{v}{\sqrt{2}}. \quad (1.8)$$

Consequently, the neutrino is massless, due to the absence of right-handed neutrinos, hence no such Yukawa interaction can be built for the neutrinos.

Since neutrinos are charge neutral, in principle they can acquire a QED invariant term $m_\nu \bar{\nu} \nu^c$, the so-called Majorana mass term. However, since the neutrinos are parts of $SU(2)$ doublets, $\bar{L} L^c$ is not SM gauge invariant. Moreover, the accidental total lepton symmetry will be violated by two units. Due to the absence of RH neutrinos, the SM neutrinos are massless. In order to accommodate the non-zero neutrino masses, one must go beyond the SM.

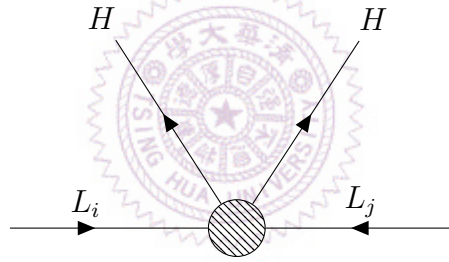
At low-energy, it is useful to consider the Lagrangian

$$\mathcal{L}_{M_\nu} = -M_D^{ij} \bar{\nu}_i^R \nu_j^L - \frac{1}{2} M_M^{ij} \bar{\nu}_i^L (\nu_j^L)^c + h.c., \quad (1.9)$$

where the first term is called the Dirac mass term and the second term the Majorana mass. In contrast to the Dirac fermions, Majorana fermions involve only left or (right-handed) field. The “physical” state $\Psi_\nu \equiv (\nu^L)^c + \nu^L$, the solution to the Dirac equation, has the property that $\Psi_\nu = \Psi_\nu^c$. In general, both mass

terms are allowed in the Lagrangian, a well-known instance is the type-I see-saw mechanism. While the $(\nu^L)^c$ acts like ν^R under Lorentz transformation, the Dirac mass term entails an extra new right-handed neutrino, often called sterile neutrino, being inert with SM interactions. That is why we got the normalized factor $\frac{1}{2}$ in the Majorana mass term owing to half d.o.f compared to the Dirac case. To tell the Majorana nature, the Neutrinoless double beta decay $0\nu\beta\beta$ decay is one of the promising probes, where an atom decay with any neutrino in the final state, $(A, Z) \rightarrow (A, Z + 2) + e^- + e^-$, violating the lepton number by 2 units.

In the SM, the charged fermions get their Dirac masses through the SSB mechanism from the renormalizable Yukawa interaction as described by Eq. (1.8,1.9), while the Majorana mass term for neutrinos can be described by an effective dim-5 gauge invariant Weinberg operator



$$\mathcal{L}_5 = \frac{c_{ij}}{\Lambda} \left(\tilde{L}_i H \right) \left(\tilde{H}^\dagger L_j \right) \xrightarrow[\langle H \rangle = \frac{v}{\sqrt{2}}]{\text{After SSB}} \mathcal{L}_5 \supset \frac{c_{ij}}{\Lambda} \frac{v^2}{2} \overline{(\nu_i^L)^c} \nu_j^L, \quad (1.10)$$

with $\tilde{L} = i\sigma_2 L^c$, $\tilde{H} = i\sigma_2 H^*$, and Λ stands for the NP energy cut-off. Then $M_\nu^{ij} \simeq \frac{c_{ij}}{\Lambda} \frac{v^2}{2}$ is the symmetric Majorana mass matrix, taking $c \sim 1$ and $m_\nu \in M_\nu \sim 1$ eV, indicates a NP scale $\Lambda \simeq \frac{\langle H \rangle^2}{m_\nu} \simeq 10^{13}$ GeV, not far from the energy scale of the unified theories.

To generate the Majorana neutrino masses, or the effective Weinberg operator, the following mechanisms have been considered:

1. New fermion field with Hypercharge $Y = 0$

\oplus Singlet fermion ν^R : $Y_{ij}^\nu \overline{\nu_i^R} \tilde{H}^\dagger L_j$ (e.g. Type-I Seesaw sterile neutrino [6])

$$(1.11)$$

$$M_\nu = Y^\nu \frac{1}{M_{\nu^R}} (Y^\nu)^T \langle H \rangle^2.$$

⊕ Triplet fermion F : $Y_{ij}^F \tilde{H}^\dagger \overline{F}_i L_j$ (e.g. Type-III Seesaw [7])

$$(1.12)$$

$$M_\nu = Y^F \frac{1}{M_F} (Y^F)^T \langle H \rangle^2.$$

2. New scalar field with Hypercharge $Y = 2$

⊕ Scalar triplet Δ : $Y_{ij}^\Delta \overline{L}_i^c i \sigma_2 \Delta L_j$ (e.g. Type-II Seesaw [8])

$$(1.13)$$

$$M_\nu = Y^\Delta \frac{\mu_\Delta}{M_\Delta^2} \langle H \rangle^2.$$

⊕ Scalar singlet S^+ : $Y_{ij}^S \overline{L}_i^c i \sigma_2 L_j S^+$ (e.g. Zee-singlet scalar [9])

This scenario is our case study, that will be elaborated on in the details.

The neutrino mass can be generated via the 1-loop diagram displayed in Fig. 1.1.

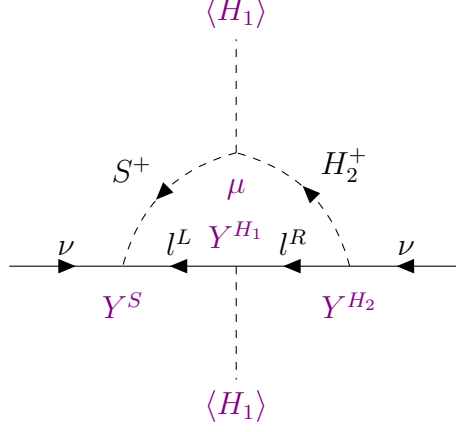


Figure 1.1: Feynman diagram for generating Majorana neutrino mass

This one-loop diagram leads to a non-zero neutrino mass given by

$$M_\nu = \frac{1}{8\pi^2} \frac{\mu \langle H_1 \rangle}{m_{\eta^+}^2 - m_{H^+}^2} \log \left(\frac{m_{\eta^+}^2}{m_{H^+}^2} \right) \left[Y^S (\langle H_1 \rangle Y^{H_1}) (Y^{H_2})^T + Y^{H_2} (\langle H_1 \rangle Y^{H_1}) (Y^S)^T \right]. \quad (1.14)$$

In principle, H_2 can couple to both the quarks and leptons. For simplicity, we focus on the phenomenological constraint on the Leptophilic Zee model's parameter space, where H_2 only couples to leptons due to some unspecified symmetries.

Chapter 2

Zee's model

The Zee model [9], a notable extension of the Standard Model, offers a compelling framework for understanding the origin of neutrino masses, a key factor in explaining the well-established neutrino oscillation data. This model addresses the limitations of the Standard Model, particularly in explaining the tiny neutrino mass, which is realized through loop correction, apart from other mechanisms such as the type-I, II, and III seesaw models. See the first term in Eq. 2.1, this contribution, breaking the lepton number $L_{e,\mu,\tau}$ by two units, leads to Majorana masses for neutrinos after SM electroweak symmetry breaking. It introduces new particles, including an additional Higgs doublet and a singly-charged scalar. These new degrees of freedom are also significant in generating observable charged lepton flavor violating (CLFV) signals, like $\mu \rightarrow e\gamma$ and $\mu \rightarrow 3e$, etc., and in potentially explaining experimental anomalies such as the anomalous MDM, baryogenesis. Being associated with the lepton mass in the loop, the model put forward an acceptable solution for the neutrino mass hierarchy other than neutrino mass generating mechanisms. The simplest extension of the Standard Model 2HDM framework that entails extra the non-conserved lepton number interaction in the singlet sector to give rise to the Majorana radiative neutrino mass. Thus,

the leptonic Yukawa in Higgs basis is put down as:

$$\mathcal{L}_{Yuk} \supset -Y_{\alpha\beta}^S \bar{L}_\alpha^c i\sigma_2 L_\beta S^+ - Y_{\alpha\beta}^{H_2} \bar{L}_\alpha H_2 l_\beta^R - Y_{\alpha\beta}^{H_1} \bar{L}_\alpha H_1 l_\beta^R + \text{h.c.}, \quad (2.1)$$

L^c is the charge conjugate of the left-handed doublet L . The first term corresponds to the singlet charged breaking lepton number invariance in SM, the latter corresponds to the 2HDM part. The relevant gauge invariant Higgs potential terms are

$$V(H_1, H_2, S^+) \supset \mu H_1^T i\sigma_2 H_2 S^- + \lambda_6 |H_1|^2 H_1^\dagger H_2 + \text{h.c.} \quad (2.2)$$

for CP-conserved in the Higgs sector, all quartic coupling is made to be real. Note that, Y^S is an antisymmetric matrix and can be rephased to be real, on the other hand, Y^{H_2} is generally complex, but here be considered real and leptophilic for simplicity, and the SM-like Yukawa coupling $Y^{H_1} = \frac{M_l}{\langle H_1 \rangle}$ in Higgs basis chosen to be diagonal without loss of generality. In the unitary gauge, the scalar components are

$$H_2 = \begin{pmatrix} H_2^+ \\ \frac{1}{\sqrt{2}}(H_2^0 + iA) \end{pmatrix}, \quad H_1 = \begin{pmatrix} 0 \\ \frac{H_1^0}{\sqrt{2}} \end{pmatrix}, \quad (2.3)$$

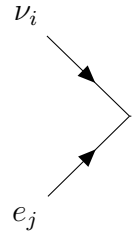
accompanied with the singlet scalar S^+ . Going to the mass eigenstates, they are related to by the following transformation

$$\begin{pmatrix} H_{SM} \\ H_N \end{pmatrix} = \begin{pmatrix} c_\alpha & s_\alpha \\ -s_\alpha & c_\alpha \end{pmatrix} \begin{pmatrix} H_1^0 \\ H_2^0 \end{pmatrix} \text{ and } \begin{pmatrix} \eta^+ \\ H^+ \end{pmatrix} = \begin{pmatrix} c_\beta & s_\beta \\ -s_\beta & c_\beta \end{pmatrix} \begin{pmatrix} S^+ \\ H_2^+ \end{pmatrix}, \quad (2.4)$$

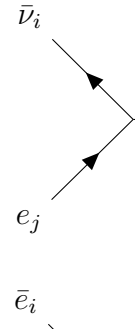
where α and β are the mixing angles. Whereas the mixing in neutral scalar induced by the Higgs potential's quartic coupling $c_\alpha s_\alpha \sim \lambda_6$ in which we consider alignment/decoupling limit ($\alpha \rightarrow 0$) being compatible with LHC search [10, 11, 12],

$H_1^0 \equiv H_{SM}^1$ is then regarded as SM-like Higgs at 125 GeV and with the redefinition of $H_0 \equiv \frac{1}{\sqrt{2}}(H_N + iA)$. The mixing angle $c_\beta s_\beta = \frac{\mu \langle H_1 \rangle}{m_{\eta^+}^2 - m_{H^+}^2}$ is proportional to the coefficient of the cubic coupling μ in Eq. 2.2, which breaks the lepton number by two units and contributes to non-zero Majorana neutrino mass matrix through quantum correction.

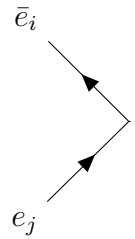
The relevant Feynman's rules for our calculation are derived below



$$\nu_i \quad e_j \quad \eta^+ (H^+) = -ic_\beta (-s_\beta) Y_{ij}^S \hat{L}, \quad (2.5)$$

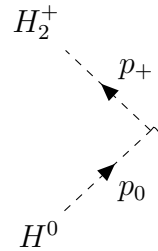


$$\bar{\nu}_i \quad e_j \quad H^+ (\eta^+) = -ic_\beta (s_\beta) Y_{ij}^{H_2} \hat{R}, \quad (2.6)$$



$$\bar{e}_i \quad e_j \quad H_0 = -i \left(Y_{ij}^{H_2} \hat{R} + Y_{ji}^{H_2*} \hat{L} \right). \quad (2.7)$$

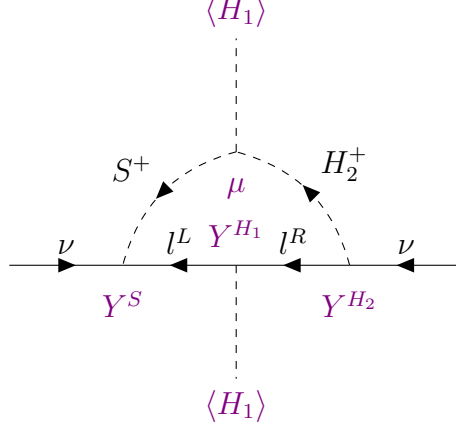
The one for the W^\pm coupling, will be employed in the next section, is derived from the kinematic term of doublet Higgs $|D_\mu H_2|^2$ reads



$$H_2^+ \quad p_+ \quad H^0 \quad p_0 \quad W^+ = -i \frac{g}{\sqrt{2}} (p_0 + p_+). \quad (2.8)$$

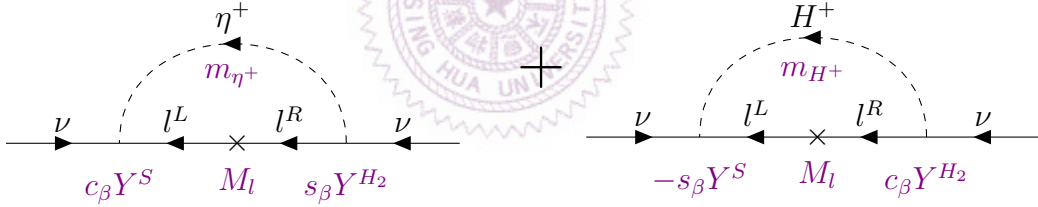
¹Henceforth, which also meant $H_2^0 \equiv H_N$.

The pivotal study in this chapter, the Zee model offers a non-trivial mechanism to generate a tiny radiative neutrino mass by quantum loop effects mediated by the newly heavy charged scalars. Particularly in one-loop order, we derived



$$M_\nu = \frac{\mu \langle H_1 \rangle}{16\pi^2} C_0(m_\nu^2, m_\nu^2, m_l^2, m_{\eta^+}^2, m_{H^+}^2) \left[Y^S (\langle H_1 \rangle Y^{H_1}) (Y^{H_2})^T + Y^{H_2} (\langle H_1 \rangle Y^{H_1}) (Y^S)^T \right], \quad (2.9)$$

alternatively, in the mass eigenbasis of charged scalar



$$M_\nu = \frac{s_\beta c_\beta}{8\pi^2} [B_0(m_\nu^2, m_l^2, m_{\eta^+}^2) - B_0(m_\nu^2, m_l^2, m_{H^+}^2)] \left[Y^S M_l (Y^{H_2})^T + Y^{H_2} M_l (Y^S)^T \right]. \quad (2.10)$$

where B_0 and C_0 are the N-point function in the Passarino-Veltman (PV) convention, see the definition and analytical expressions in [14, 15, 19]. In the limit $m_{H^+}, m_{\eta^+} \gg m_l (\in M_l) \gg m_\nu = 0$ (no tree level neutrino's mass), the results is boiled down to concise formula

$$M_\nu = \frac{s_\beta c_\beta}{8\pi^2} \log \left(\frac{m_{\eta^+}^2}{m_{H^+}^2} \right) \left[Y^S M_l (Y^{H_2})^T + Y^{H_2} M_l (Y^S)^T \right]. \quad (2.11)$$

According to the order estimation of mixing mass matrix, given the neutrino mass

$M_\nu \sim 1 \text{ eV}$, the order of Yukawa coupling is $|Y^{S,H_2}| \sim \frac{\mathcal{O}(10^{-2}-10^{-3})}{\sqrt{|c_\beta s_\beta|}}$ in the dominant heavier scalar, and $|Y^{S,H_2}| \sim \sqrt{\frac{m_{H^+}}{\epsilon}} \frac{\mathcal{O}(10^{-2}-10^{-3})}{\sqrt{|c_\beta s_\beta|}}$ in the nearly mass degeneracy case $\Delta m \equiv m_{H^+} - m_{\eta^+} = \epsilon$.

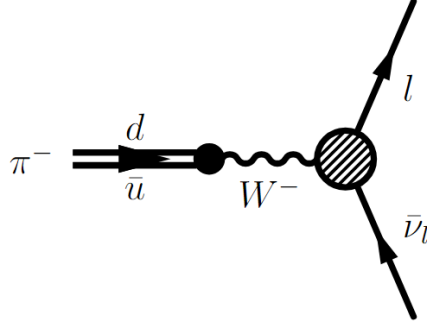


Chapter 3

Universality test in Pion decay

In SM, gauge interactions are uniform across all lepton flavors, adhering to lepton flavor universality (LFU). This universality is slightly broken only by the Higgs Yukawa couplings, which are very small, around 1% for the τ lepton. Thus, LFU is an approximate accidental symmetry of the SM at the Lagrangian level. LFU has been verified with extremely high accuracy in several systems: $Z \rightarrow ll$ decay [$\sim 0.1\%$], $K \rightarrow (\pi)l\nu$ decay [$\sim 0.1\%$], $\tau \rightarrow l\nu\nu$ decay [$\sim 0.1\%$], $\pi \rightarrow l\nu$ decay [$\sim 0.01\%$]. LFU violation (LFUV) refers to different interactions for electrons, muons, and taus leptons, distinguishable at the Lagrangian level. Notably, any modification to the $Wl\nu$ coupling would affect decay rate ratios, such as $R_{e/\mu}^\pi = \Gamma(\pi \rightarrow e\nu) / \Gamma(\pi \rightarrow \mu\nu)$. Precise measurements of the ratios $R_{e/\mu}^{\pi,K}$ and other decay channels are thus crucial for probing any SM extensions that cause nonuniversal corrections to $Wl\nu$ couplings, see review of recent works in LUV at ref. [13].

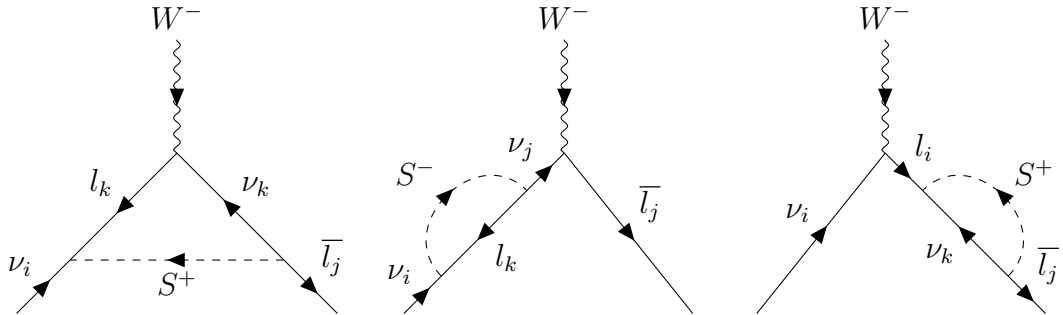
First one of the concerned issues that the Zee model is capable to address is the LFUV, particularly in the pion decay process $\pi \rightarrow l\nu$ decay in this study. On top of that, by briefly examining the potential effects of the model, we calculate the new contributions that modify the $Wl\nu$ boson coupling.



Experimental evidence, supported by theory and observed in the presence of helicity suppression ¹, has demonstrated the existence of a vector boson mediator and its dominant effect in pion decay, that is currently known as W^\pm boson. Henceforth, even though without the assumption of free-coupling to the quark sector of the second Higgs doublet, we are safe to ignore any tree-level interactions other than W^\pm boson. Only the first two terms in Eq. 2.1 contributes to the LFUV test at the one-loop level we must take into account

$$\begin{aligned}\mathcal{L}_{Yuk}^{Wl\nu} &\supset -Y_{\alpha\beta}^S \bar{L}_\alpha^c i\sigma_2 L_\beta S^+ - Y_{\alpha\beta}^{H_2} \bar{L}_\alpha H_2 l_\beta^R + h.c. \\ &= -Y_{\alpha\beta}^S (\bar{\nu}_\alpha^c l_\beta - \bar{l}_\alpha^c \nu_\beta) S^+ - Y_{\alpha\beta}^{H_2} \bar{\nu}_\alpha l_\beta^R H_2^+ - Y_{\alpha\beta}^{H_2} \bar{l}_\alpha l_\beta^R H_0 + h.c.,\end{aligned}\tag{3.1}$$

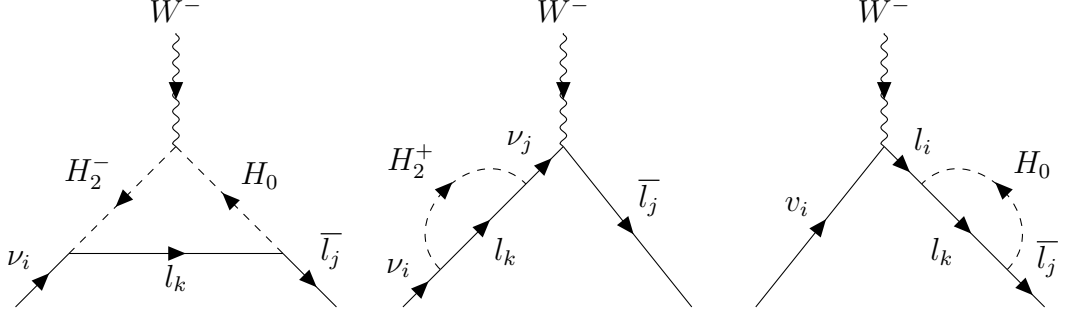
For simplicity, the neutrino and lepton masses are supposedly suppressed, except the lepton mass term presenting the helicity suppression effect. Additionally, instead of mass eigenstates, we will use the flavor state S^+, H_2^+, H_0 ² for this cursory calculation. The operations from the singlet are depicted below



¹The helicity suppression explains the dominant decay in muons (99.99%) rather than electron.

²Definition of $H_0 \equiv \frac{1}{\sqrt{2}} (H_2^0 + iA)$.

Whilst, the actions from the doublet are



Note that any contribution involving lepton mass is suppressed by tiny lepton mass presumption. These six one-loop diagrams represent four loop integrals below

$$\Gamma_W^\mu = \int \frac{d^4 q}{(2\pi)^4} \frac{(\psi_i - \not{q}) \gamma^\mu (\not{l}_j + \not{q})}{(q^2 - m_S^2) (l_j + q)^2 (\nu_i - q)^2}, \quad (3.2)$$

$$\Sigma_\nu^\alpha = \int \frac{d^4 q}{(2\pi)^4} \frac{\psi_i - \not{q}}{(q^2 - m_\alpha^2) (\nu_i - q)^2}, \quad (3.3)$$

$$\Sigma_l^\alpha = \int \frac{d^4 q}{(2\pi)^4} \frac{\not{l}_j + \not{q}}{(q^2 - m_\alpha^2) (l_j + q)^2}, \quad (3.4)$$

$$\Gamma_W^{H_2} = \int \frac{d^4 q}{(2\pi)^4} \frac{(\nu_i + l_j) \cdot (2q + \nu_i - l_j) \not{q}}{q^2 \left[(\nu_i + q)^2 - m_{H_2^+}^2 \right] \left[(l_j - q)^2 - m_{H_0}^2 \right]}. \quad (3.5)$$

The terms $\Gamma_W^{H_2^3}$ and Γ_W^μ denote the vertex corrections for doublets and singlets, respectively. Additionally, Σ_l^α and Σ_ν^α indicate the wavefunction corrections for leptons and neutrinos, where $\alpha \in \{S, H_2^+, H_0\}$. Leveraging the PV-function con-

³Indeed, this is not exact correction of the $Wl\nu$ vertex. For simplicity, we used a trick of redefinition $\Gamma_W^{H_2} \equiv (\nu_i + l_j)_\mu (\Gamma_W^{H_2})^\mu$ instead, with the aid of pion's four momentum $p_\mu^\pi \equiv (\nu_i + l_j)_\mu$ inserted on, then we will pull out p_μ^π in the amplitude expression below. The result, therefore, is still valid within pion decay context.

vention to put them into the form

$$\Gamma_W^\mu = 2\psi_i l_j^\mu C_{12} - 2l_j l_j^\mu (C_2 + C_{22}) + 2l_j \nu_i^\mu (C_0 + C_1 + C_2 + C_{12}) \quad (3.6)$$

$$- 2\psi_i \nu_i^\mu (C_1 + C_{11}) + \gamma^\mu \psi_i l_j (C_0 + C_1 + C_2) + \gamma^\mu (B_0^\pi + m_S^2 C_0 - 2C_{00}),$$

$$\Sigma_\nu^\alpha = \psi_i (B_0^\alpha + B_1^\alpha), \quad (3.7)$$

$$\Sigma_l^\alpha = l_j (B_0^\alpha + B_1^\alpha), \quad (3.8)$$

$$\Gamma_W^{H_2} = \psi_i (B_0^{H_2^+} + B_1^{H_2^+}) + l_j (B_0^{H_0} + B_1^{H_0}), \quad (3.9)$$

where the PV functions are broken down as

$$B_i^\alpha \equiv B_i^\alpha (0, m_\alpha^2, 0),$$

$$B_i^\pi \equiv B_i^\pi (m_\pi^2, 0, 0), \quad (3.10)$$

$$C_{ij\dots} \equiv C_{ij\dots} (0, 0, m_S^2, 0, 0, 0).$$

Then, the total amplitude for these diagrams are

$$M_{1-loop}^\mu = -i (Y_{ik}^S Y_{jk}^{S*} \epsilon_S + Y_{ik}^{H_2^*} Y_{jk}^{H_2} \epsilon_{H_2}) \overline{u_l} \gamma^\mu \hat{L} v_{\nu_i}, \quad (3.11)$$

with

$$\epsilon_S = \frac{1}{16\pi^2} [- (B_0^S + B_1^S) + B_0^\pi - 2C_{00} + m_S^2 C_0 \quad (3.12)$$

$$+ m_\pi^2 (2C_0 + 2C_1 + C_2 + C_{12} - C_{22})],$$

$$\epsilon_{H_2} = \frac{1}{16\pi^2} \left[\frac{1}{2} (B_0^{H_0} + B_1^{H_0}) - \frac{1}{2} (B_0^{H_2^+} + B_1^{H_2^+}) \right] \quad (3.13)$$

is the short-hand for one-loop contributions from singlet and doublet, respectively.

A useful and traditional way to ensure that no contributions are missed is by verifying the UV convergence of the outcome. The only PV functions that exhibit

UV divergence are

$$B_0 \supset \Lambda_{UV}, \quad B_1 \supset -\frac{\Lambda_{UV}}{2}, \quad C_{00} \supset -\frac{\Lambda_{UV}}{4}, \quad (3.14)$$

with Λ_{UV} is regularized UV-divergent value, from which M_{1-loop}^μ is checked the UV convergence on the fly. Consequently, the final result is wrapped up in the Fermi constant

$$\tilde{G}_F^{\pi \rightarrow ij} = G_F^{SM} (1 - Y_{ik}^S Y_{jk}^{S*} \epsilon_S - Y_{ik}^{H_2*} Y_{jk}^{H_2} \epsilon_{H_2}), \quad (3.15)$$

$$\left| \tilde{G}_F^{\pi \rightarrow ij} \right|^2 = (G_F^{SM})^2 (1 - 2 \text{Re} : Y_{ik}^S Y_{jk}^{S*} \epsilon_S + Y_{ik}^{H_2*} Y_{jk}^{H_2} \epsilon_{H_2} :) \quad (3.16)$$

The branching ratio in pion decay is therefore

$$\begin{aligned} \frac{Br(\pi \rightarrow e \nu_e)}{Br(\pi \rightarrow \mu \nu_\mu)} &= \frac{\Gamma(\pi \rightarrow e \nu_e)}{\Gamma(\pi \rightarrow \mu \nu_\mu)} = \frac{m_e^2 (m_\pi^2 - m_e^2)^2}{m_\mu^2 (m_\pi^2 - m_\mu^2)^2} \frac{\left| \tilde{G}_F^{\pi \rightarrow ee} \right|^2}{\left| \tilde{G}_F^{\pi \rightarrow \mu\mu} \right|^2} \\ &= \frac{m_e^2 (m_\pi^2 - m_e^2)^2}{m_\mu^2 (m_\pi^2 - m_\mu^2)^2} \frac{(1 - 2 |Y_{ek}^S|^2 \text{Re} : \epsilon_S : - 2 |Y_{ek}^{H_2}|^2 \text{Re} : \epsilon_{H_2} :)}{(1 - 2 |Y_{\mu k}^S|^2 \text{Re} : \epsilon_S : - 2 |Y_{\mu k}^{H_2}|^2 \text{Re} : \epsilon_{H_2} :)} \end{aligned} \quad (3.17)$$

and then, putting the experimental values

$$Br(\pi \rightarrow e \nu_e) = (1.23 \pm 0.004) \times 10^{-4}, \quad (3.18)$$

$$Br(\pi \rightarrow \mu \nu_\mu) = (99.9877 \pm 0.00004) \%,$$

turns Eq. 3.17 into in terms of the new parameter constraint

$$\begin{aligned} & \left(|Y_{e\tau}^S|^2 - |Y_{\mu\tau}^S|^2 \right) \text{Re} : \epsilon_S : + \left(|Y_{ek}^{H_2}|^2 - |Y_{\mu k}^{H_2}|^2 \right) \text{Re} : \epsilon_{H_2} : \\ & = 0.00116 \pm 0.00162 \approx \mathcal{O}(10^{-3}). \end{aligned} \quad (3.19)$$

The analytical expression of PV functions extracted from [14, 15] helps us derive

$$\epsilon_S = \frac{1}{16\pi^2} \left[4 + \frac{1}{3} (1 + 2x) \pi^2 + 4 \log(-x) + (1 + 2x) \log^2 x + (2 + 4x) \text{Li}_2(1 + x) \right], \quad (3.20)$$

$$\epsilon_{H_2} = \frac{1}{32\pi^2} \log \left(\frac{m_{H_2^+}}{m_{H_0}} \right), \quad (3.21)$$

with the variable being defined as $x = \frac{m_S^2}{m_\pi^2}$. In the mass range $m_S \in (100 - 1000)$ GeV and degeneracy of doublet $m_{H_2^+} \approx m_{H_0}$, whereby $\text{Re} : \epsilon_S : \in \mathcal{O}(10^{-8} - 10^{-5})$, otherwise, the $\epsilon_{H_2} \in \mathcal{O}(1)$ takes over in the case of $m_{H_2^+} \neq m_{H_0}$. The final constraint is fairly weak,

$$\left\{ \begin{array}{l} \left| |Y_{e\tau}^S|^2 - |Y_{\mu\tau}^S|^2 \right| < \mathcal{O}(10^2 - 10^5) \quad m_S \in (100 - 1000) \text{ and } m_{H_2^+} \approx m_{H_0}, \\ \left| |Y_{ek}^{H_2}|^2 - |Y_{\mu k}^{H_2}|^2 \right| < \mathcal{O}(10^{-3}) \quad m_{H_2^+} \neq m_{H_0} \end{array} \right., \quad (3.22)$$

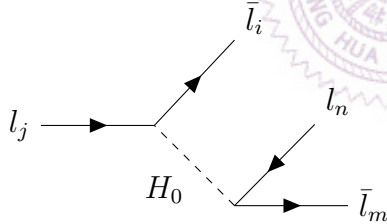
compared to the other constraints in this study below, henceforth being out of our interest and will not be counted toward this study's parameter scan constraints. The conclusion also tells us the Zee model staying safe within the universality test in pion decay.

Chapter 4

Trilepton decay $l_i \rightarrow l_j \bar{l}_m l_n$

constraint

The only contribution to LFV trilepton decay $l_i \rightarrow l_j \bar{l}_m l_n$ comes from the new neutral H_0 scalar, This allows us to explore all constraints on the Y^{H_2} coupling.



$$\rightarrow \Gamma(l_i \rightarrow l_j \bar{l}_m l_n) = \frac{m_i^5 \mathbf{Y}}{n! 3.2^9 \pi^3}. \quad (4.1)$$

The decay rate is derived in the approximation $m_j, m_n, m_m \ll m_i$, which we can ignore the final state masses, and the factor \mathbf{Y} holds in the information of Yukawa coupling of the second Higgs doublet

$$\begin{aligned} \mathbf{Y} = & \frac{1}{16m_{H_0}^4} \left(|2Y_{ji}^{H_2} Y_{nm}^{H_2*} - Y_{mi}^{H_2} Y_{nj}^{H_2*}|^2 + |2Y_{ij}^{H_2} Y_{mn}^{H_2*} - Y_{im}^{H_2} Y_{jn}^{H_2*}|^2 + 4|Y_{ji}^{H_2} Y_{mn}^{H_2}|^2 \right. \\ & \left. + 4|Y_{ij}^{H_2} Y_{nm}^{H_2}|^2 + 3|Y_{mi}^{H_2} Y_{nj}^{H_2}|^2 + 3|Y_{im}^{H_2} Y_{jn}^{H_2}|^2 + 4|Y_{mi}^{H_2} Y_{jn}^{H_2}|^2 + 4|Y_{im}^{H_2} Y_{nj}^{H_2}|^2 \right). \end{aligned} \quad (4.2)$$

Employing the branching ratio

$$Br(l_i \rightarrow l_j \bar{l}_m l_n) = \frac{\mathbf{Y}}{n! 128 G_F^2} Br(l_i \rightarrow l_j \bar{\nu}_m \nu_n), \quad (4.3)$$

where G_F^i is the Fermi constant determined in the lepton l_i decay rate process and $n!$ counts for undistinguished outgoing particles, we plugin the experiment data to set out the upper-bound constraint in table 4.1 below

Process	Exp. data	Coupling	Constraint $\left(\frac{m_{H_0}}{GeV}\right)^4$
$\mu^- \rightarrow e^- e^+ e^-$	$< 10^{-12}$	$ Y_{ee}^{H_2} ^2 (Y_{e\mu}^{H_2} ^2 + Y_{\mu e}^{H_2} ^2)$	$< 2.9 \times 10^{-21}$
$\tau^- \rightarrow e^- e^+ e^-$	$< 2.7 \times 10^{-8}$	$ Y_{ee}^{H_2} ^2 (Y_{e\tau}^{H_2} ^2 + Y_{\tau e}^{H_2} ^2)$	$< 4.47 \times 10^{-16}$
$\tau^- \rightarrow \mu^- \mu^+ \mu^-$	$< 2.1 \times 10^{-8}$	$ Y_{\mu\mu}^{H_2} ^2 (Y_{\tau\mu}^{H_2} ^2 + Y_{\mu\tau}^{H_2} ^2)$	$< 3.48 \times 10^{-16}$
$\tau^- \rightarrow e^- \mu^+ e^-$	$< 1.5 \times 10^{-8}$	$ Y_{\mu e}^{H_2} ^2 Y_{e\tau}^{H_2} ^2 + 2 Y_{e\mu}^{H_2} ^2 Y_{e\tau}^{H_2} ^2$ $+ Y_{e\mu}^{H_2} ^2 Y_{\tau e}^{H_2} ^2 + 2 Y_{\mu e}^{H_2} ^2 Y_{\tau e}^{H_2} ^2$	$< 7.45 \times 10^{-16}$
$\tau^- \rightarrow \mu^- e^+ \mu^-$	$< 1.7 \times 10^{-8}$	$ Y_{e\mu}^{H_2} ^2 Y_{\mu\tau}^{H_2} ^2 + 2 Y_{e\mu}^{H_2} ^2 Y_{\tau\mu}^{H_2} ^2$ $+ Y_{\mu e}^{H_2} ^2 Y_{\tau\mu}^{H_2} ^2 + 2 Y_{\mu e}^{H_2} ^2 Y_{\mu\tau}^{H_2} ^2$	$< 8.45 \times 10^{-16}$
$\tau^- \rightarrow \mu^- \mu^+ e^-$	$< 2.7 \times 10^{-8}$	$ 2Y_{\mu\tau}^{H_2} Y_{\mu e}^{H_2*} - Y_{e\tau}^{H_2} Y_{\mu\mu}^{H_2*} + 4 Y_{\mu\tau}^{H_2} ^2 Y_{e\mu}^{H_2} ^2$ $+ 2Y_{\tau\mu}^{H_2*} Y_{e\mu}^{H_2} - Y_{\tau e}^{H_2*} Y_{\mu\mu}^{H_2} + 4 Y_{\tau\mu}^{H_2} ^2 Y_{\mu e}^{H_2} ^2$ $+ 7 Y_{e\tau}^{H_2} ^2 Y_{\mu\mu}^{H_2} ^2 + 7 Y_{\tau e}^{H_2} ^2 Y_{\mu\mu}^{H_2} ^2$	$< 2.69 \times 10^{-15}$
$\tau^- \rightarrow e^+ \mu^- e^-$	$< 1.8 \times 10^{-8}$	$ 2Y_{e\tau}^{H_2} Y_{e\mu}^{H_2*} - Y_{\mu\tau}^{H_2} Y_{ee}^{H_2*} + 4 Y_{e\tau}^{H_2} ^2 Y_{\mu e}^{H_2} ^2$ $+ 2Y_{\tau e}^{H_2*} Y_{\mu e}^{H_2} - Y_{\tau\mu}^{H_2*} Y_{ee}^{H_2} + 4 Y_{\tau e}^{H_2} ^2 Y_{e\mu}^{H_2} ^2$ $+ 7 Y_{\mu\tau}^{H_2} ^2 Y_{ee}^{H_2} ^2 + 7 Y_{\tau\mu}^{H_2} ^2 Y_{ee}^{H_2} ^2$	$< 1.79 \times 10^{-15}$

Table 4.1: Trilepton $l_i \rightarrow l_j \bar{l}_m l_n$ decay constraints table

The table 4.1 can be cast into simpler expressions using the basic inequality

Process	Exp. data	Coupling	Constraint $(\frac{m_{H_0}}{GeV})^4$
$\mu^- \rightarrow e^- e^+ e^-$	$< 10^{-12}$	$ Y_{ee}^{H_2} ^2 Y_{e\mu}^{H_2} Y_{\mu e}^{H_2} $	$< 1.45 \times 10^{-21}$
$\tau^- \rightarrow e^- e^+ e^-$	$< 2.7 \times 10^{-8}$	$ Y_{ee}^{H_2} ^2 Y_{e\tau}^{H_2} Y_{\tau e}^{H_2} $	$< 2.24 \times 10^{-16}$
$\tau^- \rightarrow \mu^- \mu^+ \mu^-$	$< 2.1 \times 10^{-8}$	$ Y_{\mu\mu}^{H_2} ^2 Y_{\tau\mu}^{H_2} Y_{\mu\tau}^{H_2} $	$< 1.74 \times 10^{-16}$
$\tau^- \rightarrow e^- \mu^+ e^-$	$< 1.5 \times 10^{-8}$	$ Y_{\mu e}^{H_2} Y_{e\tau}^{H_2} Y_{e\mu}^{H_2} Y_{e\tau}^{H_2} $	$< 1.32 \times 10^{-16}$
$\tau^- \rightarrow \mu^- e^+ \mu^-$	$< 1.7 \times 10^{-8}$	$ Y_{e\mu}^{H_2} Y_{\mu\tau}^{H_2} Y_{e\mu}^{H_2} Y_{\tau\mu}^{H_2} $	$< 1.49 \times 10^{-16}$
$\tau^- \rightarrow \mu^- \mu^+ e^-$	$< 2.7 \times 10^{-8}$	$\frac{ Y_{\mu e}^{H_2} Y_{e\mu}^{H_2} Y_{\tau e}^{H_2} Y_{e\tau}^{H_2} + Y_{\mu\mu}^{H_2} ^2 Y_{\tau e}^{H_2} Y_{e\tau}^{H_2} }{-\frac{1}{8} Y_{\mu\mu}^{H_2} (Y_{\mu\tau}^{H_2} Y_{\mu e}^{H_2} Y_{e\tau}^{H_2} + Y_{\tau\mu}^{H_2} Y_{e\mu}^{H_2} Y_{\tau e}^{H_2})}$	$< 1.68 \times 10^{-16}$
$\tau^- \rightarrow e^+ \mu^- e^-$	$< 1.8 \times 10^{-8}$	$\frac{ Y_{\mu e}^{H_2} Y_{e\mu}^{H_2} Y_{\tau e}^{H_2} Y_{e\tau}^{H_2} + Y_{ee}^{H_2} ^2 Y_{\tau\mu}^{H_2} Y_{\mu\tau}^{H_2} }{-\frac{1}{8} Y_{ee}^{H_2} (Y_{\mu\tau}^{H_2} Y_{e\mu}^{H_2} Y_{e\tau}^{H_2} + Y_{\tau\mu}^{H_2} Y_{\mu e}^{H_2} Y_{\tau e}^{H_2})}$	$< 1.11 \times 10^{-16}$

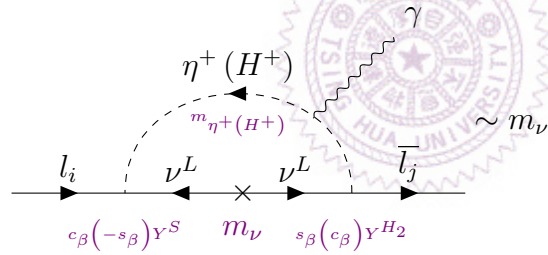
Table 4.2: Simple expression of Trilepton $l_i \rightarrow l_j \bar{l}_m l_n$ decay constraints

$a^2 + b^2 \geq 2ab$, which is shown in table 4.2. The well-known values of the lepton decay branching ratios $Br(\mu \rightarrow e \bar{\nu}_e \nu_\mu) \approx 100\%$ and $Br(\tau \rightarrow l \bar{\nu}_l \nu_\tau) \approx 17.5\%$ are used here. These constraints roughly tell us the upper bound of the new doublet Higg coupling $|Y^{H_2}| < \mathcal{O}(10^{-4}) \frac{m_{H_0}}{GeV}$.

Chapter 5

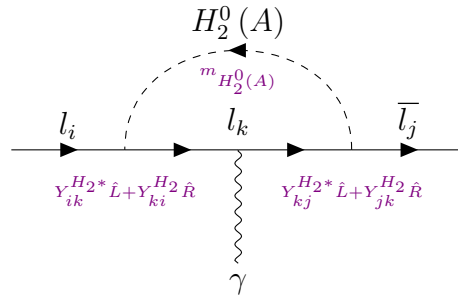
Lep-to-lep-gamma $L \rightarrow l\gamma$

Another of the LFV decays we should count in is the lep-to-lep-gamma channel. The tiny neutrino mass insertion suppresses the mixing doublet-singlet coupling term, thereby negligible

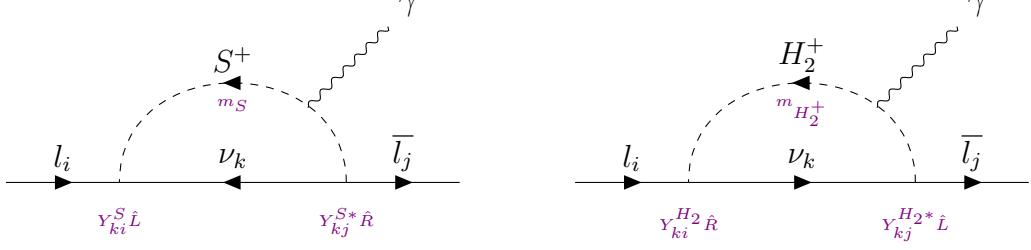


$$\sim m_\nu \frac{c_\beta s_\beta}{m_{\eta^+(H^+)}^2} Y^S Y^{H_2} \simeq 0. \quad (5.1)$$

While the main effect comes from the new neutral scalar H_0



and these two sub-contributions from charged scalars



As per Eq. E.18, to extract the branching ratio, dipole terms are only needed and read off following the general formula in Eq. E.21¹, putting down properly in

$$F_2^{H_2^+(S^+)} = \frac{-e}{3.2^7 \pi^2} \frac{m_i + m_j}{m_{H_2^+(S)}^2} Y_{ki}^{H_2(S)} Y_{kj}^{H_2(S)*}, \quad (5.2)$$

$$G_2^{H_2^+(S^+)} = \frac{e}{3.2^7 \pi^2} \frac{m_i - m_j}{m_{H_2^+(S)}^2} Y_{ki}^{H_2(S)} Y_{kj}^{H_2(S)*}, \quad (5.3)$$

for charged scalar impacts, and in effect of neutral ones otherwise

$$F_2^{H_2^0(A)} = \frac{e}{3.2^7 \pi^2} \frac{m_i + m_j}{m_{H_2^0(A)}^2} \left[(Y_{ki}^{H_2} Y_{kj}^{H_2*} + Y_{jk}^{H_2} Y_{ik}^{H_2*}) \right. \\ \left. \mp \frac{3m_k}{m_i + m_j} \left(3 + 4 \log \frac{m_k}{m_{H_2^0(A)}} \right) (Y_{ki}^{H_2} Y_{jk}^{H_2} + Y_{ik}^{H_2*} Y_{kj}^{H_2*}) \right], \quad (5.4)$$

$$G_2^{H_2^0(A)} = \frac{e}{3.2^7 \pi^2} \frac{m_i - m_j}{m_{H_2^0(A)}^2} \left[(Y_{ki}^{H_2} Y_{kj}^{H_2*} - Y_{jk}^{H_2} Y_{ik}^{H_2*}) \right. \\ \left. \pm \frac{3m_k}{m_i - m_j} \left(3 + 4 \log \frac{m_k}{m_{H_2^0(A)}} \right) (Y_{ki}^{H_2} Y_{jk}^{H_2} - Y_{ik}^{H_2*} Y_{kj}^{H_2*}) \right]. \quad (5.5)$$

The (\mp) sign difference in the neutral one case is induced by the CP property distinction of scalar H_2^0 and pseudo scalar A , whilst $m_S, m_{H_2^+}$ are the convention masses respective to charged singlet and doublet. The second part in Eq. (5.4-5.5) representing the chiral enhancement is canceled out in the neutral scalars degenerated case. The flavor states S^+, H_2^+ adopted are possibly converted to the

¹Recall that we initially assumed in the case of the much heavier new scalar mediators than leptons

mass eigenstates, by substituting

$$\frac{1}{m_S^2} \rightarrow \frac{c_\beta^2}{m_{\eta^+}^2} + \frac{s_\beta^2}{m_{H^+}^2}, \quad (5.6)$$

$$\frac{1}{m_{H_2^+}^2} \rightarrow \frac{s_\beta^2}{m_{\eta^+}^2} + \frac{c_\beta^2}{m_{H^+}^2} \quad (5.7)$$

to get the physical result after mass diagonalization. From the experiment value

$$Br(\mu \rightarrow e\gamma) : 5.7 \times 10^{-13}, \quad Br(\tau \rightarrow e\gamma) : 3.3 \times 10^{-8}, \quad Br(\tau \rightarrow \mu\gamma) : 4.4 \times 10^{-8},$$

and the branching ratio is theoretically evaluated by following through

$$Br(l_i \rightarrow l_j \gamma) = \frac{24\pi^2}{m_i^2 G_F^2} (|F_2|^2 + |G_2|^2) Br(l_i \rightarrow l_j \nu \bar{\nu}), \quad (5.8)$$

we are able to give a ballpark estimate of $\frac{|Y^{S,H_2}|^2}{m_{S,H_2}^2} < \mathcal{O}(10^{-6} - 10^{-7}) \text{ GeV}^{-2}$ ². From Eq. (5.4,5.5), given the mass of neutral scalars is much heavier than charged scalars, the constraint likely suppresses the LFV trilepton decays constraints, see in table 4.1, on account of the dominant contribution of charged scalars. On the other hand, in the more massive charged scalars scenario, the neutral one takes over the space and waive off constraints from singlet coupling Y^S . The only constraint of Y^S comes from the Michel parameters, let them room to cook up. Moreover, in this case, the constraint from $L \rightarrow l\gamma$ is possibly suppressed by the trilepton decays in Tab. 4.1. The table 5.1 refers to the degeneracy of neutral scalar as

²The notation m_{S,H_2}^2 stands for a set of $\{m_{\eta^+}^2, m_{H^+}^2, m_{H_2^0}^2, m_A^2\}$

Process	Exp. data	Coupling	Constraint
$\mu^- \rightarrow e^- \gamma$	$< 5.7 \times 10^{-13}$	$\frac{ Y_{\mu e}^{G_2} ^4}{m_{S,H_2}^4} + \frac{ Y_{\mu e}^{F_2} ^4}{m_{S,H_2}^4}$	$< 2.93 \times 10^{-16}$
$\tau^- \rightarrow e^- \gamma$	$< 3.3 \times 10^{-8}$	$\frac{ Y_{\tau e}^{G_2} ^4}{m_{S,H_2}^4} + \frac{ Y_{\tau e}^{F_2} ^4}{m_{S,H_2}^4}$	$< 1.70 \times 10^{-11}$
$\tau^- \rightarrow \mu^- \gamma$	$< 4.4 \times 10^{-8}$	$\frac{ Y_{\tau \mu}^{G_2} ^4}{m_{S,H_2}^4} + \frac{ Y_{\tau \mu}^{F_2} ^4}{m_{S,H_2}^4}$	$< 2.26 \times 10^{-11}$

Table 5.1: $L \rightarrow l\gamma$ constraints table

$m_{H_2^0} \approx m_A \equiv m_{H_0}$, and the coupling combinations are defined as follows:

$$\frac{|Y_{ij}^{F_2}|^2}{m_{S,H_2}^2} = \left[2 \frac{(Y_{ki}^{H_2} Y_{kj}^{H_2*} + Y_{jk}^{H_2} Y_{ik}^{H_2*})}{m_{H_0}^2} - \sum_{\alpha=S,H_2^+} \frac{Y_{ki}^\alpha Y_{kj}^{\alpha*}}{m_\alpha^2} \right], \quad (5.9)$$

$$\frac{|Y_{ij}^{G_2}|^2}{m_{S,H_2}^2} = \left[2 \frac{(Y_{ki}^{H_2} Y_{kj}^{H_2*} - Y_{jk}^{H_2} Y_{ik}^{H_2*})}{m_{H_0}^2} + \sum_{\alpha=S,H_2^+} \frac{Y_{ki}^\alpha Y_{kj}^{\alpha*}}{m_\alpha^2} \right]. \quad (5.10)$$

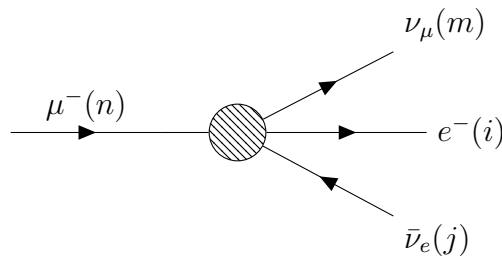


Chapter 6

Muon decay

Muon decay was measured at TRIUMF and PSI in the '80s with polarized muons from π decays that represent a cornerstone in the study of weak interactions, serving as a prototypical system for theoretical predictions and experimental validations in particle physics. The decay of polarized muons, in particular, offers a rich landscape for probing the underlying symmetries and mechanisms governing leptonic interactions.

6.1 Michel parameters



The point-like interaction in muon decay is governed by the 4-Fermi theory that is matched to the Zee model's couplings by effective low-energy treatment and the Fierz transformation. In this way, we study Michel parameters from the muon decay process to make constraints on the new couplings. The differential

decay rate of the muon is in the form:

$$d\Gamma = \frac{m_\mu^5}{3 * 2^9 * \pi^4} * (a + 4b + 6c) \left\{ 3(1 - x) + 2\rho \left(\frac{4}{3}x - 1 \right) - \xi \cos \theta \left[(1 - x) + 2\delta \left(\frac{4}{3} - 1 \right) \right] \right\} x^2 dx, \quad (6.1)$$

where ρ, ξ, δ are Michel parameters [1] measured from experiment, which are defined

$$\rho = \frac{3b + 6c}{a + 4b + 6c} = 0.74979 \pm 0.00026, \quad (6.2)$$

$$\delta = \frac{3b' - 6c'}{-3a' + 4b' - 14c'} = 0.75047 \pm 0.00034, \quad (6.3)$$

$$|\xi| = \left| \frac{3a' - 4b' + 14c'}{a + 4b + 6c} \right| = 1.0009_{-0.0007}^{+0.0016}. \quad (6.4)$$

The functions $a(a'), b(b'), c(c')$ are in terms of coupling parameters Y^{S,H_2} [2] that we are going to constrain. Herein, we assumed the zero mass of outgoing particles, that caused suppression of the Michel parameter associated to the electron mass η [16]. In Eq. 6.1, the lepton-number nonconservation is not possible to detect in muon decay, and these two parameters δ, ξ merely contribute to emitted electron distribution angle. The full treatment of the massive final state's phase space, which is useful for studying the effect of Dirac and Majorana neutrino mass in Michel parameters, is performed calculations in Appendix 7.

The symmetry and anti-symmetry between left-right couplings are encoded in ρ and δ , non-prime and prime parameters in the other words, respectively. Consequently, if a model has only one chirality gets in that will turn out the same behavior with SM, say, the predicted value $\rho = \delta = \frac{3}{4}$ same as Standard Model, and then constrain $|\xi| \leq 1$. The relative left-right difference effect is ascribed to ξ , which gives rise to changes in the angle of electron distribution. And if the true experiment turns out $|\xi| > 1$, it is definitely a hint of new physics involving

both left-right interactions in the new charged vector boson or the lepton number violation interaction in the Yukawa sector in the context of Zee model.

6.2 Fermi constant

Integrating Eq. 6.1 over outgoing electron energy, the Muon decay rate is obtained

$$\Gamma = \frac{m_\mu^5}{3 * 2^9 * \pi^3} (a + 4b + 6c) = \frac{m_\mu^5 (G_F^\mu)^2}{192\pi^3}, \quad (6.5)$$

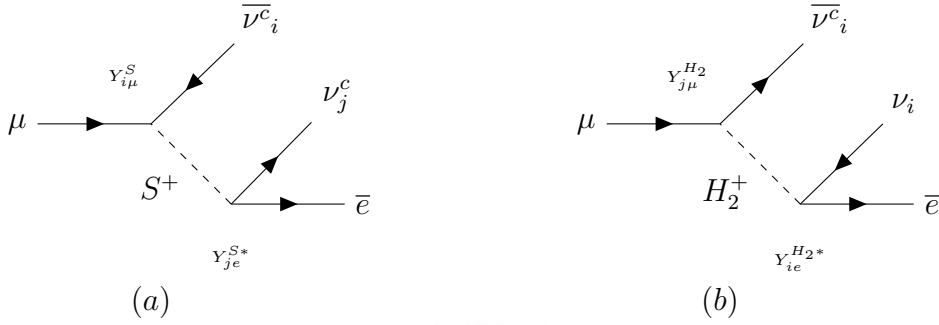
we then are able to extract the Fermi constant in terms of new coupling constants

$$(a + 4b + 6c) = 8 (G_F^\mu)^2. \quad (6.6)$$

Because the lifetime of the muon is well-measured, which is thus, by far, the best determination of the Fermi constant $G_F^\mu = 1.1663787(6) \times 10^{-5} \text{ GeV}^{-2}$, and in fact, it is more than 100 times better than the other independent determination methods. In the new model scenario, the new physics positively contributes to the Fermi constant, which makes the value larger than the SM contribution. Since the new charged mediators are in consideration, thus, an independent determination of the Fermi constant from the neutral current, which is in this report extracted from Z boson decay $G_F^Z = 1.1668(11) \times 10^{-5} \text{ GeV}^{-2}$, can help to bound the allowable region of new coupling magnitudes. Furthermore, the tension between independent determinations of G_F , such as electroweak fits, μ -decay, and CKM unitarity are potentially resorted to setting a stringent NP constraint via the Standard Model EFT (SMEFT) approach [17].

6.3 Zee model constraints in Muon decay

In the compass of this study, besides the lep-to-lep-gamma process, the additional come-up of the singlet scalar strikes up in muon decay, which gets contributions of doublet charged Higgs either. The Feynman diagrams scale up from 2 to 8 after mass diagonalization, inducing the singlet-doublet mixing terms. The first two contributions are from singlet and doublet, respectively



Before SSB, the two Michel parameters $\rho = \delta = \frac{3}{4}$ remain unchanged from their Standard Model predictions despite the presence of the unmixed effects from singlet and doublet charged scalar above get into. This is because of only one chirality involved. In contrast, the parameter ξ can reflect new physics effects through the parameters b and b' parameters, as defined in Eq (D.7-D.8)

$$b(b') = \left(\sqrt{2}G_F^{SM} + \frac{|Y_{e\mu}^S|^2}{4m_S^2} \right)^2 + \frac{1}{16m_S^4} \sum_{i,j \neq \{e,\mu\}} |Y_{i\mu}^S|^2 |Y_{je}^S|^2 + (-) \frac{1}{16m_{H_2^+}^4} \sum_{i,j} |Y_{i\mu}^{H_2}|^2 |Y_{je}^{H_2}|^2. \quad (6.7)$$

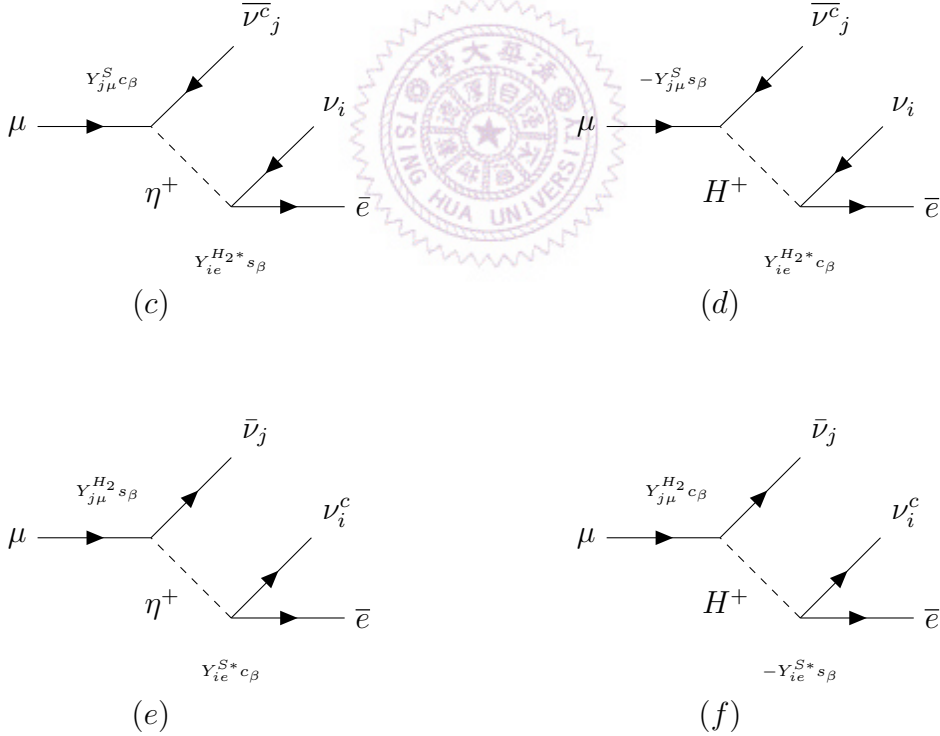
Notably, as mentioned in Appendix D, because of the spin-flip difference, the scalar-form coupling from the doublet and vector-form coupling from the singlet, as described in Eq. 6.8 after Fierz transformation, has no intertwine. The aforementioned intrinsic difference in chirality between scalar and vector-form couplings brought up the sign change of b relative to b' . In contrast, the first diagram with Lepton Number Violation (LNV) Yukawa couplings Y^S puts on the vector-like

form after Fierz transformation, for instance

$$\begin{aligned}
\overline{\nu}_e^c \hat{L}_\mu \bar{e} \hat{R} \nu_\mu^c &\xrightarrow[\text{Transform}]{\text{Fierz}} -\frac{1}{4} [\bar{\nu}_\mu \gamma^\mu \nu_e \bar{e}_L \gamma_\mu \mu_L + \bar{\nu}_\mu \gamma^\mu \gamma_5 \nu_e \bar{e}_L \gamma_\mu \gamma_5 \mu_L] \\
&\xrightarrow[\text{Transform}]{\text{Fierz}} \frac{1}{2} \bar{e} \gamma^\mu \hat{L} \nu_e \bar{\nu}_\mu \gamma_\mu \hat{L} \mu,
\end{aligned} \tag{6.8}$$

therefore exhibiting a constructive interference with W boson, shown in the first term of Eq. 6.7. The interference effect thereof just only shows up in Fermi constant constraint, where we will pick up that later.

However, after SSB, the next four diagrams appearing present the mixing properties between normal Y^{H_2} and LNV Y^S Yukawa couplings that open the possibility of detecting new physics in Michel parameters



These two distinct processes display the lepton number violation $\Delta L = -2$ for the first two diagrams and $\Delta L = 2$ for the latter two. The interference effect between singlet and doublet scalar gives rise to non-trivial contribution to decay parameters, which interestingly displays pseudo-left-right mixing effect through

the combination of coupling parameters, see Eq. (D.6-D.10) for more definition details

$$a_{-2} = a'_{-2} = \left(\frac{1}{m_{\eta^+}^2} - \frac{1}{m_{H^+}^2} \right)^2 \frac{c_\beta^2 s_\beta^2}{16} |Y_{j\mu}^S Y_{ie}^{H_2^*} - Y_{i\mu}^S Y_{je}^{H_2^*}|^2, \quad (6.9)$$

$$c_{-2} = -c'_{-2} = \left(\frac{1}{m_{\eta^+}^2} - \frac{1}{m_{H^+}^2} \right)^2 \frac{c_\beta^2 s_\beta^2}{16} |Y_{j\mu}^S Y_{ie}^{H_2^*} + Y_{i\mu}^S Y_{je}^{H_2^*}|^2, \quad (6.10)$$

and

$$a_2 = -a'_2 = \left(\frac{1}{m_{\eta^+}^2} - \frac{1}{m_{H^+}^2} \right)^2 \frac{c_\beta^2 s_\beta^2}{16} |Y_{j\mu}^{H_2} Y_{ie}^{S*} - Y_{i\mu}^{H_2} Y_{je}^{S*}|^2, \quad (6.11)$$

$$c_2 = c'_2 = \left(\frac{1}{m_{\eta^+}^2} - \frac{1}{m_{H^+}^2} \right)^2 \frac{c_\beta^2 s_\beta^2}{16} |Y_{j\mu}^{H_2} Y_{ie}^{S*} + Y_{i\mu}^{H_2} Y_{je}^{S*}|^2, \quad (6.12)$$

corresponding to $\Delta L = -2$, $\Delta L = 2$ respectively, which has no effect on b , b' at all. Consequently, the total contribution to parameters $a(a') = a(a')_2 + a(a')_{-2}$ and $c(c') = c(c')_2 + c(c')_{-2}$ alters the two Michel parameters ρ , δ from their SM values

$$\begin{aligned} \Delta\rho &= \frac{3}{16} \left(\frac{1}{m_{\eta^+}^2} - \frac{1}{m_{H^+}^2} \right)^2 \frac{c_\beta^2 s_\beta^2}{a + 4b + 6c} \text{Re} (Y_{j\mu}^{H_2} Y_{ie}^{S*} Y_{i\mu}^{H_2^*} Y_{je}^S + Y_{j\mu}^S Y_{ie}^{H_2^*} Y_{i\mu}^{S*} Y_{je}^{H_2}) \\ &= (-47 - 5) \times 10^{-5}, \end{aligned} \quad (6.13)$$

$$\begin{aligned} \Delta\delta &= \frac{21}{16} \left(\frac{1}{m_{\eta^+}^2} - \frac{1}{m_{H^+}^2} \right)^2 \frac{c_\beta^2 s_\beta^2}{-3a' + 4b' - 14c'} \text{Re} (Y_{j\mu}^{H_2} Y_{ie}^{S*} Y_{i\mu}^{H_2^*} Y_{je}^S - Y_{j\mu}^S Y_{ie}^{H_2^*} Y_{i\mu}^{S*} Y_{je}^{H_2}) \\ &= (1.3 - 8.1) \times 10^{-4}. \end{aligned} \quad (6.14)$$

Finally, all NP effects from four diagrams in muon decay add up in ξ constraint

$$\begin{aligned}
\Delta\xi &= \frac{1}{2} \left(\frac{1}{m_{\eta^+}^2} - \frac{1}{m_{H^+}^2} \right)^2 \frac{c_\beta^2 s_\beta^2}{a + 4b + 6c} \text{Re} \left(Y_{j\mu}^S Y_{ie}^{H_2*} Y_{i\mu}^{S*} Y_{je}^{H_2} - \frac{3}{2} Y_{j\mu}^{H_2} Y_{ie}^{S*} Y_{i\mu}^{H_2*} Y_{je}^S \right) \\
&- \frac{1}{2} \left(\frac{1}{m_{\eta^+}^2} - \frac{1}{m_{H^+}^2} \right)^2 \frac{c_\beta^2 s_\beta^2}{a + 4b + 6c} \left(|Y_{j\mu}^{H_2}|^2 |Y_{ie}^S|^2 + |Y_{i\mu}^{H_2}|^2 |Y_{je}^S|^2 \right) - \frac{1}{8m_{H_2^+}^4} \sum_{i,j} \frac{|Y_{i\mu}^{H_2}|^2 |Y_{je}^{H_2}|^2}{a + 4b + 6c} \\
&= (2 - 25) \times 10^{-4},
\end{aligned} \tag{6.15}$$

and Fermi constant. As mentioned earlier, the Fermi constant is often deemed as an anomaly source of new physics contribution, in which the Zee model contributions play the new physics role, and as in the extended usage in Appendix F, Z boson decay is benchmarked for Standard Model contribution $G_F^{SM} \equiv G_F^Z$ compared to Fermi constant G_F^μ precisely measured in muon decay Eq. 6.6

$$\begin{aligned}
\Delta G_F^2 &= (G_F^\mu)^2 - (G_F^{SM})^2 = \frac{a + 4b + 6c}{8} - (G_F^{SM})^2 \\
&= \frac{G_F^{SM}}{2\sqrt{2}m_S^2} |Y_{e\mu}^S|^2 + \frac{1}{32m_S^4} \sum_{i,j} |Y_{i\mu}^S|^2 |Y_{je}^S|^2 \\
&\quad + \frac{1}{32m_{H_2^+}^4} \sum_{i,j} |Y_{i\mu}^{H_2}|^2 |Y_{je}^{H_2}|^2 + \frac{a + 6c}{8} \\
&= (-1.6 - 3.6) \times 10^{-13}.
\end{aligned} \tag{6.16}$$

The first three terms are caused by purely singlet or doublet effects Eq. 6.7, while the last term comes from singlet-doublet mixing effect Eq. (6.9-6.12). The likewise analytic calculation is performed for tau lepton decay, and the results are obtained by substituting the mother particle $\mu \rightarrow \tau$ and the child particles $\mu \rightarrow \{e, \mu\}$. Where the decay parameter's experiment values in 1σ

$$\begin{aligned}
\rho_e &= 0.747 \pm 0.010 & \rho_\mu &= 0.763 \pm 0.020, \\
\delta_e &= 0.734 \pm 0.028 & \delta_\mu &= 0.778 \pm 0.037, \\
\xi_e &= 0.994 \pm 0.040 & \xi_\mu &= 1.030 \pm 0.059
\end{aligned} \tag{6.17}$$

are not strictly precise to muon decay parameters, and henceforth are out of our interest.

Roughly speaking, from the above expression of Fermi constant constraint, where $\Delta G_F^2 < \mathcal{O}(10^{-13}) \text{ GeV}^{-2}$ and on the assumption $m_{H^+} \gg m_{\eta^+}$, the coupling strength $\frac{|Y^{S,H_2}|^2}{m_{\eta^+}^2} < \mathcal{O}(10^{-5}) \text{ GeV}^{-2}$ cannot be too large. Along with Eq. 6.14 of the Michel parameter δ , offhandedly $\frac{|Y^{S,H_2}|^2}{m_{\eta^+}^2} > \frac{\mathcal{O}(10^{-7})}{|c_\beta s_\beta|} \text{ GeV}^{-2}$ evaluated, where $a + 4b + 6c \sim -3a' + 4b' - 14c' \sim G_F^2 \sim \mathcal{O}(10^{-10}) \text{ GeV}^{-2}$ and $c_\beta s_\beta = \frac{\mu < H_1 >}{m_{\eta^+}^2 - m_{H^+}^2}$. Therefore, the scalar mixing angle $s_{2\beta} \approx \beta > \mathcal{O}(10^{-2})$, in the other words, the cubic coupling μ in Eq. 2.2 is forbidden to be arbitrarily small, and the lower bound first-step estimation is inferred

$$\mu > m_{H^+}^2 \times \mathcal{O}(10^{-4}) \text{ GeV}, \quad (6.18)$$

in particular case of the much heavier one in $\mathcal{O}(1) \text{ TeV}$ scale mass range induces $\mu > \mathcal{O}(10^2) \text{ GeV}$.

1σ Michel parameters constraints, in Eq. (6.14,6.15), thus impose a larger scale, at least one order of magnitude, compared to the bound of neutrino oscillation and LFV decay constraints as described by Eq. 2.11 and Chap. (4,5). The very light scalar (about $m_{\eta^+} < \mathcal{O}(100) \text{ MeV}$) is an easy-to-see global fitting solution that reconciles all the constraints considered so far. Nevertheless, the light charged scalar will couple to the photon, consequently being able to seek out in many experiment channels and ruled out very well, at least below $\mathcal{O}(10) \text{ GeV}$. Otherwise, there is no way out since Michel parameters offer a very strong constraint, e.g. $|Y^{S,H_2}|^2 \sim (10^{-2} - 10^{-1})$ for $m_{S,H_2} = 100 \text{ GeV}$, eliminating all feasible parameter space within 1σ uncertainty of the experiment (based on hand-waving estimation and roughly numerical study). This conclusion is a novelty of the study.

Chapter 7

Conclusion and outlook

The order of magnitude of our constraints are roughly summarized in the following:

Exp.	Coupling form	Order of magnitude
Michel Parameters at 1σ	$\frac{ Y^{S,H_2} ^2}{m_{S,H_2^+}^2}$	$\sim (10^{-6} - 10^{-5}) \text{ GeV}^{-2}$
Michel Parameters at 2σ	$\frac{ Y^{S,H_2} ^2}{m_{S,H_2^+}^2}$	$< (10^{-6} - 10^{-5}) \text{ GeV}^{-2}$
G_F	$\frac{ Y^{S,H_2} ^2}{m_{S,H_2^+}^2}$	$< (10^{-6} - 10^{-5}) \text{ GeV}^{-2}$
Neutrino mass	$ Y^{S,H_2} ^2$	$\sim (10^{-6} - 10^{-4})$
$l_i \rightarrow l_j \bar{l}_m l_n$	$\frac{ Y^{H_2} ^2}{m_{H_0}^2}$	$< (10^{-9} - 10^{-8}) \text{ GeV}^{-2}$
$L \rightarrow l\gamma$	$\frac{ Y^{S,H_2} ^2}{m_{S,H_2}^2}$	$< (10^{-7} - 10^{-6}) \text{ GeV}^{-2}$

Table 7.1: Order of magnitude of roughly constraints

The constraint from the Michel parameters in the first two lines in Tab. 7.1 are

different. Note that the 1σ value, Eq. 6.4, indicates NP beyond SM, while the 2σ only leads to an upper bound. If we take the 1σ constant of Michel parameters seriously, then it will give us a nontrivial constraint. For instance, if taking $m_{S,H_2^+} = 100$ GeV, which is very close to the current experiment limit [18], then we need roughly $|Y^{S,H_2}|^2 \sim (10^{-2} - 10^{-1})$ to accommodate the NP, and that will conflict with the ν oscillation data and the LFV limits, which require $|Y^{S,H_2}|^2 \sim (10^{-6} - 10^{-4})$ and $|Y^{S,H_2}|^2 < (10^{-5} - 10^{-4})$ for $m_{H_0} = 100$ GeV, respectively. And the Zee model could be ruled out.

However, if using the 2σ allowed range for the Michel parameters, there is plenty of room left for the Zee model. And the LFV still play the dominant role over the Michel parameter. However, note that, the constraints from LFV decays is confined in the doublet coupling sector. To constrain the singlet couplings, one must consider the neutrino oscillation data. On the other hand, muon decays involve both doublet and singlet sectors and provide a new, although weak, constraint.

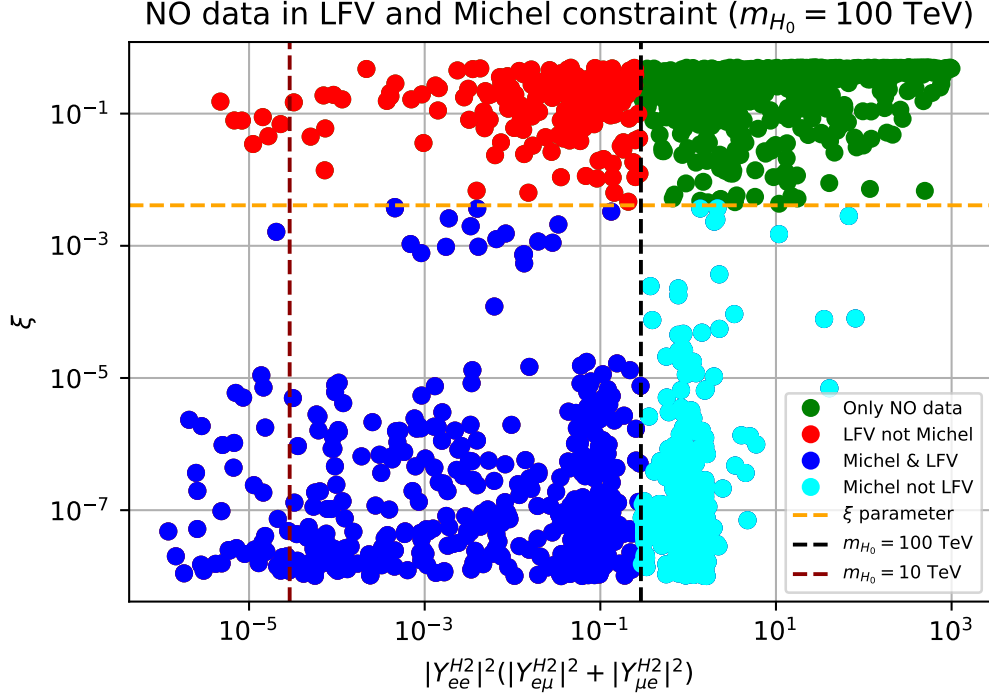


Figure 7.1: Parameter space constraint of Zee model from experiments. All data is generated from neutrino oscillation (NO) constraints in Normal Hierarchy (NH) mass ordering. The green ones are data satisfying only neutrino oscillation constraints, the cyan ones are data satisfying further Michel parameter constraint but not LFV, the blue ones satisfy both Michel and LFV constraints, and the final red ones tell how Michel constraint excludes data from LFV. The black dashed line partitions LFV constrained data and the yellow dashed line partitions Michel parameter constrained data. For the purpose of illustrating Michel parameter constraint, we did not show the $L \rightarrow l\gamma$ and G_F constraints here

Just for illustration, $c_\beta = 0.9$, $m_{H_0} = 100$ TeV, $m_{H^+} = 210$ and $m_{\eta^+} = 200$ GeV are adapted in Fig. 7.1. The point on the left-hand side of the black dashed line are the allowed configuration satisfying the LFV constraints. Moreover, the region above the yellow dashed line is excluded by the Michel parameter, particularly the ξ parameter. Notably, comparing to other previous studies employed only LFV decays constraints, the red points represent our new finding, which is excluded by Michel parameters but allowed by FLV constraint.

Due to the limitations of our searching algorithm, we were unable to generate a sufficient number of data points to fully demonstrate the novelty of the Michel parameter constraints in other model parameter space. For instance, if we consider

the case where $m_{H_0} = 10$ TeV, the black dashed line in Fig. 7.1 would shift to the left by four orders of magnitude (as indicated by the dark red dashed line), and there is still parameter space available (as indicated by the leftmost red points), potentially showing the impact of the Michel parameter on the current experimental limits. We are working to extend our numerical study to the case with m_{H_0} around $\mathcal{O}(1)$ TeV, and explore the usefulness of the Michel parameter constraint on the Zee model.



Bibliography

- [1] L. Michel, *Interaction between four half spin particles and the decay of the μ meson*, *Proc. Phys. Soc. A* **63** (1950) 514.
- [2] T. Kinoshita and A. Sirlin, *Polarization of electrons in muon decay with general parity-nonconserving interactions*, *Phys. Rev.* **108** (1957) 844.
- [3] G. Mention, M. Fechner, T. Lasserre, T. A. Mueller, D. Lhuillier, M. Cribier et al., *Reactor antineutrino anomaly*, *Phys. Rev. D* **83** (2011) 073006.
- [4] K. N. Abazajian, M. A. Acero, S. K. Agarwalla, A. A. Aguilar-Arevalo, C. H. Albright, S. Antusch et al., *Light sterile neutrinos: A white paper*, 2012.
- [5] C. Jarlskog, *Commutator of the quark mass matrices in the standard electroweak model and a measure of maximal CP nonconservation*, *Phys. Rev. Lett.* **55** (1985) 1039.
- [6] O. Sawada and A. Sugamoto, eds., *Proceedings: Workshop on the Unified Theories and the Baryon Number in the Universe: Tsukuba, Japan, February 13-14, 1979*, (Tsukuba, Japan), Natl.Lab.High Energy Phys., 1979.
- [7] R. Foot, H. Lew, X. G. He and G. C. Joshi, *Seesaw Neutrino Masses Induced by a Triplet of Leptons*, *Z. Phys. C* **44** (1989) 441.
- [8] T. P. Cheng and L.-F. Li, *Neutrino masses, mixings, and oscillations in $su(2) \times u(1)$ models of electroweak interactions*, *Phys. Rev. D* **22** (1980) 2860.

- [9] A. Zee, *A Theory of Lepton Number Violation, Neutrino Majorana Mass, and Oscillation*, *Phys. Lett. B* **93** (1980) 389.
- [10] R. K. Barman, R. Dcruz and A. Thapa, *Neutrino masses and magnetic moments of electron and muon in the zee model*, *Journal of High Energy Physics* **2022** (2022) .
- [11] D. Chowdhury and O. Eberhardt, *Update of global two-higgs-doublet model fits*, *Journal of High Energy Physics* **2018** (2018) .
- [12] J. Bernon, J. F. Gunion, H. E. Haber, Y. Jiang and S. Kraml, *Scrutinizing the alignment limit in two-higgs-doublet models: $m_h = 125$ GeV*, *Phys. Rev. D* **92** (2015) 075004.
- [13] D. Bryman, V. Cirigliano, A. Crivellin and G. Inguglia, *Testing lepton flavor universality with pion, kaon, tau, and beta decays*, *Annual Review of Nuclear and Particle Science* **72** (2022) 69–91.
- [14] A. Denner, *Techniques for the calculation of electroweak radiative corrections at the one-loop level and results for w-physics at lep200*, 2007.
- [15] L. Duc Truyen, *Electron muon elastic scattering in one-loop qed with soft-photon corrections*, 2020. 10.13140/RG.2.2.33520.48641.
- [16] C. Bouchiat and L. Michel, *Theory of μ -meson decay with the hypothesis of nonconservation of parity*, *Phys. Rev.* **106** (1957) 170.
- [17] A. Crivellin, M. Hoferichter and C. A. Manzari, *Fermi constant from muon decay versus electroweak fits and cabibbo-kobayashi-maskawa unitarity*, *Physical Review Letters* **127** (2021) .
- [18] PARTICLE DATA GROUP collaboration, *Review of particle physics*, *Phys. Rev. D* **110** (2024) 030001.

- [19] M. Steinhauser, *Übungen zu strahlungskorrekturen in eichtheorien, II.*
Institut für Theoretische Physik, Universität Hamburg, 22761 Hamburg
(2003) .
- [20] T. Kinoshita and A. Sirlin, *Muon decay with parity nonconserving interactions and radiative corrections in the two-component theory*, *Phys. Rev.* **107** (1957) 593.
- [21] T. D. Lee and C. N. Yang, *Theory of charged vector mesons interacting with the electromagnetic field*, *Phys. Rev.* **128** (1962) 885.
- [22] W. J. Marciano, *Fermi constants and “new physics”*, *Physical Review D* **60** (1999) .
- [23] MUON G-2 COLLABORATION collaboration, *Final report of the e821 muon anomalous magnetic moment measurement at bnl*, *Phys. Rev. D* **73** (2006) 072003.
- [24] T. Aoyama, T. Kinoshita and M. Nio, *Theory of the Anomalous Magnetic Moment of the Electron*, *Atoms* **7** (2019) 28.

Appendices



Appendix A

Fierz transformation

Fierz transformation is a mathematical tool used in quantum field theory and particle physics to rearrange or transform complex field operator's products into a more manageable form. This rearrangement is particularly useful when dealing with four-fermion interactions. Its core transformation is the Fierz identity. This identity allows the rearrangement of bilinear products of spinor fields. A bilinear product involves two spinor fields and gamma matrices. The Fierz identity expresses a product of two such bilinears in terms of a sum of bilinears with the spinor fields rearranged. In this study, the Fierz identity is formulated for the set of gamma matrices $\{\Gamma_S = 1, \Gamma_V = \gamma_\mu, \Gamma_T = \sigma_{\mu\nu}, \Gamma_A = \gamma_\mu\gamma_5, \Gamma_P = \gamma_5\}$.

$$\sum_{\alpha} g_{\alpha} \bar{\psi}_i \Gamma_{\alpha} \psi_j \bar{\psi}_m \Gamma_{\alpha} \psi_n = \sum_{\beta} \tilde{g}_{\beta} \bar{\psi}_i \Gamma_{\beta} \psi_n \bar{\psi}_m \Gamma_{\beta} \psi_j \quad (\text{A.1})$$

by a transformation matrix between g_α and \tilde{g}_β that one can read off for α, β running over the set $\{S, V, T, A, P\}$

$$\begin{bmatrix} \tilde{g}_S \\ \tilde{g}_V \\ \tilde{g}_T \\ \tilde{g}_A \\ \tilde{g}_P \end{bmatrix} = \frac{1}{4} \begin{pmatrix} 1 & 4 & 12 & -4 & 1 \\ 1 & -2 & 0 & -2 & -1 \\ \frac{1}{2} & 0 & -2 & 0 & \frac{1}{2} \\ -1 & -2 & 0 & -2 & 1 \\ 1 & -4 & 12 & 4 & 1 \end{pmatrix} \begin{bmatrix} g_S \\ g_V \\ g_T \\ g_A \\ g_P \end{bmatrix} \quad (\text{A.2})$$

where i, j, m, n are flavor indices.



Appendix B

Full massive Lorenz index two-body phase space

The massive two-body phase space is useful to study the effect of Dirac and Majorana neutrino. Considering k, p are 4-momentum neutrinos, and the exchange momentum

$$q^2 = m_\mu^2 + m_e^2 - 2m_\mu E_e = 2m_\mu \left(\frac{m_\mu^2 + m_e^2}{2m_\mu} - E_e \right) = 2m_\mu (W - E_e). \quad (\text{B.1})$$

The exchange energy minimum must be the total mass of neutrinos, therefore,

$$E_e^{max} = W - \frac{(m_k + m_p)^2}{2m_\mu}. \quad (\text{B.2})$$

The massive two-body phase spaces then are written down in terms of

$$I^{\alpha\beta} = \int \frac{d^3k}{E_k} \frac{d^3p}{E_p} \delta^4(q - p - k) k^\alpha p^\beta = A^{3/2} \frac{\pi}{6} q^2 g_{\alpha\beta} + B A^{1/2} \frac{\pi}{3} q_\alpha q_\beta \quad (\text{B.3})$$

$$I_{k(p)}^\alpha = \int \frac{d^3k}{E_k} \frac{d^3p}{E_p} \delta^4(q - p - k) k^\alpha (p^\alpha) = \pi \left(1 \mp \frac{\Delta}{q^2} \right) q^\alpha \quad (\text{B.4})$$

$$I = \int \frac{d^3k}{E_k} \frac{d^3p}{E_p} \delta^4(q - p - k) = 2\pi A^{1/2}, \quad (\text{B.5})$$

where

$$A = 1 - \frac{2\Sigma}{q^2} + \frac{\Delta^2}{q^4} \quad (\text{B.6})$$

$$B = 1 + \frac{\Sigma}{q^2} - \frac{2\Delta^2}{q^4} \quad (\text{B.7})$$

$$\Sigma = m_k^2 + m_p^2 \quad (\text{B.8})$$

$$\Delta = m_p^2 - m_k^2. \quad (\text{B.9})$$



Appendix C

Effective Field Theory model

Departing from the call of new charged mediator playing a part in the lepton decays and potentially being able to reach in current experiment searches. Many UV models that entail newly charged bosons require a benchmark model on a low-energy scale. To address this, we employ the EFT approach, utilizing SM materials and introducing new charged bosons that respect the $U(1)_{EM}$ group. This bottom-up approach, where we start with what we observe and carefully, piece by piece, build our model, in such a way that adheres to the given symmetries, by involving new fields and new adding-by-hand interaction terms, analogous to the Yukawa sector in the Standard Model. Apart from the typical approach in which we add non-renormalizable contributions along with the UV regulator $\frac{1}{\Lambda}$, where Λ is a new physics mass scale, herein, we introduce renormalizable couplings along between new particles and SM particles.

C.1 Charged vector boson

To construct an EFT Lagrangian with a new charged vector boson, we have to satisfy conventionally fundamental symmetries and invariances, at the low-energy scale, these are typically Lorentz invariance and $U(1)_{EM}$ group. In the first step,

we bring in the kinetic term of charged vector field $V_{\mu\nu}^{\pm} \equiv \partial_{\mu}V_{\nu}^{\pm} - \partial_{\nu}V_{\mu}^{\pm}$ in free interaction obeying Lorentz invariance

$$\mathcal{L}_{V^{\pm}} = \epsilon V_{\mu\nu}^{+} V^{-\mu\nu} + m^2 V_{\mu}^{+} V^{-\mu}, \quad (\text{C.1})$$

where the factor magnitude is defined through E.O.M reduced to the Klein-Gordon equation

$$\partial_{\mu} \frac{\partial \mathcal{L}_{V^{\pm}}}{\partial (\partial_{\mu} V_{\nu}^{\pm})} - \frac{\partial \mathcal{L}_{V^{\pm}}}{\partial V_{\nu}^{\pm}} = 2a \partial^{\nu} V_{\mu\nu}^{\pm} + m^2 V_{\mu}^{\pm} = 0, \quad (\text{C.2})$$

we obtain the Lorentz gauge condition $\partial^{\mu} V_{\mu}^{\pm} = 0$ by taking derivative ∂^{μ} to E.O.M. Consequently, to derive the relativistic Schrödinger equation for charged vector field, we set $\epsilon = -\frac{1}{2}$

$$2\epsilon \partial^{\nu} (\partial_{\mu} V_{\nu}^{\pm} - \partial_{\nu} V_{\mu}^{\pm}) + m^2 V_{\mu}^{\pm} = (-2\epsilon \partial^{\nu} \partial_{\nu} + m^2) V_{\mu}^{\pm} = (\square + m^2) V_{\mu}^{\pm} = 0. \quad (\text{C.3})$$

The relative sign between m^2 and ϵ is defined by the positive definite of energy

$$\mathcal{E} = \frac{\partial \mathcal{L}_{V^{\pm}}}{\partial (\partial_t V_{\mu}^{\pm})} \partial_t V_{\mu}^{\pm} - \mathcal{L}_{V^{\pm}} = -V^{\mp,0\mu} \partial_t V_{\mu}^{\pm} + \frac{1}{2} V_{\mu\nu}^{+} V^{-\mu\nu} - m^2 V_{\mu}^{+} V^{-\mu} \quad (\text{C.4})$$

$$= \partial_i V_0^{\pm} \partial_0 V_i^{\mp} - \partial_i V_0^{+} \partial_i V_0^{-} - m^2 (V_0^{+} V_0^{-} - V_i^{+} V_i^{-}) \quad (\text{C.5})$$

$$= (\partial_i V_0^{\pm} \partial_0 V_i^{\mp} + V_0^{\pm} \partial_0^2 V_0^{\mp}) - V_0^{\pm} (\square + m^2) V_0^{\mp} + m^2 V_i^{+} V_i^{-} \quad (\text{C.6})$$

$$= m^2 V_i^{+} V_i^{-} \geq 0. \quad (\text{C.7})$$

Here, we ignored the total derivative terms $\partial_i \hat{\mathcal{O}}$ which has no effect on total energy after integration, and used the Klein-Gordon equation along with Lorentz gauge condition to extract Eq. C.6 to Eq. C.7. Indeed, the Lorentz gauge is used to constrain the Lorentz representation spin-zero component in the vector field, and in order to impose that such condition, the relative factor between $\partial_{\mu} V_{\nu}^{\pm} \partial^{\mu} V^{\mp\nu}$

and $\partial_\mu V_\nu^\pm \partial^\nu V^{\mp\mu}$ is fixed, subsequently, $F_{\mu\nu}^\pm$ was then formed.

The second step involves interaction with the gauge field, especially photon, the standard procedure is that we convert the normal partial derivative to covariant derivative $\partial_\mu \rightarrow D_\mu = \partial_\mu + ieQ_V A_\mu$, the photon field A_μ here basically played a role as an affine connection between two points in complex field space. Interestingly, it is not the end of our story, there is another photon interaction term that we can also include in our model, which basically exerts a contribution to the MDM effect

$$\mathcal{L}_{\text{int}} \supset aieQ_V F^{\mu\nu} V_\mu^+ V_\nu^-, \quad (\text{C.8})$$

with factor \underline{a} is a “free” real number due to the antisymmetric photon field tensor $F^{\mu\nu}$. This is a mysterious emergence while we expected the full coupling with the photon field should be induced through the covariant derivative. In SM, V^\pm is indeed the W^\pm boson, and this bizarre effect originates from non-abelian properties and the connately neutral vector boson coming along with the charged one. To sustain the covariant derivative-based method and resolve the anomaly, hence, the neutral vector boson would do the job, nevertheless, we will not consider that and assume only the new charged boson appears. One more legit term is the quartic potential of V_μ^\pm , such as $b|V_\mu^\pm|^4$, which we also ignored here thanks to its non-contribution to our relevant process.

Crucially, the coefficient \underline{a} in Eq. C.8 must be fixed as a constant to ensure convergence of the magnetic dipole moment. The proper selection of \underline{a} avoids the divergence that would otherwise arise in the calculation of the MDM, a detailed address of this issue and proof within the context of this effective theory will be the subject of a discussion in Appendix E. Therein, we will pinpoint the necessity of the contribution Eq. C.8 for the renormalization of the MDM and its complementary role in the EFT framework, ensuring that the predictions of our model remain

physically meaningful.

In the final step of our consideration, we formalize the interaction Lagrangian representing the dynamics between the charged vector bosons and the fermionic matter fields. This interaction is crucial, as it, in general, encapsulates the effects we aim to investigate, particularly those pertaining to the chiral properties of the weak force.

$$\mathcal{L}_{\text{int}} \supset \bar{\psi}_i \left(V_{ij}^L \hat{L} + V_{ij}^R \hat{R} \right) \gamma^\mu \psi_j V_\mu^- + \text{h.c.}, \quad (\text{C.9})$$

where the couplings V_{ij}^L and V_{ij}^R represent the left-handed and right-handed interaction strengths, respectively, between fermions and the V^\pm boson. In the Standard Model, the right-handed coupling V_{ij}^R is absent, reflecting the purely left-handed nature of weak interactions. The introduction of a non-zero right-handed coupling signifies new physics that allows for right-handed currents. This chiral asymmetry is responsible for the observed parity violation in weak processes and could lead to discrepancies in weak interaction measurements if the right-handed terms contribute significantly.

The Lagrangian is constructed in generic form to reflect the potential chiral asymmetry from the UV models extended SM, for instance, the $\text{SU}(3)_c \times \text{SU}(3)_L \times \text{U}(1)_X$ (331) model, Left-Right Symmetric Models (LRSM), Extra-Dimensional (ED) Models, or other GUTs models, topdown ultimately. Which is a novelty we unveiled, and sets the foundation for exploring the resulting phenomenological consequences.

C.2 Charged scalar boson

According to the same vision and procedure as we have done with the new charged vector, the Lagrangian for a new charged scalar boson is laid out below

$$\mathcal{L}_{\text{EFT}} \supset |D_\mu \phi|^2 - m_\phi^2 |\phi|^2 + \bar{\psi}_i \left(Y_{ij}^L \hat{L} + Y_{ij}^R \hat{R} \right) \psi_j \phi + \text{h.c}, \quad (\text{C.10})$$

differ from the charged vector case, information of photon interaction is completely encoded in covariant derivative $D_\mu = \partial_\mu + ieQ_\phi A_\mu$ and interacting with fermion is described by the third term. Easy to see that the coefficients in Lagrangian are valid choices, in the sense both E.O.M and energy positive definite are satisfied. In free interaction, the E.O.M

$$\partial_\mu \frac{\partial \mathcal{L}_\phi}{\partial (\partial_\mu \phi^*)} - \frac{\partial \mathcal{L}_\phi}{\partial \phi^*} = (\square + m^2) \phi = 0, \quad (\text{C.11})$$

and the energy density

$$\mathcal{E} = \frac{\partial \mathcal{L}_\phi}{\partial (\partial_t \phi^*)} (\partial_t \phi^*) - \mathcal{L}_\phi = |\partial_t \phi|^2 + |\vec{\nabla} \phi|^2 + m^2 |\phi|^2 \geq 0 \quad (\text{C.12})$$

is positive definite. In Eq. C.8, the third term highlights our focus on experimental phenomenology, paralleling our approach in the charged vector case. This investigation delves into the effects within the weak interaction regime, a domain where each chiral type manifests distinct characteristics. From the context of EFT, this allows us to offer matching constraints to constraints of several UV models, which we'll briefly touch off in Appendix F through the lens of the experiment. Moreover, by leveraging our computational resources, we can effectively navigate the parameter space constraints of the triplet Higgs model.

C.3 Feynman rule

Here we souped up an Effective Lagrangian at the low-energy scale able to be all in one expressed in the following:

$$\mathcal{L}_{\text{EFT}} = \mathcal{L}_{\text{SM}} + \mathcal{L}_S + \mathcal{L}_Y + \mathcal{L}_{F-V^\pm} + \mathcal{L}_{V^\pm} + \mathcal{L}_\gamma, \quad (\text{C.13})$$

Where \mathcal{L}_{SM} is the well-know SM Lagrangian, and each other parts are defined

$$\mathcal{L}_S = |D_\mu \phi|^2 - m_\phi^2 |\phi|^2, \quad (\text{C.14})$$

$$\mathcal{L}_F = i\bar{\psi} \not{D}\psi - m_f^2 \bar{\psi}\psi, \quad (\text{C.15})$$

$$\mathcal{L}_{V^\pm} = -\frac{1}{2}\tilde{V}_{\mu\nu}^+ \tilde{V}^{-\mu\nu} + m_V^2 V_\mu^+ V^{-\mu} + ieQ_V a F^{\mu\nu} V_\mu^+ V_\nu^-, \quad (\text{C.16})$$

$$\mathcal{L}_{F-S} = \bar{\psi}_i \left(Y_{ij}^L \hat{L} + Y_{ij}^R \hat{R} \right) \psi_j \phi + \text{h.c}, \quad (\text{C.17})$$

$$\mathcal{L}_{F-V^\pm} = \bar{\psi}_i \left(V_{ij}^L \hat{L} + V_{ij}^R \hat{R} \right) \gamma^\mu \psi_j V_\mu^\pm + \text{h.c} \quad (\text{C.18})$$

according to the $U(1)_{\text{EM}}$ gauge transformation

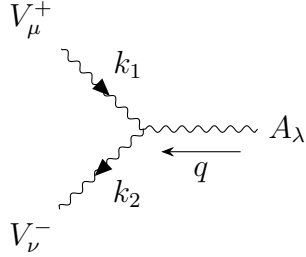
$$\partial_\mu \rightarrow D_\mu = \partial_\mu + ieQA_\mu \quad (\text{C.19})$$

$$A_\mu \rightarrow A_\mu - \partial_\mu \alpha(x) \quad (\text{C.20})$$

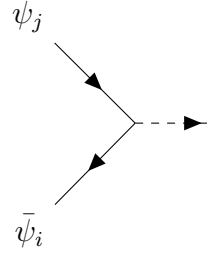
$$V_{\mu\nu}^- = \partial_\mu V_\nu^- - \partial_\nu V_\mu^- \rightarrow \tilde{V}_{\mu\nu}^- = D_\mu V_\nu^- - D_\nu V_\mu^- \quad (\text{C.21})$$

$$\{\psi, \phi, V_\mu^\pm\} \rightarrow e^{ieQ\alpha(x)} \{\psi, \phi, V_\mu^\pm\}. \quad (\text{C.22})$$

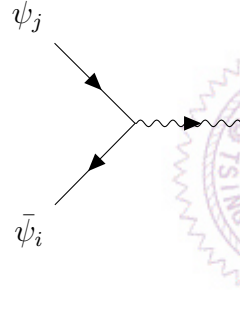
Be cautious, we assumed that either new charged vector or new charged scalar even though we wrote it in one line for simplification, but no interference between those. Couplings $Y_{ij}^{R,L}, V_{ij}^{R,L}$ are complex element symmetric matrices such that their left-right relative phases are $k\pi$ ($k \in \mathbb{Z}$) for CP invariant condition, and a factor from an additional magnetic-moment contribution $ieQ_V a F^{\mu\nu} V_\mu^+ V_\nu^-$ is purely real due to anti-symmetric of Electromagnetic Field Strength tensor $F_{\mu\nu}$. After



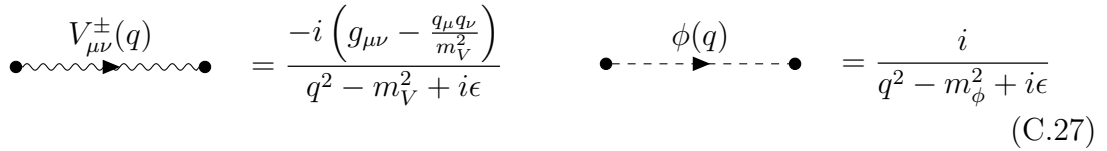
$$= -ieQ_V \left[(k_2 - a.q)_\mu g_{\lambda\nu} + (k_1 + a.q)_\nu g_{\mu\lambda} - (k_1 + k_2)_\lambda g_{\mu\nu} \right] \quad (\text{C.24})$$



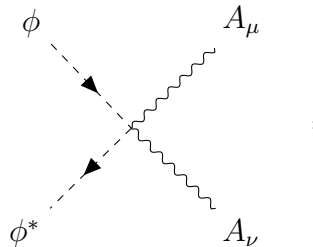
$$= i \left(Y_{ij}^L \hat{L} + Y_{ij}^R \hat{R} \right) \quad (\text{C.25})$$



$$= i \left(V_{ij}^L \hat{L} + V_{ij}^R \hat{R} \right) \gamma_\mu \quad (\text{C.26})$$



$$= \frac{-i \left(g_{\mu\nu} - \frac{q_\mu q_\nu}{m_V^2} \right)}{q^2 - m_V^2 + i\epsilon} \quad \bullet \text{---} \phi(q) \text{---} \bullet = \frac{i}{q^2 - m_\phi^2 + i\epsilon} \quad (\text{C.27})$$



$$= 2ie^2 Q_\phi^2 g_{\mu\nu} \quad (\text{C.28})$$

The final Feynman rule is the representative quadratic photon interaction term of scalar QED, which is not relevant to our consideration. We let Eq. C.24 in the generic form with the free factor \underline{a} . In SM, it will similarly cast the rule of the

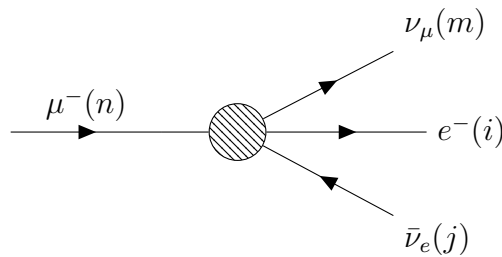
W^- boson as $Q_V = -1$ and $a = 1$.



Appendix D

Michel parameters

This investigation delves into the decay dynamics of muons within the framework of the new EFT model, exploring both the parity-nonconserving nature of weak forces and the implications of lepton universality. The theoretical analysis herein is centered around a generalized formulation for the decay-electron distribution accommodateting polarized muon decay scenario by Michel parameters. By leveraging the polarization observables in muon decay, we aim to constrain the parameters governing weak interactions, offering insights into the validity of different theoretical constructs. This chapter is structured to initially delve into the theoretical foundation surrounding the decay parameter based on the EFT four-fermion interaction theory. This effort showcases the involvement of new physics (NP) in influencing experimental values, particularly focusing on the consequences these parameters have in polarized muon decays. Subsequently, we probe the detectable impact of NP on the Fermi constant by considering the muon lifetime.



The point-like interaction in muon decay is governed by the 4-Fermi theory

that is matched to the EFT couplings by the Fierz transformation. In this way, we study Michel parameters from the muon decay process to make constraints on the new couplings, and calculations in this chapter are generally able to apply to all other fermion decay modes if the massless of the final states is supposed. The differential decay rate of the muon is in the form:

$$d\Gamma = \frac{m_\mu^5}{3 * 2^9 * \pi^4} * (a + 4b + 6c) \left\{ 3(1 - x) + 2\rho \left(\frac{4}{3}x - 1 \right) - \xi \cos \theta \left[(1 - x) + 2\delta \left(\frac{4}{3} - 1 \right) \right] \right\} x^2 dx, \quad (\text{D.1})$$

where ρ, ξ, δ are Michel parameters [1] measured from experiment, which are defined [2]

$$\rho = \frac{3b + 6c}{a + 4b + 6c} \quad (\text{D.2})$$

$$\delta = \frac{3b' - 6c'}{-3a' + 4b' - 14c'} \quad (\text{D.3})$$

$$\xi = \frac{3a' - 4b' + 14c'}{a + 4b + 6c}. \quad (\text{D.4})$$

Note that, we consider either case, only a new scalar or new vector, where the

coupling combinational parameters are defined in the new scalar case

$$a = \frac{|Y_{ij}^L Y_{nm}^{R*}|^2 + |Y_{ij}^R Y_{nm}^{L*}|^2}{16m_\phi^4} \quad (\text{D.5})$$

$$a' = \frac{|Y_{ij}^L Y_{nm}^{R*}|^2 - |Y_{ij}^R Y_{nm}^{L*}|^2}{16m_\phi^4} \quad (\text{D.6})$$

$$b = \frac{|Y_{ij}^L Y_{nm}^{L*}|^2 + |Y_{ij}^R Y_{nm}^{R*}|^2}{16m_\phi^4} + \frac{g^4}{16m_W^4} \quad (\text{D.7})$$

$$b' = \frac{|Y_{ij}^R Y_{nm}^{R*}|^2 - |Y_{ij}^L Y_{nm}^{L*}|^2}{16m_\phi^4} + \frac{g^4}{16m_W^4} \quad (\text{D.8})$$

$$c = \frac{|Y_{ij}^L Y_{nm}^{R*}|^2 + |Y_{ij}^R Y_{nm}^{L*}|^2}{32m_\phi^4} \quad (\text{D.9})$$

$$c' = \frac{|Y_{ij}^R Y_{nm}^{L*}|^2 - |Y_{ij}^L Y_{nm}^{R*}|^2}{32m_\phi^4}, \quad (\text{D.10})$$

or in the new vector mediator

$$a = \frac{|V_{ij}^L V_{nm}^{R*}|^2 + |V_{ij}^R V_{nm}^{L*}|^2}{m_V^4} \quad (\text{D.11})$$

$$a' = \frac{|V_{ij}^L V_{nm}^{R*}|^2 - |V_{ij}^R V_{nm}^{L*}|^2}{m_V^4} \quad (\text{D.12})$$

$$b = \frac{|V_{ij}^L V_{nm}^{L*}|^2 + |V_{ij}^R V_{nm}^{R*}|^2}{4m_\phi^4} + \frac{g^4}{16m_W^4} + \frac{g^2}{4m_W^2 m_V^2} \text{Re}(V_{ij}^R V_{nm}^{R*}) \quad (\text{D.13})$$

$$b' = \frac{|V_{ij}^R V_{nm}^{R*}|^2 - |V_{ij}^L V_{nm}^{L*}|^2}{4m_\phi^4} + \frac{g^4}{16m_W^4} + \frac{g^2}{4m_W^2 m_V^2} \text{Re}(V_{ij}^R V_{nm}^{R*}) \quad (\text{D.14})$$

are in terms of coupling parameters that we are going to constrain. Because of

$|a'| \leq a, |b'| \leq b, |c'| \leq c$, these below inequalities always hold [20]

$$|\xi\delta| \leq \rho, \quad (\text{D.15})$$

$$0 \leq \rho \leq 1, \quad (\text{D.16})$$

and

$$0 \leq |\xi| \leq 3 - \frac{2}{3}\rho. \quad (\text{D.17})$$

The symmetry and anti-symmetry between left-right couplings are encoded in ρ and δ respectively, particularly non-prime and prime parameters. Consequently, if only one chirality gets in that will turn out the same behavior, say, the predicted value $\rho = \delta = \frac{3}{4}$ same as Standard Model, and then constrain $|\xi| \leq 1$. The relative left-right difference effect is ascribed to ξ , which gives rise to changes in the angle of electron distribution. And if the true experiment turns out $|\xi| \geq 1$, it is definitely a hint of new physics involving both left-right interactions, at least in the vector boson sector or the lepton number violation interaction in the Yukawa sector.

As long as the neutrinos are massless and unobserved, the scalar case is non-sensitive to the LFV process on account of the non-interference between spin-0 (new scalar) and spin-1 (W boson), while this effect is characterized by the new vector case through the overlapped term.

To simplify, we further assume the universality and diagonal properties of the coupling parameters matrix, and then our case is reduced to

- For scalar case

$$a = \frac{|Y^L|^2 |Y^R|^2}{8m_\phi^4} \quad (\text{D.18})$$

$$a' = 0 \quad (\text{D.19})$$

$$b = \frac{|Y^L|^4 + |Y^R|^4}{16m_\phi^4} + \frac{g^4}{16m_W^4} \quad (\text{D.20})$$

$$b' = \frac{|Y^R|^4 - |Y^L|^4}{16m_\phi^4} + \frac{g^4}{16m_W^4} \quad (\text{D.21})$$

$$c = \frac{|Y^L|^2 |Y^R|^2}{64m_\phi^4} \quad (\text{D.22})$$

$$c' = 0. \quad (\text{D.23})$$

- For vector case

$$a = 2 \frac{|V^L|^2 |V^R|^2}{m_V^4} \quad (\text{D.24})$$

$$a' = 0 \quad (\text{D.25})$$

$$b = \frac{|V^L|^4 + |V^R|^4}{4m_V^4} + \frac{g^4}{16m_W^4} + \frac{g^2}{4m_W^2 m_V^2} |V^R|^2 \quad (\text{D.26})$$

$$b' = \frac{|V^R|^4 - |V^L|^4}{4m_V^4} + \frac{g^4}{16m_W^4} + \frac{g^2}{4m_W^2 m_V^2} |V^R|^2. \quad (\text{D.27})$$

The SM-like coupling means giving no deviation from SM contribution of Michel parameters, which are in the situation of only Y^L and V^R being involved, will be unbounded by the Michel parameters experiment as those are in sets of SM value prediction $\rho = \delta = \frac{3}{4}, \xi = -1$. As is straightforward to the eye, the universality condition implies the $\delta = \frac{3}{4}$.



Appendix E

$L \rightarrow l\gamma$ decay process

In this chapter follow, we will delve deep into the heart of this lep-to-lep-gamma process, exploring its significance and physics implications through the lens of Feynman diagram calculations and analytical dissections. This study takes us to a deeper understanding and extracts results of Magnetic Dipole Moment (MDM) and the Lepton Flavour Violation (LFV) decay $L \rightarrow l\gamma$, then profoundly demonstrates the anomaly-free of gauge invariance of the EFT model through vanishing anapole, whose exploration is crucial for the validation of our theory. Moreover, as a progress, we will also uncover the indispensable role of extra photon coupling in contributing to the MDM of the charged vector models.

E.1 Gauge invariant and Anapole vanishing

Using \mathcal{L}_{EFT} above to investigate the contribution to the LFV decay, that consists of all possible leading effects which only come from scalar field ϕ and vector field V_μ^\pm mediator. The matrix element for the process $l_j \rightarrow l_i\gamma$ emitting a real photon $\mathcal{M}^\mu = \bar{u}_i(p)\Gamma^\mu u_j(p+q)$, the interaction vertex Γ^μ can be formally decomposed

into form factors

$$\Gamma^\mu(q^2 = 0) = \gamma^\mu F_1 + \gamma^\mu \gamma_5 G_1 + i\sigma^{\mu\nu} q_\nu F_2 + i\sigma^{\mu\nu} q_\nu \gamma_5 G_2, \quad (\text{E.1})$$

where F_1, G_1 associated to γ^μ are Dirac and Anapole form factors, gauge invariance property enforces $G_1 = 0$ though; F_2, G_2 associated to $\sigma^{\mu\nu} q_\nu$ are Magnetic Dipole (MDM) and Electric Dipole Moment (EDM) respectively. To universal interactions from the EFT Lagrangian are charged scalar ϕ and vector V^\pm considered separately, where

$$F_1(G_1) = \sum_i^{[a,b,c,d]} F_1^{\phi,i} (G_1^{\phi,i}) + \sum_i^{[a,b,c,d]} F^{V,i} (G_1^{V,i}) \quad (\text{E.2})$$

$$F_2(G_2) = \sum_i^{[a,b,c,d]} F_2^{\phi,i} (G_2^{\phi,i}) + \sum_i^{[a,b,c,d]} F^{V,2} (G_2^{V,i}) \quad (\text{E.3})$$

we sum $\sum_i^{[a,b,c,d]}$ overall diagram contributions of each class and represent them by Passarino-Veltman (PV) convention functions [19, 14, 15]

$$C_{i,j,\dots}^{V(\phi),a} = C_{i,j,\dots}^{V(\phi),a} (m_2^2, 0, m_1^2, m_k, m_{V(\phi)}, m_{V(\phi)}) \quad (\text{E.4})$$

$$C_{i,j,\dots}^{V(\phi),d} = C_{i,j,\dots}^{V(\phi),d} (m_2^2, 0, m_1^2, m_{V(\phi)}, m_k, m_k) \quad (\text{E.5})$$

$$B_{i,j,\dots}^{V(\phi),b} = B_{i,j,\dots}^{V(\phi),b} (m_1^2, m_k, m_{V(\phi)}) \quad (\text{E.6})$$

$$B_{i,j,\dots}^{V(\phi),b} = B_{i,j,\dots}^{V(\phi),b} (m_2^2, m_k, m_{V(\phi)}) \quad (\text{E.7})$$

fully expressed form factors in terms of PV function are found in Appendix G. Expanding the exact calculation of PV functions, we showed that $F_1 = G_1 = 0$, that means γ^μ terms vanish in the $l_i \rightarrow l_j + \gamma$ decay process described by generic EFT Lagrangian Eq. (C.13). Under CP transformation, the EDM G_2 term $\bar{\psi} \sigma_{\mu\nu} \gamma_5 F^{\mu\nu} \rightarrow -\bar{\psi} \sigma_{\mu\nu} \gamma_5 F^{\mu\nu}$ is non-invariant, which presumably are hints stemming from higher symmetry CP violation sources. As tangibly, the interaction terms in

Eq. C.13 encoded the higher symmetry model, which in general can be non-CP conserved. On the other side, the anapole term G_1 is not only P violated but also does not preserve gauge invariance, thus, anapole inevitably vanishes in the gauge invariant theory, otherwise the EFT theory is incomplete. In the classical regime, where the gauge invariant Lagrangian became obvious, to ascertain if there is not an anomaly in our model, checking gauge invariant in the loop level contribution is conducted, which is verified through satisfying Ward Identity

$$q_\mu \Gamma^\mu(q^2 = 0) = \not{q} F_1(q^2 = 0) + \not{q} \gamma_5 G_1(q^2 = 0) = 0 \quad (\text{E.8})$$

with on-shell ($q^2 = 0$) photon four-momentum. In case of LFV decay, or $l_j \neq l_i$, both $F_1(q^2 = 0) = G_1(q^2 = 0) = 0$ conditions are obligated to satisfy. We are henceforth employing the assumption of a heavy charged boson $m_{V,\phi} \gg m_l$ and taking the approximated expansion at order $\mathcal{O}\left(\frac{m_l^2}{m_{V,\phi}^2}\right)$ for simplicity.

E.2 Charged vector form factors

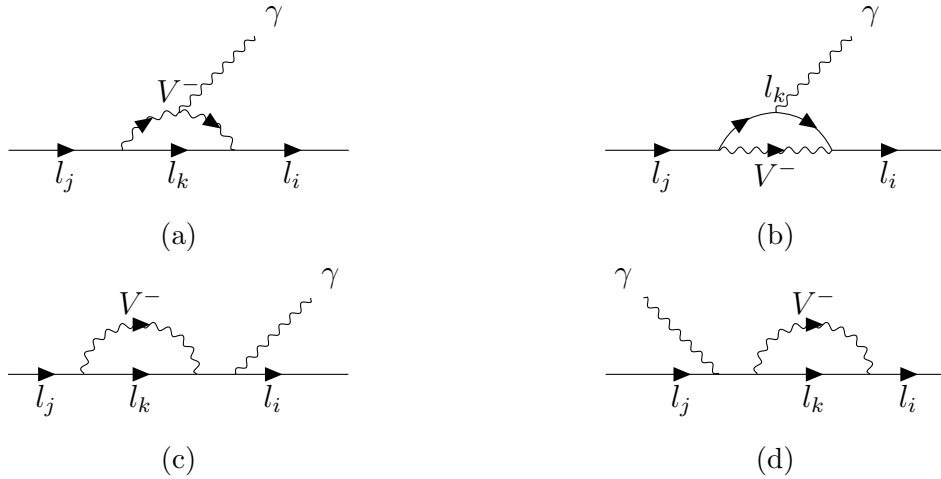


Figure E.1: $l_j \rightarrow l_i \gamma$ with new charged vector contribution

1.

$$G_1^{V,a} = \frac{eQ_V}{24} \left\{ \left(V_L^{*ki} V_L^{kj} - V_R^{*ki} V_R^{kj} \right) \left[\frac{6(m_j^2 - m_j m_i + m_i^2 - 3m_k^2)}{m_V^2} \left(\frac{1}{\epsilon} + \log \left[\frac{\mu^2}{m_V^2} \right] \right) \right. \right. \\ \left. \left. - 18 + \frac{(7m_j^2 - 7m_j m_i + 7m_i^2 - 33m_k^2)}{m_V^2} \right] + \left(V_L^{*ki} V_R^{kj} - V_R^{*ki} V_L^{kj} \right) \frac{18(m_i - m_j) m_k}{m_V^2} \right\} \quad (\text{E.9})$$

2.

$$G_1^{V,b} = \frac{eQ_k}{24} \left\{ \left(V_L^{*ki} V_L^{kj} - V_R^{*ki} V_R^{kj} \right) \left[\frac{6(m_j^2 - m_j m_i + m_i^2 - 3m_k^2)}{m_V^2} \left(\frac{1}{\epsilon} + \log \left[\frac{\mu^2}{m_V^2} \right] \right) \right. \right. \\ \left. \left. - 18 + \frac{(7m_j^2 - 7m_j m_i + 7m_i^2 - 33m_k^2)}{m_V^2} \right] + \left(V_L^{*ki} V_R^{kj} - V_R^{*ki} V_L^{kj} \right) \frac{18(m_i - m_j) m_k}{m_V^2} \right\} \quad (\text{E.10})$$

3.

$$G_1^{V,c} = \frac{eQ_l}{4(m_i + m_j)} \left\{ m_j \left(V_L^{*ki} V_L^{kj} - V_R^{*ki} V_R^{kj} \right) \left[\left(\frac{m_j^2 - 3m_k^2}{m_V^2} \right) \left(\frac{1}{\epsilon} + \log \left[\frac{\mu^2}{m_V^2} \right] \right) - 3 \right. \right. \\ \left. \left. + \frac{(7m_j^2 - 33m_k^2)}{6m_V^2} \right] + \left(Y_L^{*ki} Y_R^{kj} - Y_R^{*ki} Y_L^{kj} \right) \left[\left(6m_k + 6\frac{m_k^3}{m_V^2} \right) \left(\frac{1}{\epsilon} + \log \left[\frac{\mu^2}{m_V^2} \right] \right) \right. \right. \\ \left. \left. + 2m_k - \frac{m_k(3m_j^2 + 2m_k^2)}{m_V^2} \right] \right\} \quad (\text{E.11})$$

4.

$$G_1^{V,d} = \frac{eQ_l}{4(m_i + m_j)} \left\{ m_i \left(V_L^{*ki} V_L^{kj} - V_R^{*ki} V_R^{kj} \right) \left[\left(\frac{m_i^2 - 3m_k^2}{m_V^2} \right) \left(\frac{1}{\epsilon} + \log \left[\frac{\mu^2}{m_V^2} \right] \right) - 3 \right. \right. \\ \left. \left. + \frac{(7m_i^2 - 33m_k^2)}{6m_V^2} \right] - \left(V_L^{*ki} V_R^{kj} - V_R^{*ki} V_L^{kj} \right) \left[\left(6m_k + 6\frac{m_k^3}{m_V^2} \right) \left(\frac{1}{\epsilon} + \log \left[\frac{\mu^2}{m_V^2} \right] \right) \right. \right. \\ \left. \left. + 2m_k - \frac{m_k(3m_i^2 + 2m_k^2)}{m_V^2} \right] \right\} \quad (\text{E.12})$$

The absence of the parameter \underline{a} indicates that the additional interaction term in-

volving the photon and the newly introduced charged vector does not get part in this form factor, therefore solely influencing the MDM/EDM. The pattern explicitly presents how the diagram's anapole form factor contributions are rooted out to preserve the gauged invariance. $\frac{G_1^{V,c}+G_1^{V,d}}{Q_l} = \frac{G_1^{V,b}}{Q_V} = \frac{G_1^{V,a}}{Q_k}$ corresponds to terms proportional to $(V_L^{*ki}Y_L^{kj} - V_R^{*ki}Y_R^{kj})$ and UV finite of $(V_L^{*ki}V_R^{kj} - V_R^{*ki}V_L^{kj})$ terms, meanwhile UV divergence in $(V_L^{*ki}V_R^{kj} - V_R^{*ki}V_L^{kj})$ terms pertaining to $G_1^{V,c}$ and $G_1^{V,d}$ form factors canceling out each others. That manifestly combinatorial each other subtracting off even in $l_i = l_j$ case, which brings the Ward Identity $q_\mu \bar{u}_i \Lambda^\mu (q^2 = 0) u_i = \bar{u}_i \not{q} \gamma_5 G_1 \bar{u}_i = 0$ about to be obeyed. Otherwise, the Dirac form factor in the same expression within replacing $m_j \rightarrow -m_j$ and $V_L^{kj} \rightarrow -V_L^{kj}$, which however strikes divergence as $l_i = l_j$, but this divergence can be resolved through the application of the renormalization technique nonetheless.

E.3 Charged scalar form factors

In place of discussing anapole terms, we will illustrate the cancellation of the Dirac term as $m_i \neq m_j$, and the behavior of the anapole will be similarly followed.

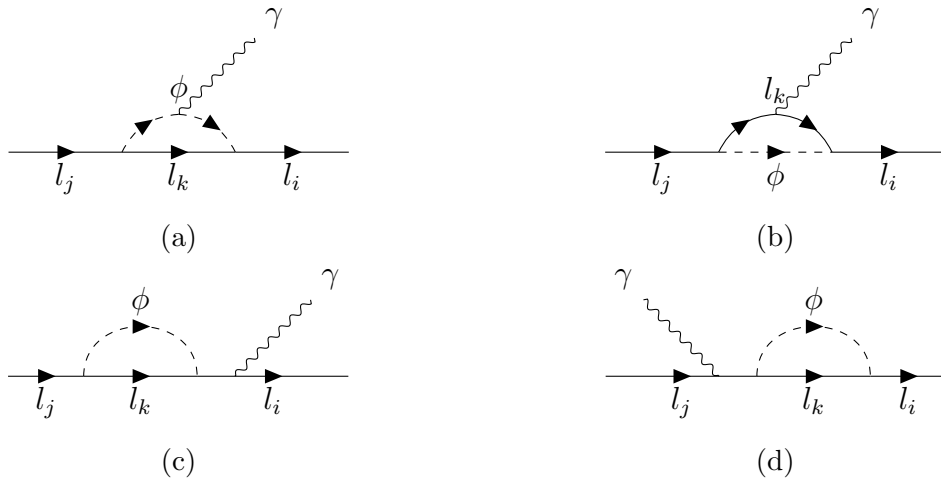


Figure E.2: $l_j \rightarrow l_i \gamma$ with new charged scalar contribution

1.

$$F_1^{\phi,a} = \frac{eQ_\phi}{8} \left\{ \left(Y_L^{*ki} Y_L^{kj} + Y_R^{*ki} Y_R^{kj} \right) \left[2 \left(\frac{1}{\epsilon} + \log \left[\frac{\mu^2}{m_\phi^2} \right] \right) + 1 \right. \right. \\ \left. \left. + \frac{2(m_j^2 + m_j m_i + m_i^2 - 3m_k^2)}{3m_\phi^2} \right] + 2 \left(Y_L^{*ki} Y_R^{kj} + Y_R^{*ki} Y_L^{kj} \right) \frac{(m_i + m_j) m_k}{m_\phi^2} \right\} \quad (\text{E.13})$$

2.

$$F_1^{\phi,c} = \frac{eQ_l}{8(m_j - m_i)} \left\{ m_j \left(Y_L^{*ki} Y_L^{kj} + Y_R^{*ki} Y_R^{kj} \right) \left[2 \left(\frac{1}{\epsilon} + \log \left[\frac{\mu^2}{m_\phi^2} \right] \right) - \frac{2(m_j^2 - 3m_k^2)}{3m_\phi^2} + 1 \right] \right. \\ \left. + 4 \left(Y_L^{*ki} Y_R^{kj} + Y_R^{*ki} Y_L^{kj} \right) \left[\left(m_k - \frac{m_k^3}{m_\phi^2} \right) \left(\frac{1}{\epsilon} + \log \left[\frac{\mu^2}{m_\phi^2} \right] \right) + m_k - \frac{m_k(m_j^2 + 2m_k^2)}{2m_\phi^2} \right] \right\} \quad (\text{E.14})$$

3.

$$F_1^{\phi,d} = \frac{eQ_l}{8(m_i - m_j)} \left\{ m_i \left(Y_L^{*ki} Y_L^{kj} + Y_R^{*ki} Y_R^{kj} \right) \left[2 \left(\frac{1}{\epsilon} + \log \left[\frac{\mu^2}{m_\phi^2} \right] \right) - \frac{2(m_i^2 - 3m_k^2)}{3m_\phi^2} + 1 \right] \right. \\ \left. + 4 \left(Y_L^{*ki} Y_R^{kj} + Y_R^{*ki} Y_L^{kj} \right) \left[\left(m_k - \frac{m_k^3}{m_\phi^2} \right) \left(\frac{1}{\epsilon} + \log \left[\frac{\mu^2}{m_\phi^2} \right] \right) + m_k - \frac{m_k(m_i^2 + 2m_k^2)}{2m_\phi^2} \right] \right\} \quad (\text{E.15})$$

4.

$$F_1^{\phi,b} = \frac{eQ_k}{8} \left\{ \left(Y_L^{*ki} Y_L^{kj} + Y_R^{*ki} Y_R^{kj} \right) \left[2 \left(\frac{1}{\epsilon} + \log \left[\frac{\mu^2}{m_\phi^2} \right] \right) + 1 \right. \right. \\ \left. \left. + \frac{2(m_j^2 + m_j m_i + m_i^2 - 3m_k^2)}{3m_\phi^2} \right] + 2 \left(Y_L^{*ki} Y_R^{kj} + Y_R^{*ki} Y_L^{kj} \right) \frac{(m_i + m_j) m_k}{m_\phi^2} \right\} \quad (\text{E.16})$$

Equivalent to the charged vector case, from the above expressions, $F_1^{\phi,c} + F_1^{\phi,d} \propto F_1^{\phi,b} \propto F_1^{\phi,a}$ in such terms accompanied by $(Y_L^{*ki} Y_L^{kj} + Y_R^{*ki} Y_R^{kj})$, respectively

propositional to their own particle's charge emitting photon. They all sum up to zero if we impose $Q_l + Q_\phi + Q_k = 0$. In the $\left(Y_L^{*ki}Y_R^{kj} + Y_R^{*ki}Y_L^{kj}\right)$ terms, both $F_1^{\phi,c}$ and $F_1^{\phi,d}$ offset UV divergent parts of each other, and then the UV finite part of F_1^ϕ of altogether vanish if charge conversation is held on. The same conclusion for anapole form factors G_1^ϕ in expressions substituted F_1^ϕ by $m_j \rightarrow -m_j$ and $Y_L^{kj} \rightarrow -Y_L^{kj}$.

E.4 $L \rightarrow l\gamma$ and $(g - 2)_l$

The ongoing dialogue between theoretical predictions and experimental measurements in the realm of the lepton $g - 2$ and flavor violation decay, particularly muon, continues to be a fertile ground for discovering new physics. The measurement of the muon's anomalous magnetic moment a_μ thus remains a key focus in high-energy physics, symbolizing the intricate interplay between theorist and experimentalist sides.

Meanwhile, EFT models can potentially provide possible candidate of new physics that could account for the measuremental values, allowing for bridging the gap between the currently observed phenomena in the MDM/LFV measurements and the enormous of possible explanations of underlying theoretical framework, paving the way for a deeper understanding of fundamental physics. This not only aids in pinpointing the specific nature of the new interactions or particles but also helps in guiding future experimental searches.

E.4.1 $L \rightarrow l\gamma$ LFV decay

In the intriguing landscape of particle physics, LFV decay stands out as a phenomenon that defies the Standard Model's predictions, offering a window into potential new physics. The parity of these decays, in which a lepton of one fla-

vor, such as a muon, transforms into another, like an electron, without conserving flavor, has fueled extensive theoretical speculation. Various models attempting to account for LFV have emerged, each proposing novel mechanisms and particles beyond the Standard Model, such as models addressing massive neutrinos, leptoquark (LQ) model, R-parity violating supersymmetry, etc. Amidst these diverse theoretical constructs, EFT plays on a bottom-up approach, which provides a versatile framework, enabling physicists to systematically analyze LFV processes without committing to a specific underlying theory smoothing the path for a deeper understanding of these rare decays.

Eq .E.1 tells us how to perform the calculation of the LFV decay rate

$$i\mathcal{M}_\nu = \bar{l}_i(k_i) \sigma^{\mu\nu} (F_2 + G_2\gamma_5) l_j(k_j) q_\mu \quad (\text{E.17})$$

where $q = k_j - k_i$ is the on-shell emitting photon four-momentum. Assuming that the heavy mass of decaying particle $m_j \gg m_i$ we then derive the decay rate

$$\Gamma(l_j \rightarrow l_i \gamma) = \frac{m_j^3}{8\pi} (|F_2|^2 + |G_2|^2), \quad (\text{E.18})$$

in which the squared amplitude and two-body phase space used are the following

$$|\mathbf{M}|^2 = 4m_j^4 (|F_2|^2 + |G_2|^2) \quad (\text{E.19})$$

$$\int dP_2 = \int \frac{d^3k_i}{2k_i^0 (2\pi)^3} \frac{d^3q}{2q^0 (2\pi)^3} (2\pi)^4 \delta^4(k_j - k_i - q) = \frac{\pi}{2}. \quad (\text{E.20})$$

E.4.2 $(g - 2)_l$ anomalous magnetics dipole moment

The measurement of the muon's anomalous magnetic moment denoted as $(g - 2)$, stands as a cornerstone in precision particle physics and probes the frontiers of

the Standard Model. Achieving sub-parts-per-million (ppm) precision, this measurement offers a window into physics beyond the Standard Model. The muon magnetic dipole moment, expressed as $\vec{\mu} = ge\frac{e}{2m}\vec{S}$, where \vec{S} is the muon's spin angular momentum, is foundational to these explorations, Dirac exactly predicted by his equation $g = 2$ in the classical limit, and then Schwinger derived $a_\mu \equiv \frac{(g-2)_\mu}{2} = \frac{\alpha}{2\pi}$ in QED first order quantum correction. Recent experimental results, particularly from the Fermilab Muon $g - 2$ experiment, have corroborated earlier findings from the Brookhaven National Laboratory, intensifying the 4.2σ discrepancies between experimental data and Standard Model predictions.

On the theoretical front, efforts to reconcile these discrepancies have been robust. Theoretical physicists have proposed various extensions to the Standard Model, such as supersymmetry, leptoquarks, and dark photons, as potential explanations for the observed anomaly. These models introduce new particles or interactions that could contribute to the muon $g - 2$ value, thus potentially resolving the tension between theory and experiment. Moreover, refined calculations incorporating quantum electrodynamics, hadronic contributions, and electroweak interactions have been performed, offering nuanced insights into the muon's behavior. These theoretical updates are critical for enhancing our understanding of fundamental physics, providing new directions for theoretical exploration and experimental verification.

As is customary, the EFT model proposed embarks on the game to lay on a preliminary robust stone that bridges to the higher-scale UV theories. The MDM/EDM form factor formulated in Eq. E.1 is useful to acquire LFV decay rate

Eq. E.18 as well, newly charged scalar and vector contribution are¹

$$F_2^\phi = \frac{-e}{3 \cdot 2^7 m_\phi^2 \pi^2} \left[(m_i + m_j) (Q_\phi - 2Q_k) (Y_L^{*ki} Y_L^{kj} + Y_R^{*ki} Y_R^{kj}) \right. \\ \left. + 6m_k \left(Q_\phi + 3Q_k + 2Q_k \log \left[\frac{m_k^2}{m_\phi^2} \right] \right) (Y_L^{*ki} Y_R^{kj} + Y_R^{*ki} Y_L^{kj}) \right] \quad (\text{E.21})$$

and

$$F_2^V = \frac{e}{3 \cdot 2^7 m_V^2 \pi^2} \left[(m_i + m_j) (Q_V - 8Q_k + 9aQ_V) (V_L^{*ki} V_L^{kj} + V_R^{*ki} V_R^{kj}) \right. \\ \left. - 6m_k (5a - 1) Q_V (V_L^{*ki} V_R^{kj} + V_R^{*ki} V_L^{kj}) \right] + (a - 1) \frac{eQ_V}{2^6 m_V^2 \pi^2} \times \\ \left[(V_L^{*ki} V_L^{kj} + V_R^{*ki} V_R^{kj}) (m_i + m_j) - 2m_k (V_L^{*ki} V_R^{kj} + V_R^{*ki} V_L^{kj}) \right] \left(\frac{1}{\epsilon} + \log \left[\frac{\mu^2}{m_V^2} \right] \right). \quad (\text{E.22})$$

As mentioned earlier, the quantity F_2^V exhibits UV divergence apparently popping up in Eq. E.22 unless $a = 1$. This critical function of the extra adding-by-hand ED interaction term in the charged vector sector physicalizes F_2^V to meaningful experimental prediction. Within UV theories like SM, that additional term $aieQ_V F^{\mu\nu} V_\mu^+ V_\nu^-$ naturally came out through the gauged covariant derivative approach. Nevertheless, from the EFT point of view, the matter likely springs from the missing piece of the neutral gauge boson.

The other way to cancel the divergence in the extra arbitrary magnetic moment interaction term by the ζ -limiting ($\zeta \rightarrow 0$) formalism is a technical aspect of the field theory discussed by T. D. Lee and C. N. Yang [21], which introduced a negative metric deemed as ghost particle, spin-0 component in vector field with negative norm, provides a way to regulate the theory that would otherwise make the theory non-renormalizable.

¹The MDM's form factor expressions are under the approximation of the heavily charged boson and expand to second order $\mathcal{O}\left(\frac{m_i^2}{m_{V,\phi}^2}\right)$.

We'll see that, if only one chirality is involved, the charged scalar and vector contributions display negative and positive effects, respectively, on the charged ($Q_l < 0$) lepton's anomalous MDM $a_l = \frac{2m_l F_2^{V,\phi}}{-eQ_l}$ value as the l_k is neutral, for instance in the SM context, or some beyond the SM contexts, like leptoquark or lepton number violation interaction structure. Conversely, the oppositely changed sign of effect would happen as the mediator is neutral ($Q_{V,\phi} = 0$) or the positively charged fermion ($Q_k > 1$) inside the loop.

The EDM form factor is achieved by switching out $m_i \rightarrow -m_i$ and $V_L^{*ki} (Y_L^{*ki}) \rightarrow -V_L^{*ki} (Y_L^{*ki})$, roughly speaking

$$G_2^{\phi,V} \propto (m_j - m_i) (R^{*ki} R^{kj} - L^{*ki} L^{kj}) f_1 + m_k (R^{*ki} L^{kj} - L^{*ki} R^{kj}) f_2 \quad (\text{E.23})$$

where L, R are the left and right couplings of the newly introduced charged boson and two form factors f_1, f_2 . In $l_i = l_j$, the electric dipole value obtained from the EDM form factor is only proportional to $(R^* L - L^* R)$. Then if the initial premise, which states that the left and right coupling's relative phase is different by an integer of pi for CP invariance (CPV-free), holds true, the EDM thus equals zero for a completely CPV-free theory.

Appendix F

EFT Coupling Constraints in muon decay experiments

In this chapter, we are going to discuss the constraints within the SM context, where no new charged fermion is introduced, and the non-Lepton Flavor Violation (nLFV) of the coupling scenario equivalent to flavor diagonal coupling is assumed. We also go about investigating two universality and non-universality cases, which eventually lead to some interesting conclusions. In the last section, we will apply the EFT calculation framework to simple coupling patterns inspired by UV models.

F.1 Case of universal coupling

In this numerical analysis, we assumed the universal coupling within flavor-conserved and SM particle conditions. The input parameters used are:

- $\rho = 0.74979(26)$
- $\delta = 0.75047(34)$
- $|\xi| = 1.0009^{+0.0016}_{-0.0007}$
- $G_F^\mu = 1.1663787(6) \times 10^{-5} \text{ GeV}^{-2}$

- $G_F^{Zl^+l^-} = 1.1661(16) \times 10^{-5} \text{ GeV}^{-2}$
- $G_F^Z = 1.1668(11) \times 10^{-5} \text{ GeV}^{-2}$

Considering saying, according to Eq. D.4, the δ in this scenario should be identical to SM's predicted value of $3/4$, leading the universality coupling assumption to be invalid within the 1σ uncertainty regime of Michel parameters. Thus, we hereafter extended the Michel parameters scan to 2σ and used $G_F^{Zl^+l^-}$ extracted from $\Gamma_{l^+l^-}^Z = 83.984(86) \text{ MeV}$ [17, 22] and G_F^Z extracted from $\Gamma_Z = 2.4952(23) \text{ GeV}$ as SM inputs, then attain the plot of the scanned allowable parameter space below.

- For new scalar

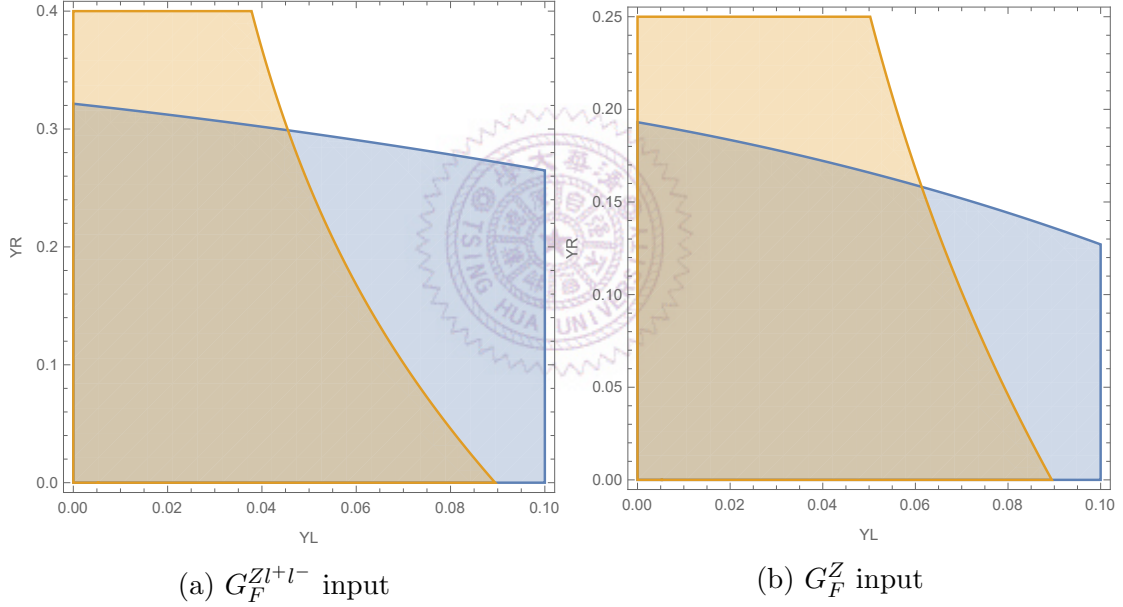


Figure F.1: Yukawa coupling Y satisfies muon decay experiment constraints, we defined $YL \equiv \frac{|Y^L|^2/m_\phi^2}{G_F}$, $YR \equiv \frac{|Y^R|^2/m_\phi^2}{G_F}$. The blue is represented by G_F and the orange one is represented by $|\xi|$ constraints.

- For new vector

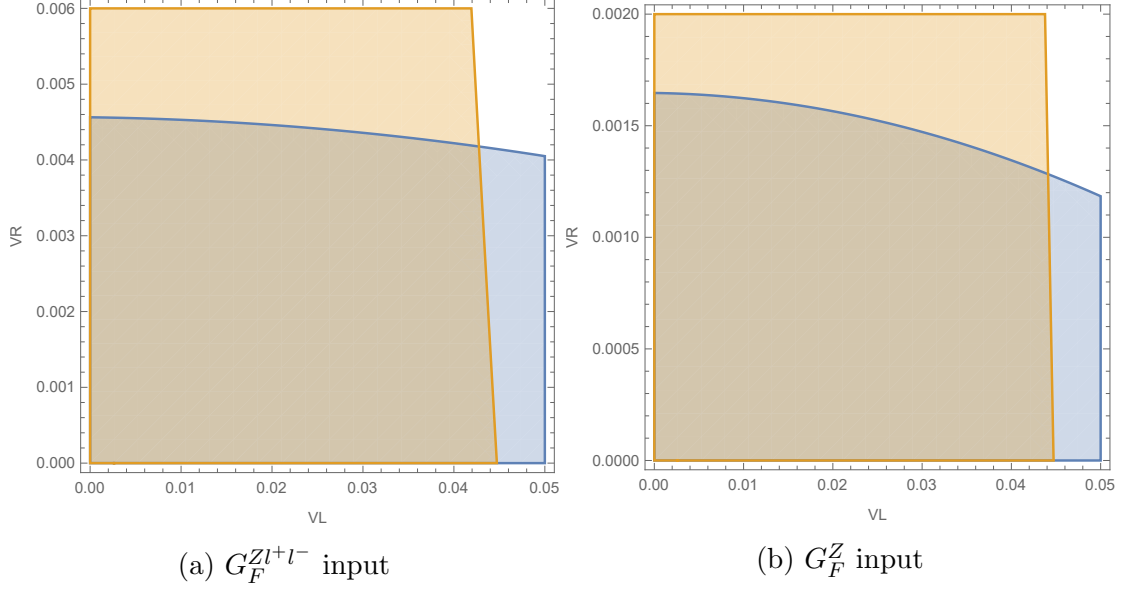


Figure F.2: Vector coupling V satisfies muon decay experiment constraints, we defined $VL \equiv \frac{|V^L|^2/m_V^2}{G_F}$, $VR \equiv \frac{|V^R|^2/m_V^2}{G_F}$. The blue is represented by G_F and the orange one is represented by $|\xi|$ constraints.

Because the parameter ρ takes no significant constraint stacking up ill against the others, we have not plotted it out. The shaded area allows couplings to survive in the new scalar and vector cases depicted in Fig. F.1-F.2, respectively, that is mainly rounded by $|\xi|$ and G_F experiments. The bounded orange region is from $|\xi| = 0.9995$ constraint deviating 2σ from the mean values, whereas the bounded blue region corresponds to $G_F^{Zl^+l^-} = 1.1645 \times 10^{-5}$ or $G_F^Z = 1.1657 \times 10^{-5} \text{ GeV}^{-2}$ at 1σ deviation. The G_F^Z bound from total Z decay demonstrated a stringent compass, henceforth, we are going to use it for studying later. Measuring up to δ and ρ parameters more efficiently, the ξ parameter thus appears to be another quantity sensitive to NP, besides G_F already investigated in most literature.

F.2 a_l contributions from new charged bosons

To simplify BSM anomalies and preserve SM symmetries, including accidental symmetries, the $Q_{V,\phi} = 1$ charged boson is the only candidate considered. Making use of the form factor Eq. E.1 got calculated from Eq. (E.22,E.21) in which we

derive the lepton's anomalous magnetic dipole

$$a_l = \frac{2m_l F_2^{V,\phi}}{e}. \quad (\text{F.1})$$

- The contribution from the scalar field is apparently a negative effect

$$F_2^\phi = \frac{|Y^L|^2 + |Y^R|^2}{16\pi^2} \frac{m_l^4 - 2m_l^2 m_\phi^2 + (-2m_l^2 m_\phi^2 + 2m_\phi^4) \text{Log}\left(\frac{m_\phi^2}{m_\phi^2 - m_l^2}\right)}{2m_l^4} \quad (\text{F.2})$$

$$= -m_l^2 \frac{|Y^L|^2 + |Y^R|^2}{96\pi^2 m_\phi^2} + \mathcal{O}\left(\frac{m_l^3}{m_\phi^3}\right) \quad (\text{F.3})$$

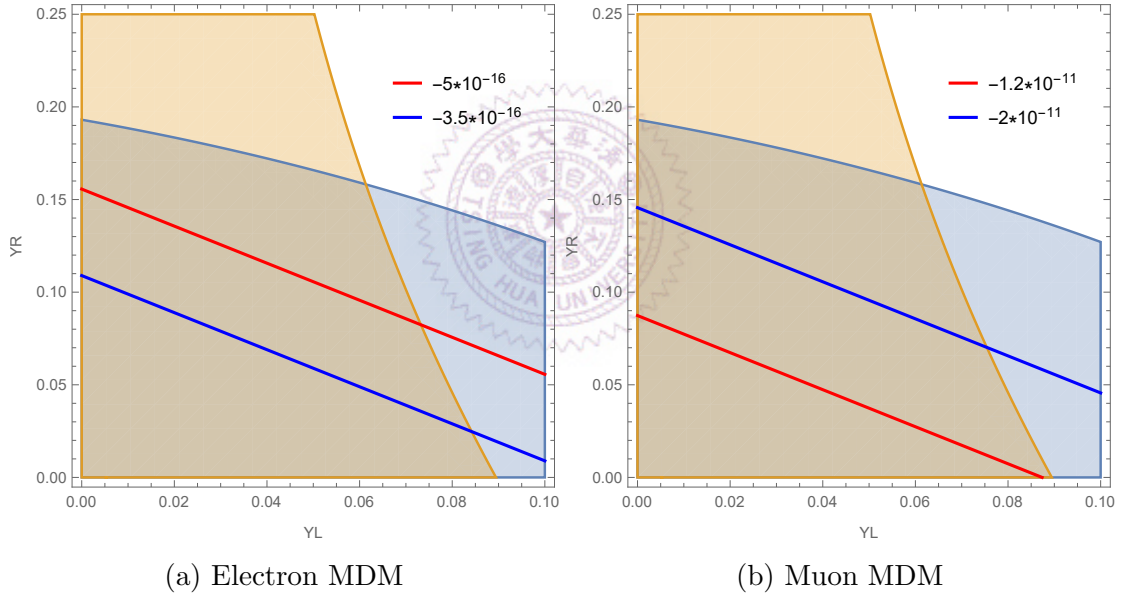


Figure F.3: MDM values from new scalar's contribution in muon decay experiment's constrained region.

- Meanwhile, the contribution from the vector field is positive

$$F_2^V = \frac{|V^L|^2 + |V^R|^2}{16\pi^2} \frac{m_l^6 + 8m_l^4 m_V^2 - 4m_l^2 m_V^4 + 2(3m_l^4 m_V^2 - 5m_l^2 m_V^4 + 2m_V^6) \text{Log}\left(\frac{m_V^2}{m_V^2 - m_l^2}\right)}{2m_l^4 m_V^2} \quad (\text{F.4})$$

$$= 5m_l^2 \frac{|V^L|^2 + |V^R|^2}{48\pi^2 m_V^2} + \mathcal{O}\left(\frac{m_l^3}{m_V^3}\right) \quad (\text{F.5})$$

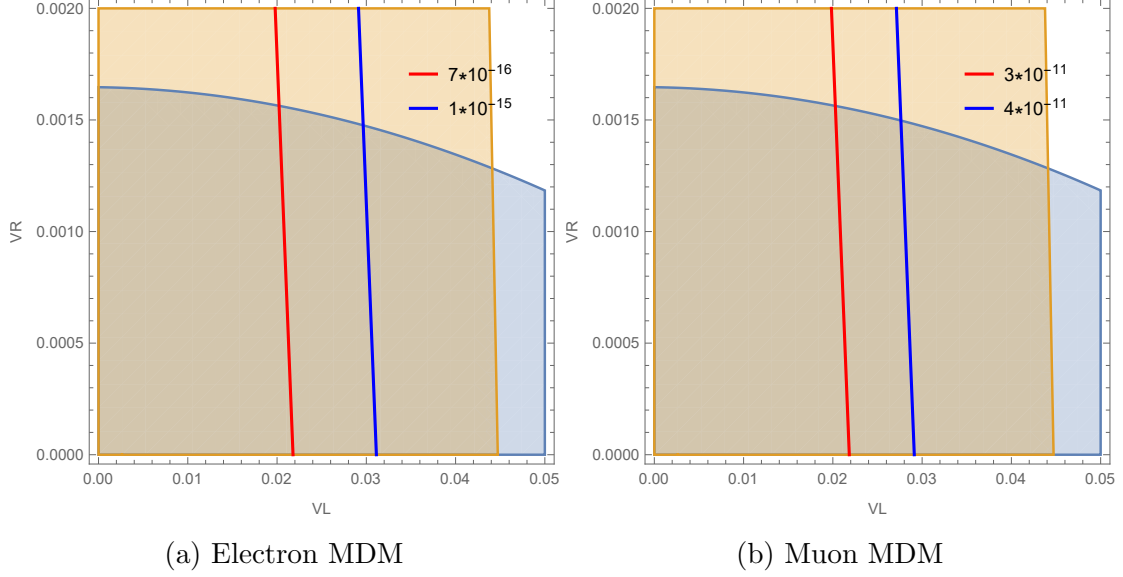


Figure F.4: MDM values from new vector's contribution in muon decay experiment's constrained region.

We can see that the MDM in the scalar case is highly constrained by the Fermi constant extracted from total Z decay, meanwhile, in the vector case, the MDM is inclined to be strongly constrained by the Michel parameter ξ . The allowed region generates merely a smidgen of MDM values, which is not enough to explain the anomaly

$$\Delta a_\mu = (2.74 \pm 0.73) \times 10^{-9} \quad [23] \quad (\text{F.6})$$

$$\Delta a_e = (-88 \pm 36) \times 10^{-14} \quad [24]. \quad (\text{F.7})$$

Frequently, in most research works, where people involved more than just only one charged boson as our simple consideration. Furthermore, the chiral enhancement happens, for example, as described in Eq. 5.4, the neutral scalar is capable of putting forward a solution for the opposite sign effect between muon and electron MDM on that account [10]. Notice that the scalar takes the negative contribution, whilst in contrast, the vector takes the positive contribution.

F.3 Case of non-universal coupling

In the non-universality case, we thus derived the allowed region graph for explaining the electron MDM with the new scalar, hereby, we tuned the coupling of muon to a very small value $\frac{|Y_{\mu\nu\mu}^R|^2}{m_\phi^2} = \frac{|Y_{\mu\nu\mu}^L|^2}{m_\phi^2} = 6 \times 10^{-10}$ so as to get the safe regime in electron couplings space satisfying the electron MDM anomaly.

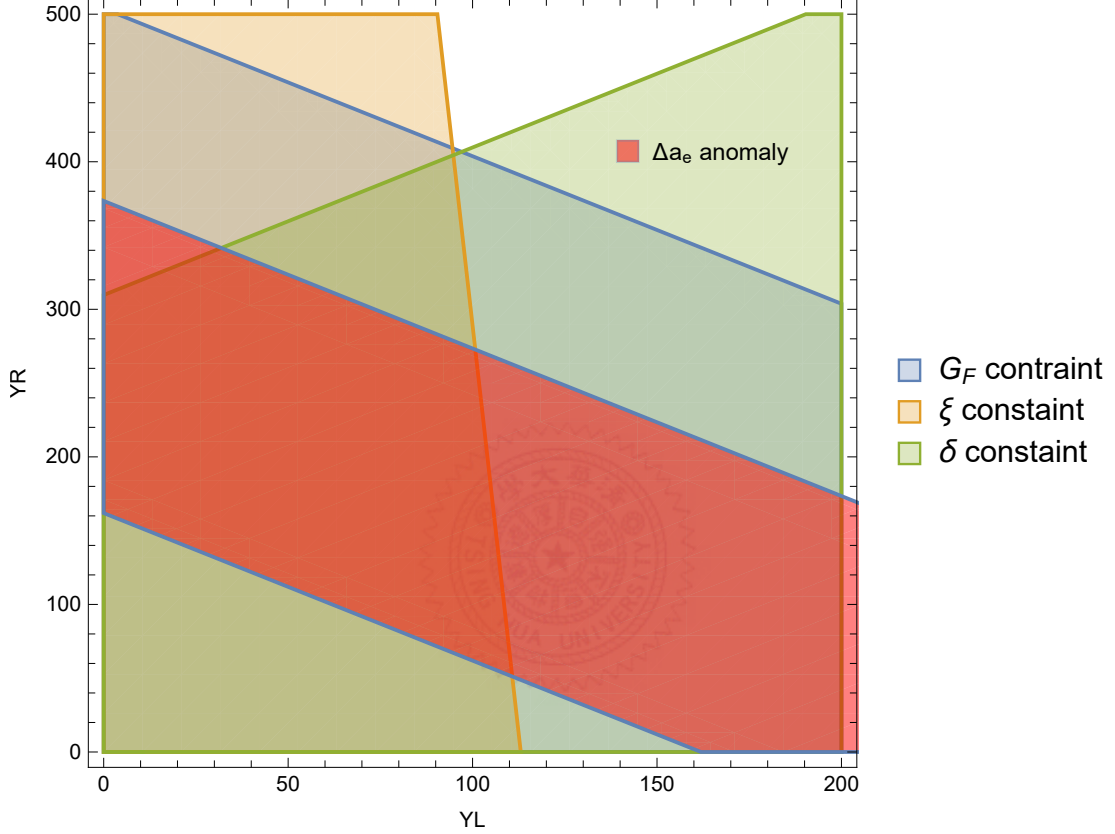


Figure F.5: Electron MDM anomaly in the new scalar's non-universality coupling of the constrained region, we defined $YL \equiv \frac{|Y_{e\nu e}^L|^2/m_\phi^2}{G_F}$, $YR \equiv \frac{|Y_{e\nu e}^R|^2/m_\phi^2}{G_F}$.

Now, the upper bound is no longer constrained by G_F as the universality case, it is instead from the Michel parameter δ constraint. That emphasizes the importance of Michel parameters in probing and constraining the NP. This fine-tuning is frustrating on the theoretical side, as the coupling of the muon is smaller by two orders of magnitude of G_F the Fermi constant, while the electron's coupling is over 100 times larger than the Fermi constant. Owing to the mass hierarchy between electron and muon, speculatively saying, the theory entailing the mass inversely

associated with Yukawa coupling may help reconcile this issue, nonetheless.

Nevertheless, the complicated behavior of constraints is put up in the new vector's non-universality case, in which we chose a benchmark point in the muon coupling regime that satisfies the muon MDM anomaly and then see how the electron couplings are constrained. The same size as G_F is demanded for the vector's couplings pictured in Fig. F.6, which is probably unreasonable given the current experimental evidences.

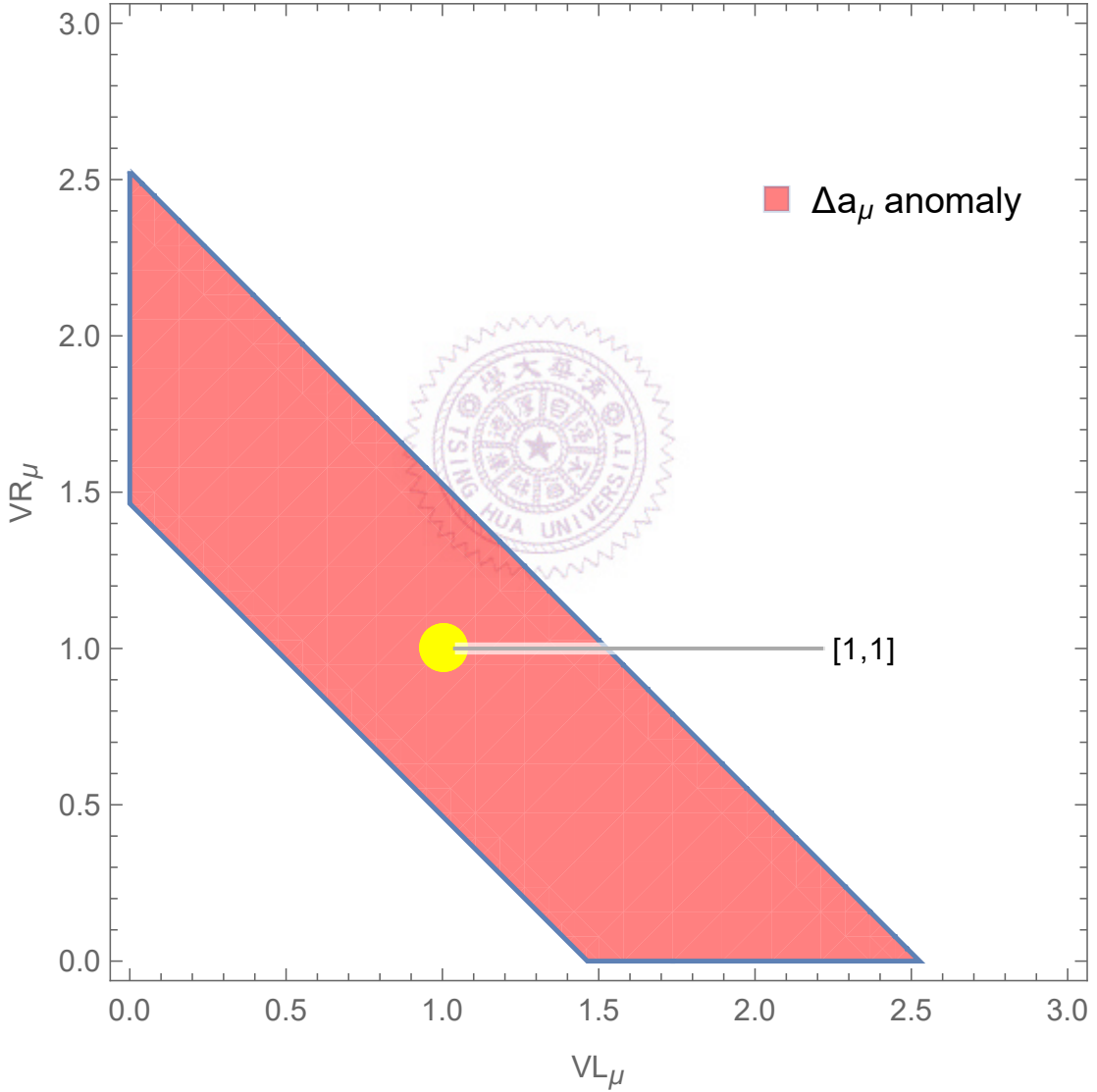


Figure F.6: Muon MDM anomaly's allowed region in the new vector's non-universality coupling case, we defined $VL_\mu \equiv \frac{|V_{\mu\nu\mu}^L|^2/m_V^2}{G_F}$, $VR_\mu \equiv \frac{|V_{\mu\nu\mu}^R|^2/m_V^2}{G_F}$.

Contrary to the new scalar case, the new vector has an interference effect

between the new vector and the SM W^\pm boson, which induces dependence on the relative phase between couplings. Depending on whether the interference is constructive or destructive, which is determined by the value of the relative phase, either the G_F or δ parameter will play the dominant role in imposing constraints.

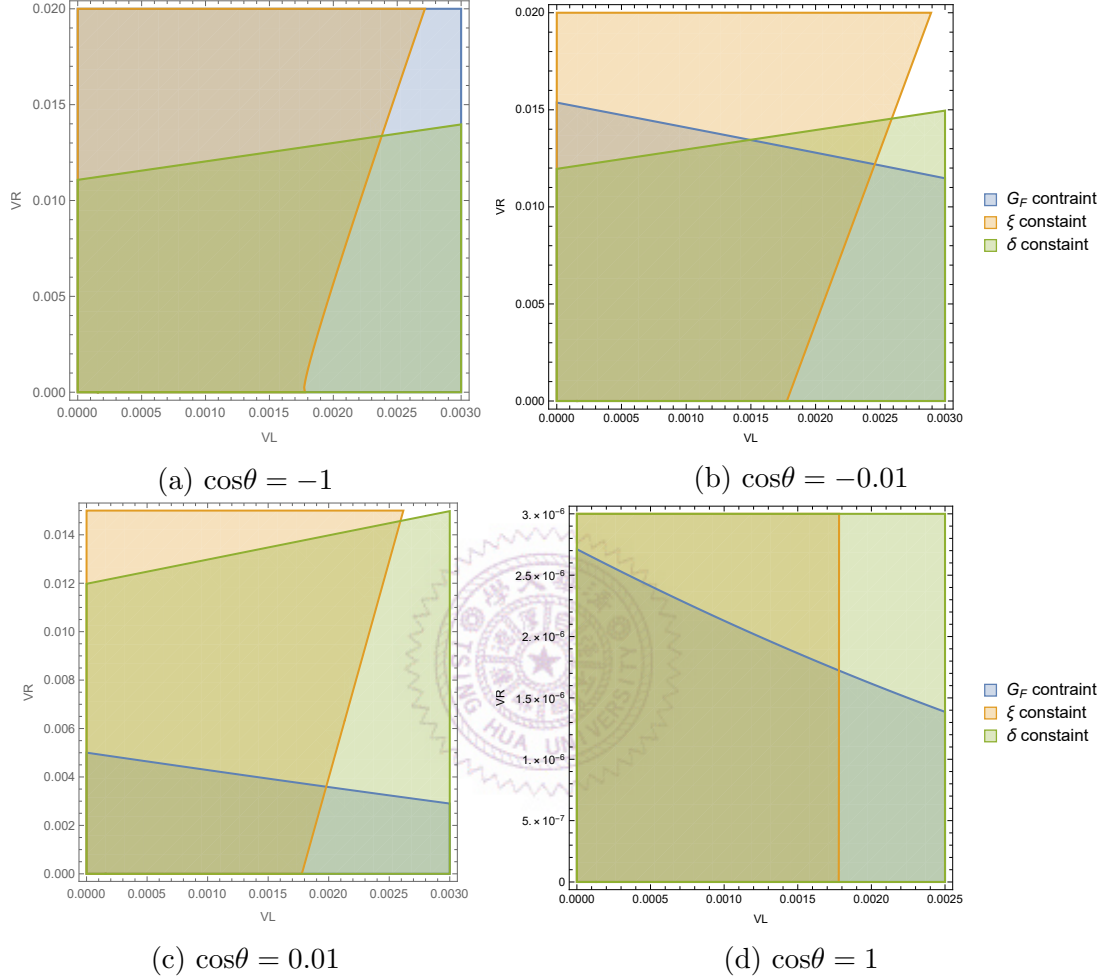


Figure F.7: The new vector non-universality coupling's constrained region, we defined $VL \equiv \frac{|V_{e\nu_e}^L|^2/m_V^2}{G_F}$, $VR \equiv \frac{|V_{e\nu_e}^R|^2/m_V^2}{G_F}$. The angle θ is the relative phase between two couplings, $V_{e\nu_e}^R$ and $V_{\mu\nu_\mu}^{*R}$.

As shown above in Fig. F.7, when $\cos\theta$ is negative, the Michel parameter δ gives a strong constraint on the upper bound. Once $\cos\theta$ turns positive, the G_F constraint dominates and lays down more stringent constraints in the electron coupling space.

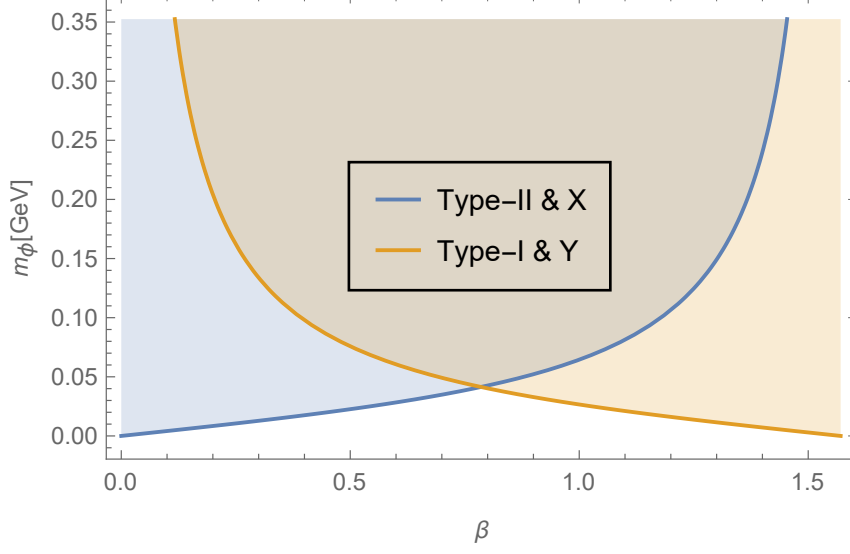


Figure F.8: 2HDM constraint

F.4 Coupling pattern from UV models

In this section, we rely on the pattern from several UV models to set out limits on the mass range search for new particles. In 2HDM, the coupling conformations are summarized in table F.1 involving only one chiral interaction

$$Y^L = -\frac{\sqrt{2}m_l\xi_l}{\langle H_{SM} \rangle}, \quad (\text{F.8})$$

$\langle H_{SM} \rangle$ is the SM VEV mixing, characterized by β angle, between non-trivial vacuum expectations of two Higgs doublets

$$\langle H_{SM} \rangle = \langle H_1 \rangle \sin \beta + \langle H_2 \rangle \cos \beta. \quad (\text{F.9})$$

Following the available procedure derived in this study, the constraint relation of mass and coupling value is shown in Fig F.8.

Type	Description	up-type quarks couple to	down-type quarks couple to	charged leptons couple to	Coupling ξ_i
Type I	Fermiophobic	H_2	H_2	H_2	$\cot \beta$
Type II	MSSM-like ¹	H_2	H_1	H_1	$-\tan \beta$
Type X	Lepton-specific	H_2	H_2	H_1	$-\tan \beta$
Type Y	Flipped	H_2	H_1	H_2	$\cot \beta$

Table F.1: 2HDM type of couplings

On the other hand, the searching mass limit for a heavy W' gauge boson other than SM's W boson can be enhanced by the Muon decay experiment. If considering sequential Standard Model (SSM) models, where the new extended gauge fields share similar properties to that of the SM, couplings with either left or right-handed are SM-like coupling

$$V^R (V^L) = g/\sqrt{2}. \quad (\text{F.10})$$

From Fig F.2, we can readily extract the lower bound of the new gauge boson mass for SSM models. The relatively strong lower limits on the mass scale for the W' boson with only left-handed and only right-handed couplings are 3.3 TeV and 637 GeV, respectively. These limits are compared to the 2016 PDG values of 3.7 TeV for left-handed coupling and 715 GeV for right-handed coupling.

These analyses serve as a test bed and provide formulas for further study. No less pivotal, the precise measurements offered by Muon decay experiments, demonstrate that here is a promising source of NP's constraint and detection.

Appendix G

$L \rightarrow l\gamma$ form factor full expression

In what follows we will present the full expression in terms of PV functions of form factor in Appendix E.

G.1 Charged vector form factors of diagrams Fig. E.1

1. Diagram a

- Dirac form factor

$$\begin{aligned}
 F_1^{V,a} = & \frac{-eQ_V}{2m_V^2} \left\{ 3 (V_{ik}^R V_{jk}^{*L} + V_{ik}^L V_{jk}^{*R}) (m_1 + m_2) m_k m_V^2 \sum_{i=0}^2 C_i^{V,a} + \right. \\
 & (V_{ik}^L V_{jk}^{*L} + V_{ik}^R V_{jk}^{*R}) \left[\sum_{i=1}^2 \left(\frac{m_1^3 m_2^3}{m_i^2} + m_V^2 \left(2m_1 m_2 + m_i^2 + 3 \frac{m_1^2 m_2^2}{m_i^2} \right) - m_1^2 m_2^2 \right) C_i^{V,a} - \right. \\
 & \sum_{i,j=1}^2 \left(\frac{m_1^4 m_2^4}{m_i^4} - 3 \frac{m_1^3 m_2^3}{m_i^2} - m_V^2 \left(2m_1 m_2 + 4 \frac{m_1^2 m_2^2}{m_i^2} \right) + 2m_1^2 m_2^2 \right) C_{ij}^{V,a} - \\
 & 2 (m_1^2 + m_2^2 + 5m_1 m_2 - 6m_V^2) C_{00}^{V,a} - 6 \sum_{i=1}^2 \left(2 \frac{m_1^2 m_2^2}{m_i^2} - 3m_1 m_2 + m_i^2 \right) C_{00i}^{V,a} - \\
 & \sum_{i,j,k=1}^2 \left(m_1^4 m_2^4 \left(\frac{1}{m_i^4} + \frac{1}{m_j^2 m_k^2} \right) - 3 \frac{m_1^3 m_2^3}{m_i^2} + m_1^2 m_2^2 \right) C_{ijk}^{V,a} - \sum_{i,j=1}^2 \left(14 \frac{m_1^2 m_2^2}{m_i^2} - 8m_1 m_2 \right) C_{00ij}^{V,a} - \\
 & \left. \sum_{i,j,k,l=1}^2 \left(2 \frac{m_1^4 m_2^4}{m_i^2 m_j^2} - \frac{m_1^3 m_2^3}{m_i^2} \right) C_{ijkl}^{V,a} - \frac{(2m_1^2 - 7m_1 m_2 + 2m_2^2 - 6m_k^2 - 4m_V^2)^2}{4} \right] \Bigg\}. \tag{G.1}
 \end{aligned}$$

- Anapole form factor

$$\begin{aligned}
G_1^{V,a} = & \frac{-eQ_V}{2m_V^2} \left\{ 3 (V_{ik}^R V_{jk}^{*L} - V_{ik}^L V_{jk}^{*R}) (m_1 - m_2) m_k m_V^2 \sum_{i=0}^2 C_i^{V,a} + \right. \\
& (V_{ik}^R V_{jk}^{*R} - V_{ik}^L V_{jk}^{*L}) \left[\sum_{i=1}^2 \left(\frac{m_1^3 m_2^3}{m_i^2} + m_V^2 \left(2m_1 m_2 - m_i^2 - 3 \frac{m_1^2 m_2^2}{m_i^2} \right) + m_1^2 m_2^2 \right) C_i^{V,a} + \right. \\
& \sum_{i,j=1}^2 \left(\frac{m_1^4 m_2^4}{m_i^4} + 3 \frac{m_1^3 m_2^3}{m_i^2} - m_V^2 \left(4 \frac{m_1^2 m_2^2}{m_i^2} - 2m_1 m_2 \right) + 2m_1^2 m_2^2 \right) C_{ij}^{V,a} + \\
& 2 (m_1^2 + m_2^2 + 5m_1 m_2 - 6m_V^2) C_{00}^{V,a} + 6 \sum_{i=1}^2 \left(2 \frac{m_1^2 m_2^2}{m_i^2} + 3m_1 m_2 + m_i^2 \right) C_{00i}^{V,a} + \\
& \sum_{i,j,k=1}^2 \left(m_1^4 m_2^4 \left(\frac{1}{m_i^4} + \frac{1}{m_j^2 m_k^2} \right) + 3 \frac{m_1^3 m_2^3}{m_i^2} + m_1^2 m_2^2 \right) C_{ijk}^{V,a} + \sum_{i,j=1}^2 \left(14 \frac{m_1^2 m_2^2}{m_i^2} + 8m_1 m_2 \right) C_{00ij}^{V,a} + \\
& \left. \sum_{i,j,k,l=1}^2 \left(2 \frac{m_1^4 m_2^4}{m_i^2 m_j^2} + \frac{m_1^3 m_2^3}{m_i^2} \right) C_{ijkl}^{V,a} + \frac{(2m_1^2 - m_1 m_2 + 2m_2^2 - 6m_k^2 - 4m_V^2)^2}{4} \right\}. \tag{G.2}
\end{aligned}$$

- MDM form factor

$$\begin{aligned}
F_2^{V,a} = & \frac{-eQ_V}{4m_V^2} \left\{ (V_{ik}^R V_{jk}^{*L} + V_{ik}^L V_{jk}^{*R}) m_k \left[(m_1^2 + m_2^2 - 4m_V^2) C_0^{V,a} + \right. \right. \\
& \sum_{i=1}^2 \left(3 \frac{m_1^2 m_2^2}{m_i^2} + m_i^2 - 6m_V^2 \right) C_i^{V,a} + 8C_{00}^{V,a} + 2 \sum_{i,j=1}^2 \frac{m_1^2 m_2^2}{m_i^2} C_{ij}^{V,a} - 1 \Big] - \\
& (V_{ik}^L V_{jk}^{*L} + V_{ik}^R V_{jk}^{*R}) \left[\sum_{i=1}^2 \left(\frac{m_1^3 m_2^3}{m_i^3} - m_1 m_2 m_i + 2m_V^2 \frac{m_1 m_2}{m_i} \right) C_i^{V,a} + 8(m_1 + m_2) C_{00}^{V,a} + \right. \\
& \sum_{i,j=1}^2 \left(\frac{m_1^3 m_2^3}{m_i^3} + 2 \frac{m_1^3 m_2^3}{m_i m_j^2} - m_1 m_2 m_i + 4m_V^2 \frac{m_1 m_2}{m_i} \right) C_{ij}^{V,a} + 24 \sum_{i=1}^2 \frac{m_1 m_2}{m_i} C_{00i}^{V,a} + \\
& 4 \sum_{i,j,k=1}^2 \frac{m_1^3 m_2^3}{m_i m_j^2} C_{ijk}^{V,a} + 2 \sum_{i,j,k,l=1}^2 \frac{m_1^3 m_2^3}{m_i m_j^2} C_{ijkl}^{V,a} + 16 \sum_{i,j=1}^2 \frac{m_1 m_2}{m_i} C_{00ij}^{V,a} - \frac{7}{12} (m_1 + m_2) \Big] \Big\} - \\
& \frac{aeQ_V}{4m_V^2} \left\{ (V_{ik}^L V_{jk}^{*L} + V_{ik}^R V_{jk}^{*R}) (m_1 + m_2) \left[\sum_{i=1}^2 \left(\frac{m_1^2 m_2^2}{m_i^2} - m_1 m_2 + 2m_V^2 \right) C_i^{V,a} + 4C_{00}^{V,a} + \right. \right. \\
& \sum_{i,j=1}^2 \left(\frac{m_1^2 m_2^2}{m_i^2} - m_1 m_2 \right) C_{ij}^{V,a} \Big] - (V_{ik}^R V_{jk}^{*L} + V_{ik}^L V_{jk}^{*R}) m_k \left[((m_1 - m_2)^2 - 4m_V^2) C_0^{V,a} + \right. \\
& \left. \sum_{i=1}^2 \frac{(m_1 m_2 - m_i^2)(3m_1 m_2 - m_i^2)}{m_i^2} C_i^{V,a} + 8C_{00}^{V,a} + 2 \sum_{i,j=1}^2 \left(\frac{m_1^2 m_2^2}{m_i^2} - m_1 m_2 \right) C_{ij}^{V,a} \right] \Big\}. \tag{G.3}
\end{aligned}$$

- EDM form factor

$$\begin{aligned}
G_2^{V,a} = & \frac{-eQ_V}{4m_V^2} \left\{ (V_{ik}^L V_{jk}^{*R} - V_{ik}^R V_{jk}^{*L}) m_k \left[(m_1^2 + m_2^2 - 4m_V^2) C_0^{V,a} + \right. \right. \\
& \sum_{i=1}^2 \left(3 \frac{m_1^2 m_2^2}{m_i^2} + m_i^2 - 6m_V^2 \right) C_i^{V,a} + 8C_{00}^{V,a} + 2 \sum_{i,j=1}^2 \frac{m_1^2 m_2^2}{m_i^2} C_{ij}^{V,a} - 1 \Big] + \\
& (V_{ik}^L V_{jk}^{*L} - V_{ik}^R V_{jk}^{*R}) \left[\sum_{i=1}^2 (-1)^i \left(\frac{m_1^3 m_2^3}{m_i^3} - m_1 m_2 m_i + 2m_V^2 \frac{m_1 m_2}{m_i} \right) C_i^{V,a} + 8(m_1 - m_2) C_{00}^{V,a} + \right. \\
& \sum_{i,j=1}^2 (-1)^i \left(\frac{m_1^3 m_2^3}{m_i^3} + 2 \frac{m_1^3 m_2^3}{m_i m_j^2} - m_1 m_2 m_i + 4m_V^2 \frac{m_1 m_2}{m_i} \right) C_{ij}^{V,a} + 24 \sum_{i=1}^2 (-1)^i \frac{m_1 m_2}{m_i} C_{00i}^{V,a} + \\
& \left. \left. 2 \sum_{i,j,k,l=1}^2 (-1)^i \frac{m_1^3 m_2^3}{m_i m_j^2} (C_{ijk}^{V,a} + C_{ijkl}^{V,a}) + 16 \sum_{i,j=1}^2 (-1)^i \frac{m_1 m_2}{m_i} C_{00ij}^{V,a} - \frac{7}{12} (m_1 - m_2) \right] \right\} - \\
& \frac{aeQ_V}{4m_V^2} \left\{ (V_{ik}^R V_{jk}^{*R} - V_{ik}^L V_{jk}^{*L}) (m_1 - m_2) \left[\sum_{i=1}^2 \left(\frac{m_1^2 m_2^2}{m_i^2} + m_1 m_2 + 2m_V^2 \right) C_i^{V,a} + 4C_{00}^{V,a} + \right. \right. \\
& \sum_{i,j=1}^2 \left(\frac{m_1^2 m_2^2}{m_i^2} + m_1 m_2 \right) C_{ij}^{V,a} \Big] + (V_{ik}^R V_{jk}^{*L} - V_{ik}^L V_{jk}^{*R}) m_k \left[((m_1 + m_2)^2 - 4m_V^2) C_0^{V,a} + \right. \\
& \left. \sum_{i=1}^2 \frac{(m_1 m_2 + m_i^2)(3m_1 m_2 + m_i^2)}{m_i^2} C_i^{V,a} + 8C_{00}^{V,a} + 2 \sum_{i,j=1}^2 \left(\frac{m_1^2 m_2^2}{m_i^2} + m_1 m_2 \right) C_{ij}^{V,a} \right] \Big\}. \tag{G.4}
\end{aligned}$$

As being showed above, only $F_2^{V,a}$ and $G_2^{V,a}$ get contribution from $ieQ_V a F^{\mu\nu} V_\mu^+ V_\nu^-$ which corresponds to the tree-level magnetic dipole moment, and for renormalization $F_2^{V,a}, G_2^{V,a}$, set $a = 1$.

2. Diagram b

- Dirac form factor

$$\begin{aligned}
F_1^{V,b} = & \frac{eQ_l}{2(m_1 - m_2)m_V^2} \left\{ (V_{ik}^R V_{jk}^{*L} + V_{ik}^L V_{jk}^{*R}) m_k \left[(m_1^2 - 4m_V^2) B_0^{V,b} + 2m_1^2 B_1^{V,b} + \right. \right. \\
& m_1^2 B_{11}^{V,b} + 4B_{00}^{V,b} + \frac{1}{6} (m_1^2 - 3m_k^2 + 15m_V^2) \Big] - (V_{ik}^L V_{jk}^{*L} + V_{ik}^R V_{jk}^{*R}) m_1 \left[(m_1^2 + 2m_V^2) B_1^{V,b} + \right. \\
& \left. \left. 2m_1^2 B_{11}^{V,b} + m_1^2 B_{111}^{V,b} + 8B_{00}^{V,b} + 6B_{001}^{V,b} + \frac{1}{12} (3m_1^2 - 10m_k^2 + 4m_V^2) \right] \right\}. \tag{G.5}
\end{aligned}$$

- Anapole form factor

$$\begin{aligned}
G_1^{V,b} = & \frac{eQ_l}{2(m_1 + m_2)m_V^2} \left\{ (V_{ik}^R V_{jk}^{*L} - V_{ik}^L V_{jk}^{*R}) m_k \left[(m_1^2 - 4m_V^2) B_0^{V,b} + 2m_1^2 B_1^{V,b} + \right. \right. \\
& m_1^2 B_{11}^{V,b} + 4B_{00}^{V,b} + \frac{1}{6} (m_1^2 - 3m_k^2 + 15m_V^2) \left. \right] - (V_{ik}^L V_{jk}^{*L} - V_{ik}^R V_{jk}^{*R}) m_1 \left[(m_1^2 + 2m_V^2) B_1^{V,b} + \right. \\
& \left. \left. 2m_1^2 B_{11}^{V,b} + m_1^2 B_{111}^{V,b} + 8B_{00}^{V,b} + 6B_{001}^{V,b} + \frac{1}{12} (3m_1^2 - 10m_k^2 + 4m_V^2) \right] \right\}.
\end{aligned} \tag{G.6}$$

3. Diagram c

- Dirac form factor

$$\begin{aligned}
F_1^{V,c} = & \frac{eQ_l}{2(m_2 - m_1)m_V^2} \left\{ (V_{ik}^R V_{jk}^{*L} + V_{ik}^L V_{jk}^{*R}) m_k \left[(m_2^2 - 4m_V^2) B_0^{V,c} + 2m_2^2 B_1^{V,c} + \right. \right. \\
& m_2^2 B_{11}^{V,c} + 4B_{00}^{V,c} + \frac{1}{6} (m_2^2 - 3m_k^2 + 15m_V^2) \left. \right] - (V_{ik}^L V_{jk}^{*L} + V_{ik}^R V_{jk}^{*R}) m_2 \left[(m_2^2 + 2m_V^2) B_1^{V,c} + \right. \\
& \left. \left. 2m_2^2 B_{11}^{V,c} + m_2^2 B_{111}^{V,c} + 8B_{00}^{V,c} + 6B_{001}^{V,c} + \frac{1}{12} (3m_2^2 - 10m_k^2 + 4m_V^2) \right] \right\}.
\end{aligned} \tag{G.7}$$

- Anapole form factor

$$\begin{aligned}
G_1^{V,c} = & \frac{-eQ_l}{2(m_2 + m_1)m_V^2} \left\{ (V_{ik}^R V_{jk}^{*L} - V_{ik}^L V_{jk}^{*R}) m_k \left[(m_2^2 - 4m_V^2) B_0^{V,c} + 2m_2^2 B_1^{V,c} + \right. \right. \\
& m_2^2 B_{11}^{V,c} + 4B_{00}^{V,c} + \frac{1}{6} (m_2^2 - 3m_k^2 + 15m_V^2) \left. \right] + (V_{ik}^L V_{jk}^{*L} - V_{ik}^R V_{jk}^{*R}) m_2 \left[(m_2^2 + 2m_V^2) B_1^{V,c} + \right. \\
& \left. \left. 2m_2^2 B_{11}^{V,c} + m_2^2 B_{111}^{V,c} + 8B_{00}^{V,c} + 6B_{001}^{V,c} + \frac{1}{12} (3m_2^2 - 10m_k^2 + 4m_V^2) \right] \right\}.
\end{aligned} \tag{G.8}$$

4. Diagram d

- Dirac form factor

$$\begin{aligned}
F_1^{V,d} = \frac{eQ_k}{2m_V^2} & \left\{ (V_{ik}^R V_{jk}^{*L} + V_{ik}^L V_{jk}^{*R}) (m_1 + m_2) m_k \left[-4m_V^2 \sum_{i=0}^2 C_i^{V,d} + 4C_{00}^{V,d} + 6 \sum_{i=1}^2 C_{00i}^{V,d} + \right. \right. \\
& \sum_{i,j=1}^2 \frac{m_1^2 m_2^2}{m_i^2} \left(C_{ij}^{V,d} + \sum_{k=1}^2 C_{ijk}^{V,d} \right) - \frac{1}{6} \Big] + (V_{ik}^L V_{jk}^{*L} + V_{ik}^R V_{jk}^{*R}) \left[\frac{1}{24} (7m_1^2 + 7m_2^2 + 12m_1 m_2 - \right. \\
& 28m_k^2 + 28m_V^2) + 2m_V^2 \sum_{i=0}^2 \left(\frac{(i-1)(i-2)}{2} (m_k^2 - m_1 m_2) + 2m_1 m_2 \right) C_i^{V,d} - \\
& 2(m_1 m_2 + m_k^2 + 2m_V^2) C_{00}^{V,d} + 12 \sum_{i=1}^2 \frac{m_1^2 m_2^2}{m_i^2} \left(C_{00i}^{V,d} + \sum_{j=1}^2 C_{00ij}^{V,d} \right) + \\
& \left. \left. \sum_{i,j=1}^2 \left[m_1 m_2 (m_k^2 + 2m_V^2) + \frac{m_1^4 m_2^4}{m_i^2 m_j^2} \right] C_{ij}^{V,d} + \sum_{i,j,k=1}^2 \frac{m_1^4 m_2^4}{m_i^2 m_j^2} \left(C_{ijk}^{V,d} + \sum_{l=1}^2 C_{ijkl}^{V,d} \right) + 24C_{0000}^{V,d} \right] \right\}. \tag{G.9}
\end{aligned}$$

• Anapole form factor

$$\begin{aligned}
G_1^{V,d} = \frac{eQ_k}{2m_V^2} & \left\{ (V_{ik}^R V_{jk}^{*L} - V_{ik}^L V_{jk}^{*R}) (m_1 - m_2) m_k \left[-4m_V^2 \sum_{i=0}^2 C_i^{V,d} + 4C_{00}^{V,d} + 6 \sum_{i=1}^2 C_{00i}^{V,d} + \right. \right. \\
& \sum_{i,j=1}^2 \frac{m_1^2 m_2^2}{m_i^2} \left(C_{ij}^{V,d} + \sum_{k=1}^2 C_{ijk}^{V,d} \right) - \frac{1}{6} \Big] + (V_{ik}^R V_{jk}^{*R} - V_{ik}^L V_{jk}^{*L}) \left[\frac{1}{24} (-3m_1^2 - 3m_2^2 + \right. \\
& 12m_1 m_2 + 28m_k^2 - 28m_V^2) + 2m_V^2 \sum_{i=0}^2 \left(\frac{(1-i)(i-2)}{2} (m_k^2 + m_1 m_2) + 2m_1 m_2 \right) C_i^{V,d} + \\
& 2(-m_1 m_2 + m_k^2 + 2m_V^2) C_{00}^{V,d} - 12 \sum_{i=1}^2 \frac{m_1^2 m_2^2}{m_i^2} \left(C_{00i}^{V,d} + \sum_{j=1}^2 C_{00ij}^{V,d} \right) + \\
& \left. \left. \sum_{i,j=1}^2 \left(m_1 m_2 (m_k^2 + 2m_V^2) - \frac{m_1^4 m_2^4}{m_i^2 m_j^2} \right) C_{ij}^{V,d} - \sum_{i,j,k=1}^2 \frac{m_1^4 m_2^4}{m_i^2 m_j^2} \left(C_{ijk}^{V,d} + \sum_{l=1}^2 C_{ijkl}^{V,d} \right) - 24C_{0000}^{V,d} \right] \right\}. \tag{G.10}
\end{aligned}$$

• MDM form factor

$$\begin{aligned}
F_2^{V,d} = \frac{eQ_k}{2m_V^2} & \left\{ (V_{ik}^R V_{jk}^{*L} + V_{ik}^L V_{jk}^{*R}) m_k \left[4m_V^2 \sum_{i=0}^2 C_i^{V,d} + 4C_{00}^{V,d} + \sum_{ij=1}^2 \left(m_1 m_2 - \frac{m_1^2 m_2^2}{m_i^2} \right) C_{ij}^{V,d} - \right. \right. \\
& 6 \sum_{i=1}^2 C_{00i}^{V,d} - \sum_{i,j,k=1}^2 \frac{m_1^2 m_2^2}{m_i^2} C_{ijk}^{V,d} - \frac{1}{3} \Big] + (V_{ik}^L V_{jk}^{*L} + V_{ik}^R V_{jk}^{*R}) \left[-m_V^2 \sum_{i=1}^2 \left(4 \frac{m_1 m_2}{m_i} + 2m_i \right) C_i^{V,d} - \right. \\
& 2m_V^2 (m_1 + m_2) C_0^{V,d} + \sum_{i,j=1}^2 \left(-\frac{m_1 m_2}{m_i} (m_k^2 + 2m_V^2) + \frac{m_1^2 m_2^2}{m_i^2} m_j \right) C_{ij}^{V,d} + 2(m_1 + m_2) C_{00}^{V,d} + \\
& \left. \left. \sum_{i,j,k=1}^2 \frac{m_1^2 m_2^2}{m_j^2} m_i C_{ijk}^{V,d} + 6 \sum_{i=1}^2 m_i C_{00i}^{V,d} + \frac{m_1 + m_2}{6} \right] \right\}. \tag{G.11}
\end{aligned}$$

- EDM form factor

$$\begin{aligned}
G_2^{V,d} = \frac{eQ_k}{2m_V^2} & \left\{ (V_{ik}^L V_{jk}^{*R} - V_{ik}^R V_{jk}^{*L}) m_k \left[4m_V^2 \sum_{i=0}^2 C_i^{V,d} - 4C_{00}^{V,d} + \sum_{ij=1}^2 \left(m_1 m_2 - \frac{m_1^2 m_2^2}{m_i^2} \right) C_{ij}^{V,d} - \right. \right. \\
& 6 \sum_{i=1}^2 C_{00i}^{V,d} + \sum_{i,j,k=1}^2 \frac{m_1^2 m_2^2}{m_i^2} C_{ijk}^{V,d} + \frac{1}{3} \left. \right] + (V_{ik}^R V_{jk}^{*R} - V_{ik}^L V_{jk}^{*L}) \left[-m_V^2 \sum_{i=1}^2 \left(4 \frac{m_1 m_2}{m_i} - 2m_i \right) C_i^{V,d} - \right. \\
& 2m_V^2 (m_1 - m_2) C_0^{V,d} - \sum_{i,j=1}^2 (-1)^i \left(\frac{m_1 m_2}{m_i} (m_k^2 + 2m_V^2) + \frac{m_1^2 m_2^2}{m_i^2} m_j \right) C_{ij}^{V,d} + 2(m_1 - m_2) C_{00}^{V,d} - \\
& \left. \left. \sum_{i,j,k=1}^2 (-1)^i \frac{m_1^2 m_2^2}{m_j^2} m_i C_{ijk}^{V,d} - 6 \sum_{i=1}^2 (-1)^i m_i C_{00i}^{V,d} + \frac{m_1 - m_2}{6} \right] \right\}. \tag{G.12}
\end{aligned}$$

G.2 Charged scalar form factor of diagrams Fig. E.2

1. Diagram a

- Dirac form factor

$$\begin{aligned}
F_1^{\phi,a} = \frac{eQ_\phi}{2} & \left\{ (Y_{ik}^R Y_{jk}^{*L} + Y_{ik}^L Y_{jk}^{*R}) (m_1 + m_2) m_k \sum_{i=0}^2 C_i^{\phi,a} - \right. \\
& (Y_{ik}^L Y_{jk}^{*L} + Y_{ik}^R Y_{jk}^{*R}) \left[(m_1 + m_2) \sum_{i,j=1}^2 \frac{m_1 m_2}{m_i} \left(\frac{C_i^{\phi,a}}{2} + C_{ij}^{\phi,a} \right) + 2C_{00}^{\phi,a} \right] \left. \right\}. \tag{G.13}
\end{aligned}$$

- Anapole form factor

$$\begin{aligned}
G_1^{\phi,a} = \frac{eQ_\phi}{2} & \left\{ (Y_{ik}^L Y_{jk}^{*R} - Y_{ik}^R Y_{jk}^{*L}) (m_1 - m_2) m_k \sum_{i=0}^2 C_i^{\phi,a} + \right. \\
& (Y_{ik}^L Y_{jk}^{*L} - Y_{ik}^R Y_{jk}^{*R}) \left[\sum_{i,j=1}^2 \left(\frac{m_1^2 m_2^2}{m_i^2} - m_1 m_2 \right) \left(\frac{C_i^{\phi,a}}{2} + C_{ij}^{\phi,a} \right) + 2C_{00}^{\phi,a} \right] \left. \right\}. \tag{G.14}
\end{aligned}$$

- MDM form factor

$$\begin{aligned}
F_2^{\phi,a} = \frac{eQ_\phi}{2} & \left[(Y_{ik}^L Y_{jk}^{*L} + Y_{ik}^R Y_{jk}^{*R}) \sum_{i,j=1}^2 \frac{m_1 m_2}{m_i} \left(\frac{C_i^{\phi,a}}{2} + C_{ij}^{\phi,a} \right) - \right. \\
& \left. (Y_{ik}^R Y_{jk}^{*L} + Y_{ik}^L Y_{jk}^{*R}) m_k \sum_{i=0}^2 C_i^{\phi,a} \right]. \tag{G.15}
\end{aligned}$$

- EDM form factor

$$G_2^{\phi,a} = \frac{eQ_\phi}{2} \left[(Y_{ik}^L Y_{jk}^{*L} - Y_{ik}^R Y_{jk}^{*R}) \sum_{i,j=1}^2 (-1)^i \frac{m_1 m_2}{m_i} \left(\frac{C_i^{\phi,a}}{2} + C_{ij}^{\phi,a} \right) + (Y_{ik}^L Y_{jk}^{*R} - Y_{ik}^R Y_{jk}^{*L}) m_k \sum_{i=0}^2 C_i^{\phi,a} \right]. \quad (\text{G.16})$$

2. Diagram b

- Dirac form factor

$$F_1^{\phi,b} = \frac{eQ_l}{2(m_1 - m_2)} \left[m_k (Y_{ik}^R Y_{jk}^{*L} + Y_{ik}^L Y_{jk}^{*R}) B_0^{\phi,b} - m_1 (Y_{ik}^L Y_{jk}^{*L} + Y_{ik}^R Y_{jk}^{*R}) B_1^{\phi,b} \right]. \quad (\text{G.17})$$

- Anapole form factor

$$G_1^{\phi,b} = \frac{-eQ_l}{2(m_1 + m_2)} \left[m_k (Y_{ik}^R Y_{jk}^{*L} - Y_{ik}^L Y_{jk}^{*R}) B_0^{\phi,b} - m_1 (Y_{ik}^L Y_{jk}^{*L} - Y_{ik}^R Y_{jk}^{*R}) B_1^{\phi,b} \right]. \quad (\text{G.18})$$

3. Diagram c

- Dirac form factor

$$F_1^{\phi,c} = \frac{-e}{2(m_2 - m_1)} \left[m_k (Y_{ik}^R Y_{jk}^{*L} + Y_{ik}^L Y_{jk}^{*R}) B_0^{\phi,c} - m_2 (Y_{ik}^L Y_{jk}^{*L} + Y_{ik}^R Y_{jk}^{*R}) B_1^{\phi,c} \right]. \quad (\text{G.19})$$

- Anapole form factor

$$G_1^{\phi,c} = \frac{-e}{2(m_2 + m_1)} \left[m_k (Y_{ik}^R Y_{jk}^{*L} - Y_{ik}^L Y_{jk}^{*R}) B_0^{\phi,c} + m_2 (Y_{ik}^L Y_{jk}^{*L} - Y_{ik}^R Y_{jk}^{*R}) B_1^{\phi,c} \right]. \quad (\text{G.20})$$

4. Diagram d

- Dirac form factor

$$F_1^{\phi,d} = \frac{eQ_k}{2} \left\{ (Y_{ik}^R Y_{jk}^{*L} + Y_{ik}^L Y_{jk}^{*R}) (m_1 + m_2) m_k \sum_{i=0}^2 C_i^{\phi,d} + \right. \\ \left. (Y_{ik}^L Y_{jk}^{*L} + Y_{ik}^R Y_{jk}^{*R}) \left[(m_1 m_2 + m_k^2) C_0^{\phi,d} + m_1 m_2 \sum_{i,j=1}^2 (C_i^{\phi,d} + C_{ij}^{\phi,d}) - 2C_{00}^{\phi,d} + \frac{1}{2} \right] \right\}. \quad (\text{G.21})$$

- Anapole form factor

$$G_1^{\phi,d} = \frac{eQ_k}{2} \left\{ (Y_{ik}^L Y_{jk}^{*R} - Y_{ik}^R Y_{jk}^{*L}) (m_1 - m_2) m_k \sum_{i=0}^2 C_i^{\phi,d} + \right. \\ \left. (Y_{ik}^R Y_{jk}^{*R} - Y_{ik}^L Y_{jk}^{*L}) \left[(m_k^2 - m_1 m_2) C_0^{\phi,d} - m_1 m_2 \sum_{i,j=1}^2 (C_i^{\phi,d} + C_{ij}^{\phi,d}) - 2C_{00}^{\phi,d} + \frac{1}{2} \right] \right\}. \quad (\text{G.22})$$

- MDM form factor

$$F_2^{\phi,d} = \frac{-eQ_k}{2} \left[(Y_{ik}^L Y_{jk}^{*L} + Y_{ik}^R Y_{jk}^{*R}) \sum_{i,j=1}^2 \frac{m_1 m_2}{m_i} \left(\frac{C_i^{\phi,d}}{2} + C_{ij}^{\phi,d} \right) + \right. \\ \left. (Y_{ik}^R Y_{jk}^{*L} + Y_{ik}^L Y_{jk}^{*R}) m_k \sum_{i=1}^2 C_i^{\phi,d} \right]. \quad (\text{G.23})$$

- EDM form factor

$$G_2^{\phi,d} = \frac{-eQ_k}{2} \left[(-Y_{ik}^L Y_{jk}^{*L} - Y_{ik}^R Y_{jk}^{*R}) \sum_{i,j=1}^2 (-1)^i \frac{m_1 m_2}{m_i} \left(\frac{C_i^{\phi,d}}{2} + C_{ij}^{\phi,d} \right) + \right. \\ \left. (Y_{ik}^R Y_{jk}^{*L} - Y_{ik}^L Y_{jk}^{*R}) m_k \sum_{i=1}^2 C_i^{\phi,d} \right]. \quad (\text{G.24})$$